COMPUTATION OF MOLECULAR PROPERTIES AT THE *AB INITIO* LIMIT

A Thesis
Presented to
The Academic Faculty

by

Berhane Temelso

In Partial Fulfillment
of the Requirements for the Degree
Doctor of Philosophy in the
School of Chemistry and Biochemistry

Georgia Institute of Technology
May 2007

COMPUTATION OF MOLECULAR PROPERTIES AT THE *AB INITIO* LIMIT

Approved by:

Dr. C. David Sherrill, Advisor
School of Chemistry and Biochemistry
Georgia Institute of Technology

Dr. Rigoberto Hernandez
School of Chemistry and Biochemistry
Georgia Institute of Technology

Dr. Jean-Luc Brédas
School of Chemistry and Biochemistry
Georgia Institute of Technology

Dr. Robert L. Whetten
School of Chemistry and Biochemistry
Georgia Institute of Technology

Dr. Ralph C. Merkle
College of Computing
Georgia Institute of Technology

Date Approved: 10 January 2006

This thesis is dedicated to my father, Temelso Gayim, to whom it would mean most.

ACKNOWLEDGEMENTS

I am deeply indebted to my advisor, Dr. C. David Sherrill, for patiently guiding me through highs and lows of graduate school. Much of what is contained in this thesis was possible because of the efforts of our collaborators (Dr. Ralph C. Merkle, Robert A. Freitas Jr, Dr. Edward F. Valeev, Dr. Arteum Bochevarov), members of my committee (Dr. Jean-Luc Brèdas, Dr. Rigoberto Hernandez, Dr. Ralph C. Merkle, Dr. Robert L. Whetten). I would be remiss without mentioning my great teachers and mentors (Michael Archibald (ICS), Dr. Jay Baltisberger (Berea), Dr. Amer Lahamer (Berea), Ted Lenio (ICS) Konelene Merhatsidke (Atse Tewodros), Dr. Henry F. Schaefer III (UGA), Astrid Shiferaw (ICS), Dr. Yukio Yamaguchi(UGA)) for their help at many critical junctures.

The love and support of my family has been indispensable and I am truly grateful to my mother, Ametsion Hagdu, for all her sacrifices and prayers; my oldest brother, Tesfaldet, for setting aside his life to make ours better; my brother Haile for all the childhood fun; my sisters Netsanet, Genet and Kokob for keeping our family together and forging a great bond despite the great distance; Nevio for being the best brother-in-law anyone could ask for; Christine, Eros, Alessia, Ariam and Naód for their fandom of the uncle they have never met; Akoy G/Michael for looking after for my family; Rich and Lila Bellando for making me part of their family and supporting me in every conceivable way; James, Tara and Jennifer for being like brothers and sisters to me; Eddie and Dee for the Christmas magic and more; Isabella, Layla and Olivia for making every visit to Berea truly great.

Finally, my gratitude goes to current members of the Sherrill Group (John Sears, Ashley Ringer, Steve Arnstein, Tait Takatani) for their camaraderie; many friends (Dr. Micah Abrams, Suhaila Abdalla, Alana Canfield, James Doto, Fekre-Selassie, Selam, and Aman Fekade, Jay Foley, Steve Gnapragasam, Dr. Cheng Guan Koay, Dr. Rick Hodes, Hebret Lemma, Yordanos Mehari, Gideon Mogos, Jeremy Moix, Gungor Ozer, E. Dinesh Pillai, Yanping Qin, Dr. Mutasem Sinnokrot, William Sommer, Abebe Teferi, Li Teh, Alexander Teklu, Dr. Shi Zhong) for sticking with me over the years; Kobe and the Lakers for the endless drama and entertainment; Octane for "the atmosphere and the attitude" and my country, Eritrea for being a place I can proudly call home.

TABLE OF CONTENTS

LIST OF TABLES

LIST OF FIGURES

LIST OF SYMBOLS OR ABBREVIATIONS

AFM	Atomic force microscope.
B3LYP	3-parameter hybrid Becke exchange/Lee-Yang-Parr correlation functional.
BHLYP	Hybrid 50% Becke 50% HF exchange/Lee-Yang-Parr correlation functional. Equivalent to BH&HLYP.
BO	Born-Oppenheimer.
CASSCF	Complete active space self-consistent field.
CBS	Complete basis set limit.
CC	Coupled cluster.
cc-pCVNZ	Correlation consistent polarized core-valence N-ζ basis set.
cc-pVNZ	Correlation consistent polarized valence N-ζ basis set.
cc-pwCVNZ	Correlation consistent polarized core-valence weighted N-ζ basis set.
CC2	The second-order approximate coupled cluster singles and doubles model.
CCSD	Coupled cluster with single and double excitations.
CCSD(T)	Coupled cluster with single and double and perturbative triple excitations.
CCSDT	Coupled cluster with single, double, and triple excitations.
CGTO	Contracted Gaussian-type orbital (GTO).
CI	Configuration interaction.
CVD	Chemical vapor deposition.
DBOC	Diagonal Born-Oppenheimer correction.
$\Delta E^{\ddagger}$	Energy of activation.
ΔE	Energy of reaction.
ΔH	Enthalpy of reaction.
$\Delta H^{\ddagger}$	Enthalpy of activation.
E_a	Activation barrier.
ELF	Electron localization functions.

EP	Epstein-Nesbet.
FCI	Full configuration interaction.
FOCI	First-order configuration interaction.
GTO	Gaussian-type orbital.
GVB	Generalized valence bond.
HEAT	High accuracy extrapolated *ab initio* thermochemistry.
HF	Hartree-Fock.
HOMO	Highest occupied molecular orbital.
HTHP	High-temperature high-pressure.
ICS	International Community School of Addis Ababa ,Ethiopia.
LCAO-MO	Linear combination of atomic orbitals - molecular orbitals.
LDA	Local density approximation.
LUMO	Lowest unoccupied molecular orbital.
MBPT	Many-body perturbation theory.
MP	Møller-Plesset perturbation theory.
MP2	Møller-Plesset perturbation theory of second order.
MP2-CCSD	Hybrid MP2-CCSD method.
MPn	Møller-Plesset perturbation theory of n-th order.
MR-CISD	Multireference configuration interaction with single and double excitations.
MRD-CI	Multireference diexcited configuration interaction.
NPE	Non-parallelity error.
OPT1	Open shell perturbation theory method 1.
OPT2	Open shell perturbation theory method 2.
QCISD	Quadratic configuration interaction with single and double excitations.
RCCSD(T)	Restricted open-shell coupled cluster with single and double and perturbative triple excitations.
RFA	Rational-function approximation.
RMP2	Restricted open-shell Møller-Plesset perturbation theory of second order.

ROHF	Restricted open-shell Hartree-Fock.
ROSPT	Restricted open-shell perturbation theory.
SCF	Self-consistent field.
SOCI	Second-order configuration interaction.
SPM	Scanning probe microscope.
STM	Scanning tunneling microscope.
TCEPA	Truncated coupled electron pair approximation.
UCCSD(T)	Unrestricted open-shell coupled cluster with single and double and perturbative triple excitations.
UGA	University of Georgia.
UHF	Unrestricted Hartree-Fock.
UMP2	Unrestricted open-shell Møller-Plesset perturbation theory of second order.
ZAPT2	Z-averaged perturbation theory of second order.
ZPVE	Zero-point vibrational energy.

SUMMARY

The accuracy of a quantum chemical calculation inherently depends on the ability to account for the completeness of the one- and n-particle spaces. The size of the basis set used can be systematically increased until it reaches the complete one-particle basis set limit (CBS) while the n-particle space approaches its exact full configuration interaction (FCI) limit by following a hierarchy of electron correlation methods developed over the last seventy years. If extremely high accuracy is desired, properly correcting for very small effects such as those resulting the Born-Oppenheimer approximation and the neglect of relativistic effects becomes indispensable. For a series of chemically interesting and challenging systems, we identify the limits of conventional approaches and use state-of-the-art quantum chemical methods along with large basis sets to get the "right answer for the right reasons." First, we quantify the importance of small effects that are ignored in conventional quantum chemical calculations and manage to achieve spectroscopic accuracy (agreement of 1 cm^{-1} or less with experimental harmonic vibrational frequencies) for BH, CH^+ and NH. We then definitively resolve the global minimum structure for Li_6, Li_6^+, and Li_6^- using high accuracy calculations of the binding energies, ionization potentials, electron affinities and vertical excitation spectra for the competing isomers. The same rigorous approach is used to study a series of hydrogen transfer reactions and validate the necessary parameters for the hydrogen abstraction and donation steps in the mechanosynthesis of diamondoids. Finally, in an effort to overcome the steep computational scaling of most high-level methods, a new hybrid methodology which scales as $\mathcal{O}(N^5)$ but performs comparably to $\mathcal{O}(N^6)$ methods is benchmarked for its performance in the equilibrium and dissociation regimes.

CHAPTER I

INTRODUCTION

The objective of electronic structure theory is to solve the Schrödinger equation for any molecular system using efficient theoretical and computational implementations developed since the inception of quantum mechanics in the 1920s. Many models and approximations have been developed to compute wavefunctions and energies from which properties like optimal geometries, electronic, vibrational and rotational energy levels, reaction barriers, etc., can be deduced. The famous Schrödinger equation is shown in Equation 1.

$$\hat{H}\Psi = E\Psi \tag{1}$$

Here the Hamiltonian, $\hat{H}$, is the total energy operator, Ψ is the wavefunction and $E = \langle\Psi|\hat{H}|\Psi\rangle$ is the expectation value of the $\hat{H}$ operator for a given system. For a system of N electrons and M nuclei, $\hat{H}$ can be written as the sum of the kinetic and potential energy operators of the molecular system

$$\hat{H} = \hat{T}_e + \hat{T}_N + \hat{V}_{ee} + \hat{V}_{eN} + \hat{V}_{NN} \tag{2}$$

where the electronic kinetic energy operator, $\hat{T}_e$, nuclear kinetic energy operator, $\hat{T}_N$, electron-electron repulsion term, $\hat{V}_{ee}$, electron-nuclear attraction operator, $\hat{V}_{eN}$ and nuclear-nuclear repulsion term, $\hat{V}_{NN}$ are given by,

$$\hat{T}_e = -\sum_{i}^{N} \frac{1}{2}\nabla_i^2 \tag{3}$$

$$\hat{T}_N = -\sum_{i}^{M} \frac{1}{2M_A}\nabla_A^2 \tag{4}$$

$$\hat{V}_{ee} = \sum_{i>j}^{N} \frac{1}{r_{ij}} \tag{5}$$

$$\hat{V}_{eN} = -\sum_{i}^{N}\sum_{A}^{M} \frac{Z_A}{r_{Ai}} \tag{6}$$

$$\hat{V}_{NN} = \sum_{B>A}^{M} \frac{Z_A Z_B}{r_{AB}} \tag{7}$$

One of the most fundamental principles that these models invoke is the Born-Oppenheimer (BO) approximation[1] which claims that light electrons move in a different timescale than nuclei and thus nuclei could be assumed to remain stationary with respect to the fast motion of the electrons. This assumption is acceptable for most applications, but there remain many exceptions for which its validity is questionable[2]. The Born-Oppenheimer approximation allows for the separation of electronic and nuclear motion since $\hat{T}_N = 0$ and $\hat{V}_{NN}$ = *constant* and the resulting electronic Hamiltonian, $\hat{H}_e$ only depends parametrically on nuclear coordinates, A.

$$\hat{H}_e = -\sum_{i}^{N} \frac{1}{2}\nabla_i^2 - \sum_{i>j}^{N} \frac{1}{r_{ij}} + -\sum_{i}^{N}\sum_{A}^{M} \frac{Z_A}{r_{Ai}} \tag{8}$$

Now that we have defined the form of our electronic Hamiltonian, it is time to find the right form for the electronic wavefunction, Ψ_e. Since the molecular problem is inherently a many-body problem, solving the Schrödinger equation for such a system is virtually intractable for all but the simplest cases, namely the hydrogen atom and hydrogenic ions such as He^+ and Li^{2+}. We thus ignore the electron-electron interaction term from the Hamiltonian and start with the more soluble problem of non-interacting electrons. The new Hamiltonian has the form

$$\hat{H}_{1e} = -\sum_{i}^{N} \frac{1}{2}\nabla_i^2 - \sum_{i}^{N}\sum_{A}^{M} \frac{Z_A}{r_{Ai}} = \sum_{i}^{N} \hat{h}(i) \tag{9}$$

The solutions to this system of non-interacting electrons are a set of orbitals, $\chi_j(x_i)$, such that

$$\hat{h}(i)\chi_j(x_i) = \varepsilon_j \chi_j(x_i) \tag{10}$$

and the total wavefunction is a product of each particle's wavefunction and the total energy is simply a sum of each eigenvalue:

$$\Psi^{HP} = \chi_i(x_1)\chi_j(x_2)\chi_k(x_3)...\chi_n(x_N) \tag{11}$$

$$E = \varepsilon_i + \varepsilon_j + \varepsilon_k + ... + \varepsilon_n \tag{12}$$

These Hartree product wavefunctions (Ψ^{HP}) give unphysical results and violate the Pauli exclusion principle. Without delving into the details (which can be found in Reference [3, 4]), we assert that the simplest wavefunction that satisfies the Pauli principle and remains physically sensible is a Slater determinant of the form

$$\Psi_e = \frac{1}{\sqrt{N!}} \begin{vmatrix} \chi_a(\mathbf{x}_1) & \chi_b(\mathbf{x}_1) & \dots & \chi_n(\mathbf{x}_1) \\ \chi_a(\mathbf{x}_2) & \chi_b(\mathbf{x}_2) & \dots & \chi_n(\mathbf{x}_2) \\ \vdots & \vdots & \ddots & \vdots \\ \chi_a(\mathbf{x}_N) & \chi_b(\mathbf{x}_N) & \dots & \chi_n(\mathbf{x}_N) \end{vmatrix}$$

which is normally denoted in a shorthand form as

$$\Psi_e = |\chi_a(\mathbf{x}_1)\chi_b(\mathbf{x}_2)...\chi_n(\mathbf{x}_N)\rangle \tag{13}$$

The Slater determinant corresponds to N indistinguishable elections occupying spin orbitals $\chi_a \cdots \chi_n$.

1.1 Hartree-Fock Theory

In Hartree-Fock (HF) theory, we assume this independent electron approach but allow each electron to interact with the average field generated by the other electrons. Hartree-Fock theory, also referred to as molecular orbital theory, self-consistent field theory and mean-field theory, attempts to find a set of spin-orbitals that minimize the electronic energy. We can now go ahead plug in our suitable wavefunction and Hamiltonian to Equation 1 and calculate the HF energy. First, Equation 8 can be decomposed into a part that contains one- and two-electron operators.

$$\hat{H}_e = \sum_i^N \hat{h}(i) + \sum_{i>j}^N \frac{1}{r_{ij}} \tag{14}$$

The contribution to the energy from the one-electron operator is

$$E_1 = \sum_i^N \langle \Psi | \hat{h}(i) | \Psi \rangle = \sum_i^N \langle \chi_i | \hat{h}(i) | \chi_i \rangle = \sum_i^N h_{ii} \tag{15}$$

while the two-electron term yields

$$E_2 = \sum_{i>j}^N \langle \Psi | \frac{1}{r_{ij}} | \Psi \rangle = \sum_{i>j}^N \langle ij || ij \rangle \tag{16}$$

where the so-called antisymmetized two-election integrals $\langle ij||ij\rangle$ are

$$\langle ij||ij\rangle = \langle ij|ji\rangle - \langle ij|ij\rangle \tag{17}$$

and $\langle ij|ij\rangle$ is defined as

$$\langle ij|ij\rangle = \int dx_1 dx_2 \chi_i^*(x_1)\chi_j^*(x_2)\frac{1}{r_{ij}}\chi_i(x_1)\chi_j(x_2) \tag{18}$$

Thus, if we know the spin orbitals χ_i, we would easily calculate the HF energy.

$$E_{HF} = E_1 + E_2 = \sum_i^N h_{ii} + \sum_{i>j}^N \langle ij||ij\rangle \tag{19}$$

In reality, we do not know the spin orbitals χ_i and we would have to construct them using the LCAO-MO (linear combination of atomic orbitals to construct molecular orbitals) approach. For the sake of convenience, we can integrate out spin from χ_i and deal with molecular orbitals, ψ_i instead. At the heart of all electronic structure theory calculations lie basis sets describing atomic orbitals, ϕ_μ which mix to form molecular orbitals.

$$\psi_i = \sum_\mu C_\mu^i \phi_\mu \tag{20}$$

where C_μ^i are expansion coefficients and the atomic orbitals, ϕ_μ are typically constructed from Gaussian-type orbitals (GTO) and the contractions thereof (CGTO)

$$\phi_\mu^{GTO}(r) = N x^l y^m z^n e^{-\alpha r^2} \tag{21}$$

$$\phi_\mu^{CGTO}(r) = \sum_\nu C_\nu^\mu \phi_\nu^{GTO}(r) \tag{22}$$

where l, m, and n are integers used to specify s, p, d, etc. type orbitals. Gaussian-type orbitals mimic the Slater type orbitals ($\phi_\mu^{STO}(r) = N x^l y^m z^n e^{-\alpha r}$) fairly well and they are easy to compute. We can compute one- and two-electron contributions to the HF energy in atomic orbital (AO) basis as

$$h_{ii} = \sum_\mu \sum_\nu C_\mu^{i*} C_\nu^{i*} \langle \mu|\nu\rangle = \sum_\mu \sum_\nu C_\mu^{i*} C_\nu^{i*} h_{\mu\nu} \tag{23}$$

$$\langle ij|kl\rangle = \sum_\mu \sum_\nu \sum_\rho \sum_\sigma C_\mu^{i*} C_\nu^{j*} C_\rho^k C_\sigma^l \langle \mu\nu|\rho\sigma\rangle \tag{24}$$

and write the Hartree-Fock energy in AO basis as

$$E_{HF} = \sum_{\mu\nu} D_{\mu\nu}[2h_{\mu\nu} + \sum_{\rho\sigma} D_{\rho\sigma}\{2(\mu\nu|\rho\sigma) - (\mu\rho|\nu\sigma)\}] \tag{25}$$

where the density matrix, $D_{\mu\nu}$ is

$$D_{\mu\nu} = \sum_{\mu\nu} C_{\mu}^{i*} C_{\nu}^{i} = C^{\dagger} C \tag{26}$$

The aim of Hartree-Fock theory is to variationally minimize the electronic energy with respect to these molecular orbital coefficients. So, we form an energy functional ($E = \langle\Psi|\hat{H}|\Psi\rangle$) and minimize it subject to a normalization condition ($\langle\Psi|\Psi\rangle = 1$) using the method of Lagrange multipliers:

$$L[\Psi] = \langle\Psi|\hat{H}|\Psi\rangle - E(\langle\Psi|\Psi\rangle - 1) \tag{27}$$

$$\delta L[\Psi] = \delta\langle\Psi|\hat{H}|\Psi\rangle - \delta E(\langle\Psi|\Psi\rangle - 1) \tag{28}$$

Without showing any of the gory detail, it may be proven that the set of solutions to this minimization problem satisfy this pseudo-eigenvalue equation:

$$\sum_{\nu} F_{\mu\nu} C_{\nu}^{i} = \varepsilon_i \sum_{\nu} S_{\mu\nu} C_{\nu}^{i} \tag{29}$$

where the Fock matrix, F and overlap matrix S are given by

$$F_{\mu\nu} = h_{\mu\nu} + \sum_{\rho\sigma} [D_{\rho\sigma}\{2(\mu\nu|\rho\sigma) - (\mu\rho|\sigma\nu)\}] \tag{30}$$

$$S_{\mu\nu} = \langle\phi_\mu|\phi_\nu\rangle \tag{31}$$

Equation 29 can be cast in a true eigenvalue problem form by transforming the Fock matrix.

$$F^t = S^{-1/2} F S^{-1/2} \tag{32}$$

$$F^t(S^{1/2}C) = \varepsilon(S^{1/2}C) \tag{33}$$

Given a set of atomic orbitals, computation of the Hartree-Fock energy involves the following steps.

- Compute the overlap, one- and two-electron integrals, and the nuclear repulsion energy

- Build the transformation matrix $S^{-1/2}$ and use it to construct an initial guess for the Fock matrix (F_0') only using the one-electron part of the Hamiltonian:

$$F_0' = (S^{-1/2})^\dagger H S^{-1/2} \tag{34}$$

- Diagonalize the initial Fock matrix to generate its eigenvectors and build the initial density matrix:

$$F_0' C_0' = \varepsilon C_0' \tag{35}$$

$$D_{\mu\nu} = C_0^\dagger C_0 \tag{36}$$

- Using the new density matrix, generate a new Fock matrix, diagonalize it, calculate the HF energy and density and iterate until convergence.

The eigenvectors of the Fock matrix are a set orbitals, χ_i, and its eigenvalues, ε_i are the orbital energies. The mean-field or Hartree-Fock electronic energy is

$$E_{HF} = \sum_{\mu\nu} D_{\mu\nu}(H_{\mu\nu} + F_{\mu\nu}) + E_{NN} \tag{37}$$

where E_{NN} is the nuclear repulsion energy. The major shortcoming of HF theory is that it does not correlate the motion of electrons of opposite spins; instead, it allows each electron to interact with the average field generated by other electrons. This lack of dynamical correlation needs to be corrected. Also, a single Slater determinant wavefunction is not sufficient for many cases when the gap between the highest occupied molecular orbital (HOMO) and lowest unoccupied molecular orbital (LUMO) approaches zero, particularly in bond-breaking regions. The "non-dynamical" correlation problem also needs the proper treatment. As will be shown below, a Slater determinant constructed from these HF orbitals will serve as reference wavefunction ($|\Psi_0\rangle$) for more accurate electron correlation methods.

1.2 Electron Correlation Methods

Although HF theory captures more than ~99% of the total energy of a system, the remaining ~1% is frequently very critical for chemical problems. This correlation energy, E_{corr} is defined as

$$E_{corr} = E - E_{HF} \tag{38}$$

The lack of accounting for instantaneous dynamical correlation between electrons and the inadequacies of a single Slater determinant reference are significant enough to warrant the development of other more sophisticated approaches that go beyond a simple mean-field approach.

As mentioned at the very beginning, HF theory provides the best single Slater determinant wavefunction for a given one-particle basis set. The other component of this problem is the n-particle problem which deals with the correlation of electrons. Starting with a HF reference wavefunction, the n-particle wavefunction is built by adding a set of excited determinants, Φ_i, from the HF reference, Φ_{HF} with a weight, a_i

$$\Psi = a_0\Phi_{HF} + \sum_i a_i\Phi_i \tag{39}$$

where the excited determinants Φ_i differ from Φ_{HF} by the replacement of one or more orbitals. Most electron correlation methods differ in the way that they determine these weights or coefficients, a_i. Therefore, the molecular problem would have two dimensions – one on each of the one- and n-particle basis. As shown below, one would have to increase both the one- and n-particle basis to get to the exact answer within the non-relativistic Born-Oppenheimer approximation.

Table 1: Completing the one- and n-particle space

	DZ	TZ	QZ	...	one-particle limit (CBS)
HF	HF/DZ			...	HF/CBS
MP2	MP2/DZ			...	MP2/CBS
CISD	CISD/DZ			...	CISD/CBS
CCSD	CCSD/DZ			...	CCSD/CBS
CCSD(T)	CCSD(T)/DZ			...	CCSD(T)/CBS
⋮	⋮	⋮	⋮	⋱	⋮
n-particle limit (FCI)	FCI/DZ			...	Exact

The most common classes of electron correlation methods are derived from configuration interaction (CI) theory, many-body perturbation theory (MBPT) and coupled cluster (CC) theory and each one is briefly described below.

1.2.1 Configuration Interaction

Configuration interaction theory is conceptually simplest to understand because of its similarities with HF theory. The trial CI wavefunction is constructed by taking a linear combination of excited determinants from a reference HF wavefunction and the CI energy is variationally minimizing with respect to the weights or CI coefficients as they are normally called.

$$\Psi_{CI} = a_0\Phi_{HF} + \sum_i a_i\Phi_i^a + \sum_{ij} a_{ij}^{ab}\Phi_{ij}^{ab} + \sum_{ijk} a_{ijk}^{abc}\Phi_{ijk}^{abc} + ... = \sum_I^N a_I\Phi_I \tag{40}$$

where i, j, k are occupied orbitals, a, b, c are virtual or unoccupied orbitals, and Φ_i^a, Φ_{ij}^{ab} and Φ_{ijk}^{abc} are possible determinants found by performing single, double and triple excitations from the reference determinant (Φ_{HF}), respectively. In a manner similar to how we solved the HF equations, the CI energy can be minimized subject to the constraint that the whole CI wavefunction remain normalized:

$$L = \langle\Psi_{CI}|H|\Psi_{CI}\rangle - \epsilon[\langle\Psi_{CI}|\Psi_{CI}\rangle - 1] \tag{41}$$

where

$$\langle\Psi_{CI}|H|\Psi_{CI}\rangle = \sum_I\sum_J a_I a_J\langle\Phi_I|H|\Phi_J\rangle = \sum_I\sum_J a_I a_J H_{IJ} \tag{42}$$

$$\langle\Psi_{CI}|\Psi_{CI}\rangle = \sum_I\sum_J a_I a_J\langle\Phi_I|\Phi_J\rangle = \sum_I a_I^2 \tag{43}$$

This is equivalent to building the CI matrix (Equation 44) and diagonalizing it:

$$H_{CI} = \begin{vmatrix} H_{00} & H_{01} & H_{02} & \dots & H_{0N} \\ H_{10} & H_{11} & H_{12} & \dots & H_{1N} \\ H_{20} & H_{21} & H_{22} & \dots & H_{2N} \\ \vdots & \vdots & \vdots & \ddots & \vdots \\ H_{N0} & H_{N1} & H_{N2} & \dots & H_{NN} \end{vmatrix} \tag{44}$$

Here, I and J represent excited determinants and N is the total number of determinants. By virtue of the Slater rules, the H_{IJ} elements are zero if Φ_I and Φ_J differ by more than two excitations. Diagonalizing Equation 44 yields the CI energy and coefficient for the reference and excited determinants. Except for systems with less than 10 electrons, performing a

CI calculation including all possible excitations from the reference determinant, even in a modest one-particle basis, is virtually impossible. Instead, the CI expansion is truncated after a limited set of excitations such as in CISD where all single and double excitations from the reference determinant are included in the CI expansion. When all possible excitations are incorporated, the resulting full configuration interaction (FCI) wavefunction is the exact solution to the non-relativistic Born-Oppenheimer time-independent Schrödinger equation within a given basis set and the accuracy of other electron correlation methods is routinely gauged by benchmarking against FCI results.

1.2.2 Many-Body Perturbation Theory

In general perturbation theory, the Hamiltonian operator, H, is broken into a reference Hamiltonian, H_0 whose solutions, Φ_0, are known and a relatively small perturbation, H′ such that

$$H = H_0 + \lambda H' \tag{45}$$

For the purposes of calculating correlation energy, the Møller-Plesset (MP) perturbation theory defines the H_0 to be the sum over the Fock operators from a HF theory, and the perturbation to be the exact electron-electron repulsion potential, V_{ee}, minus two times the expectation value of the electron-electron repulsion potential from HF theory:

$$H_0 = \sum_i F_{ii} \tag{46}$$

$$H' = H - H_0 \tag{47}$$

For the perturbation series of different degrees n=0...2, the MPn energies are

$$E_{MP0} = \sum_i \varepsilon_i = E_{HF} \tag{48}$$

$$E_{MP1} = E_{HF} \tag{49}$$

$$E_{MP2} = \sum_{j>i}^{occ} \sum_{b>a}^{unocc} \frac{|\langle ij||ab\rangle|^2}{\varepsilon_i + \varepsilon_j - \varepsilon_a - \varepsilon_b} \tag{50}$$

The energy expressions for MPn ($n > 2$) look more complicated and will not be shown here. MP2 is the cheapest means of accounting for electron correlation and it normally recovers more than 80% of the electron correlation energy for a system.

1.2.3 Coupled Cluster Theory

In coupled cluster theory, the wavefunction is constructed in an exponential *ansatz* as

$$\Psi_{cc} = e^T \Phi_0 \tag{51}$$

where

$$e^T = 1 + T + \frac{T^2}{2} + \frac{T^3}{6} + ... + \frac{T^n}{n!} \tag{52}$$

$$T = T_1 + T_2 + ... + T_N \tag{53}$$

The order of the coupled cluster wavefunction is determined based on the terms included in the cluster operator, T. Thus, for coupled cluster singles and doubles (CCSD) method, T includes the sum T_1 and T_2 and e^T are given by

$$T = T_1 + T_2 \tag{54}$$

$$e^T = 1 + (T_1 + T_2) + \frac{(T_1 + T_2)^2}{2} + ... + \frac{(T_1 + T_2)^n}{n!} \tag{55}$$

where the $\hat{T}_1$ and $\hat{T}_2$ operators acting on a HF reference determinant generate singly and doubly excited configurations with amplitudes t_i^a and t_{ij}^{ab}, respectively.

$$T_1 \Phi_0 = \sum_{i}^{occ} \sum_{a}^{unocc} t_i^a \Phi_i^a \tag{56}$$

$$T_2 \Phi_0 = \sum_{i<j}^{occ} \sum_{a<b}^{unocc} t_{ij}^{ab} \Phi_{ij}^{ab} \tag{57}$$

The coupled cluster energy expression is

$$E_{CC} = \langle \Phi_0 | H e^T | \Phi_0 \rangle \tag{58}$$

and for CCSD, it reduces to the following form in spin-orbital basis:

$$E(CCSD) = \sum_{j>i}^{occ} \sum_{b>a}^{unocc} \langle ij||ab \rangle (t_{ij}^{ab} + 2 t_i^a t_j^b) \tag{59}$$

The importance of triple excitations has been noted, but the N^8 scaling of CCSDT has prompted the development of CCSD(T) which inexpensively includes the contribution of triples using higher-order terms from perturbation theory. The CCSD(T) method is considered the "gold standard of quantum chemistry" in cases where there are no bonds being broken or near-degeneracies and it has proven to be a good benchmark for most instances where FCI calculations are not possible.

1.2.4 Scaling of Electron Correlation Methods

One of the major challenges of electron correlation methods is their steep scaling and one often needs to reach a compromise between the size of the one- and n-particle basis to get the most accurate answer at a reasonable computational cost. The scaling for a hierarchy of relevant methods for the difference classes of electron correlation methods with increasing basis set size, N is given below.

Table 2: Scaling of electron correlation methods

Scaling	Method
N^4	HF, DFT
N^5	MP2, CC2
N^6	MP3, CISD, CCSD
N^7	MP4, CCSD(T)
$\vdots$	$\vdots$

1.3 Thesis Structure

The concepts described above are used throughout this thesis, particularly as they relate to finding the proper compromise between basis set size and electron correlation treatment. In Chapter II, we seek to achieve spectroscopic accuracy for a set of diatomics by extrapolating the one-particle basis to its complete basis set (CBS) limit, capturing all the electron correlation energy using FCI, including relativistic and first-order correction to the Born-Oppenheimer approximation. Chapter III definitively resolves the global minimum structure of Li_6 and its cation and anion using large one- and n-particle basis. Chapters IV and V explore the performance of different electron correlation methods for predicting hydrogen transfer barriers and energies of reactions. The hydrogen abstraction and donation steps in the mechanosynthesis of diamondoids are also assessed in terms of the kinetic parameters derived from our high accuracy methods. In Chapter VI, the first (MP2-CCSD(I)) and second (MP2-CCSD(II)) generations of a hybrid MP2-CCSD method which scales as MP2 $\mathcal{O}(N^5)$ but has the accuracy of the more reliable CCSD is benchmarked around the equilibrium as well as the bond dissociation region for a set of small molecules. The Appendix provides the motivation and preliminary results for two interesting topics

that branched out of the other topics discussed earlier. In particular, as an extension of our work on achieving spectroscopic accuracy by accounting small effects in Chapter II and accurate hydrogen transfer barriers in Chapters IV and V, the effect of the Diagonal Born-Oppenheimer Correction (DBOC) on hydrogen transfer barriers is investigated in Appendix A. Appendix B explores some odd artifacts introduced by open-shell perturbation theories when studying symmetric hydrogen exchange reactions.

CHAPTER II

A COMPARISON OF ONE-PARTICLE BASIS SET COMPLETENESS, HIGHER-ORDER ELECTRON CORRELATION, RELATIVISTIC EFFECTS, AND ADIABATIC CORRECTIONS FOR SPECTROSCOPIC CONSTANTS OF BH, CH^+, AND NH

To investigate the relative importance of various small sources of error in theoretical predictions of molecular properties, we report spectroscopic constants for the ground electronic states of BH, CH^+, and NH which are nearly converged to the adiabatic *ab initio* limit. Computations are performed using full configuration interaction (FCI) and coupled-cluster singles, doubles and perturbative triples [CCSD(T)] methods with correlation consistent basis sets of double to sextuple-ζ quality. The equilibrium bond lengths, r_e, harmonic vibrational frequencies, ω_e, anharmonicity constants, $\omega_e x_e$, centrifugal distortion constants, $\overline{D}_e$, and other quantities are compared with experiment for each species. The systematic dependence of spectroscopic constants on the one-particle basis is used to estimate the complete basis set limit (CBS) values by using a two-point linear extrapolation scheme. The importance of core correlation, scalar relativistic corrections, higher-order electron correlation, and basis set completeness are carefully investigated. Moreover, deviations from the Born-Oppenheimer approximation are studied by computing the diagonal Born-Oppenheimer correction (DBOC). The remaining error is attributed primarily to nonadiabatic effects. Our *ab initio* limit, adiabatic results for r_e are within 0.0007 Å of experiment when nonadiabatic effects are insignificant or have been removed. Adiabatic predictions of ω_e are within 0.5 cm^{-1} of experiment.[1]

2.1 Introduction

As *ab initio* electronic structure computations become more accurate, it is important to ask how the remaining errors in state-of-the-art approaches, such as basis set completeness, non-factorizable four-body and higher electron correlation, and relativistic, adiabatic, and

[1]Previously published as B. Temelso, E.F. Valeev, and C.D. Sherrill, J. Phys. Chem. A 108 (2004) 3068.

nonadiabatic corrections, compare to each other. Within the scope of the non-relativistic Born-Oppenheimer approximation, the quality of a quantum-chemical calculation depends only on the completeness of the one- and n-particle model spaces, n being the number of electrons in the system. The choice of a basis set dictates the truncation of the one-particle expansion while the wave function model determines the completeness of the n-particle space. The ultimate goal within this scheme is to achieve the complete basis set full configuration interaction (CBS FCI) values, which represent the exact solution of the time-independent Schrödinger equation under the framework of the Born-Oppenheimer approximation. However, the restriction to the non-relativistic Born-Oppenheimer approximation itself may lead to errors which are significant in some applications, such as matching the high rovibrational levels of the water molecule as required to prove the presence of water on the sun or to model the greenhouse effect on earth[5, 6].

In gauging the maximum accuracy that can be achieved by *ab initio* electronic structure theory, the study of diatomics has been valuable because of their small size and the availability of spectroscopic data. Extensive work on spectroscopic quality *ab initio* molecular properties of small diatomic hydrides has been done by Martin[7, 8], who observed that nonadiabatic effects, which are considered to be smaller or comparable to errors in the best *ab initio* methods, could actually be much more significant corrections, as in the case of BeH and BH. He performed a convergence study of spectroscopic constants of diatomic hydrides with respect to contracted and uncontracted basis sets. By accounting for the one-particle and n-particle incompleteness, he computed benchmark-quality spectroscopic constants and compared his best results with true Born-Oppenheimer (BO) results that are derived from experimental data, thereby showing the level of accuracy that can be expected from high level electronic structure theory methods. Another paper by Martin[9] studied the spectroscopic constants of the hydroxyl anion, OH^-, by converging the one- and n-particle basis and indicating the importance of connected quadruples of the coupled-cluster expansion and scalar relativistic effects in predicting constants accurately. Feller and Sordo[10] studied first row diatomic hydrides using coupled-cluster theory with full inclusion of triple excitations (CCSDT) and concluded that the improvement of CCSDT over CCSD(T) is

minimal compared to the significant computational cost of the former even though some of the differences between CCSDT and CCSD(T) remain significant on a spectroscopic scale. Nevertheless, this does not mean that inclusion of connected quadruple and even pentuple excitations in the coupled-cluster wave function produce similarly unimportant corrections. Recent benchmarking studies on the reliability of computed spectroscopic constants have been done with less correlated methods such as coupled-cluster with singles and doubles (CCSD)[11], second-order perturbation theory (MP2)[11], and density functional theory (DFT)[12].

Significant work has been devoted to analyzing the systematic convergence of different properties with respect to increasing basis set size. As a result, various extrapolation schemes exist for determining the complete basis set values for self-consistent field (SCF) and correlation energies, particularly for Dunning's correlation consistent basis sets[13, 14, 15, 16, 17], which are known to give a systematic convergence of energies and properties towards the CBS limit. Feller[18] showed that SCF energies approach the CBS limit exponentially, while Helgaker *et al.*[19] derived an inverse-cubic form (60) for extrapolating correlation energies.

In addition to accounting for basis set and correlation incompleteness, some of the more significant corrections to standard *ab initio* techniques include relativistic[20, 21, 22], adiabatic[23, 24, 25], and nonadiabatic [26, 27] contributions. In this work, we quantify the importance of these effects in achieving benchmark quality spectroscopic constants for three diatomic hydrides.

2.2 Computational and Theoretical Methods

All FCI computations were carried out using the DETCI [28] module in the PSI 3.2 [29] program package, while ACES II [30] was used to obtain CCSD(T) results. Computations were performed on a 72-processor IBM SP as well as dual-processor Linux workstations.

For Dunning's[13, 14, 15, 16, 17] correlation consistent polarized valence N-zeta (cc-pVNZ) basis sets, only valence-valence correlation is considered (using the frozen-core approximation), while the cc-pCVNZ basis sets enable the addition of core-core and core-valence

correlation due to the presence of high-exponent inner-shell basis functions. Both sets of correlation consistent basis sets use pure angular momentum Gaussian functions. Our largest basis, (cc-pCV5Z) is of
(18s12p7d5f3g1h/10s9p7d5f3g1h) quality for first row atoms while the cc-pV5Z basis for hydrogen has a (8s4p3d2f1g/5s4p3d2f1g) contraction scheme.

The one-particle calibration was done at the CCSD(T) level by taking the most accurate SCF energies and adding extrapolated correlation energies. It has been observed that SCF energies nearly converge to their complete basis set limit with cc-pV5Z or cc-pV6Z basis sets[19, 7]. The correlation energies asymptotically approach their basis set limit as

$$E_{\text{corr}} = d + fX^{-3} \tag{60}$$

The complete basis set limit may be estimated by the two-point linear extrapolation scheme of Helgaker *et al.*[19] For basis sets of consecutive cardinal numbers X and $Y = X - 1$, the extrapolated correlation energies would have the form:

$$E_{\text{corr}}^{XY} = \frac{E_{\text{corr}}^{X} X^3 - E_{\text{corr}}^{Y} Y^3}{X^3 - Y^3} \tag{61}$$

The estimated complete basis set CCSD(T) potential energy curve is the sum of the cc-pVXZ SCF energy and the extrapolated correlation energy, E_{corr}^{XY}. This two-point linear extrapolation accelerates the convergence of energies and spectroscopic constants, which are computed as derivatives of the potential energy curve[11]. The n-particle calibration was performed by comparing CCSD(T) and FCI energies. For a given basis set, full configuration interaction gives the exact solution within the Born-Oppenheimer approximation, thus capturing all the correlation energy in a complete n-particle Hilbert space.

When nuclei and electrons move in time scales that are not greatly different, deviations from the Born-Oppenheimer (BO) approximation become significant and adiabatic and nonadiabatic effects deserve consideration. The diagonal Born-Oppenheimer correction (DBOC) [23] is a first-order adiabatic correction to the BO approximation, and instead of assuming that nuclei are infinitely heavy, it takes into account the finite mass of the nuclei. The DBOC correction involves the expectation value of the nuclear kinetic energy operator,

$\hat{T}_n$,

$$E_{\mathrm{DBOC}} = \langle \Psi_e(r;R) | \hat{T}_n | \Psi_e(r;R) \rangle \tag{62}$$

Valeev and Sherrill have recently reported on the convergence behavior of this correction with respect to basis set and correlation treatment using configuration interaction wavefunctions[25].

The importance of relativistic effects was estimated by first-order perturbation theory. The relativistic corrections were computed as expectation values of the one-electron mass-velocity and Darwin terms[31] using unrelaxed CCSD densities in PSI 3.2 [29].

Spectroscopic constants were generated from a sixth-order polynomial, $U(r)$ determined from seven energy points evenly spaced about r_e (step-size of 0.005 Å). Each energy calculation was converged to 10^{-12} Hartrees. The rotational (J) and vibrational (ν) energy levels of a diatomic is generally given by Dunham's[32] expansion,

$$E_{\nu J} = h \sum_{ln} Y_{ln} (\nu + \frac{1}{2})^l J^n (J+1)^n \tag{63}$$

Expanding the first few terms, we get:

$$E \approx U(r_e) + h\omega_e(\nu + \frac{1}{2}) + hB_e J(J+1) - h\omega_e x_e (\nu + \frac{1}{2})^2 \tag{64}$$

$$-h\alpha_e(\nu + \frac{1}{2}) J(J+1) - h\overline{D}_e J^2 (J+1)^2 + ... \tag{65}$$

where we have substituted the Dunham expansion coefficients with the more familiar spectroscopic constants: $Y_{01} \cong B_e$, $Y_{10} \cong \omega_e$, $Y_{02} \cong \overline{D}_e$, $Y_{20} \cong -\omega_e x_e$ and $Y_{11} \cong -\alpha_e$. In our polynomial expansion in r, spectroscopic constants are given in terms of derivatives of $U(r)$ in the usual way[33].

$$I_e \equiv \mu r_e^2, \quad B_e \equiv \frac{h}{8\pi^2 I_e}, \quad \omega_e \equiv \frac{1}{2\pi} \left[\frac{U''(r_e)}{\mu} \right]^{1/2}, \tag{66}$$

$$\omega_e x_e \equiv \frac{B_e^2 r_e^4}{4h\omega_e^2} \left[\frac{10 B_e r_e^2 [U'''(r_e)]^2}{3h\omega_e^2} - U^{iv}(r_e) \right], \tag{67}$$

$$\alpha_e \equiv -\frac{2B_e^2}{\omega_e} \left[\frac{2B_e r_e^3 U'''(r_e)}{h\omega_e^2} + 3 \right], \overline{D}_e \equiv \frac{4B_e^3}{\omega_e^2} \tag{68}$$

where μ is the reduced mass, I_e is the moment of inertia, B_e is the rotational constant, ω_e is the harmonic vibrational frequency, $\omega_e x_e$ is the anharmonicity constant, α_e is the vibration-rotation coupling constant, and $\overline{D}_e$ is the centrifugal distortion constant. As suggested by

Handy and Lee[34], we have computed the reduced mass, μ, and the DBOC using atomic masses instead of nuclear masses.

2.3 Results and Discussion

The spectroscopic constants are presented in Tables 3 (BH), 4 (CH^+) and 5 (NH). The complete basis set extrapolation, FCI calibration, scalar relativistic and diagonal Born-Oppenheimer corrections are included in lower sections of Tables 3 - 5.

These calculated values are compared with experimental numbers [35, 36, 37, 38] as well as adiabatic[39, 40, 41] and Born-Oppenheimer values when available. Spectroscopists normally determine experimental spectroscopic constants by fitting their rovibrational spectra directly to a simple Dunham-type expansion (63). However, this expansion is derived assuming a single Born-Oppenheimer potential energy surface, whereas the experimental data are influenced by adiabatic and nonadiabatic effects. Hence the spectroscopic constants thus derived will incorporate some effective adiabatic and nonadiabatic contributions. Watson has shown[40] that a more complete mathematical treatment of the Dunham expansion (63) allows for an approximate separation of these effects. Spectroscopists typically deduce an "equilibrium bond length" as that which satisfies $Y_{01} = \hbar/\mu r_e^2$ for a fitted Dunham coefficient Y_{01}. However, a more detailed treatment[40] shows that

$$Y_{01} = \frac{\hbar}{2\mu(r_e^{ad})^2}\left[1 + \frac{\Delta Y_{01}^D}{B_e} + \frac{m_e}{m_p}g_J\right] \tag{69}$$

where r_e^{ad} is an adiabatic bond length, ΔY_{01}^D is a Dunham correction (involving up to the fifth derivative of the potential), and g_J is the Zeeman effect rotational factor incorporating nonadiabatic contributions. Following Watson, one may correct the experimental bond length (r_e^{expt}) to obtain adiabatic (r_e^{ad}) and Born-Oppenheimer (r_e^{BO}) values as,

$$r_e^{ad} = r_e^{expt}\sqrt{1 + \Delta Y_{01}^D/B_e + m_e g_J/m_p} \tag{70}$$

$$r_e^{BO} = r_e^{ad}/(1 + m_e d_1^{ad}/M_1 + m_e d_2^{ad}/M_2) \tag{71}$$

where d_1^{ad} and d_2^{ad} are constants, m_e is mass of an electron, and M_1 and M_2 are nuclear masses. These allow for a more direct comparison to the equilibrium bond lengths (r_e^{BO}) and the DBOC-corrected bond lengths (r_e^{ad}) computed theoretically in this work. This approach

Table 3: Spectroscopic constants of the $\tilde{X}\ ^1\Sigma^+$ state of BH

Level of theory	r_e	ω_e	$\omega_e x_e$	B_e	$\overline{D}_e$	α_e
FCI/cc-pVDZ	1.25597	2340.72	48.8	11.574	0.00113	0.397
FCI/cc-pVTZ	1.23560	2348.71	49.1	11.959	0.00124	0.422
FCI/cc-pVQZ	1.23349	2356.78	48.8	12.001	0.00124	0.420
FCI/cc-pV5Z	1.23285	2358.21	49.2	12.013	0.00125	0.421
FCI/cc-pCVDZ	1.25434	2340.12	48.8	11.604	0.00114	0.392
FCI/cc-pCVTZ	1.23339	2355.26	49.0	12.002	0.00125	0.421
CCSD(T)/cc-pVDZ	1.25578	2342.65	48.6	11.578	0.00113	0.395
CCSD(T)/cc-pVTZ	1.23540	2350.84	49.0	11.963	0.00124	0.421
CCSD(T)/cc-pVQZ	1.23329	2358.91	48.7	12.004	0.00124	0.419
CCSD(T)/cc-pV5Z	1.23266	2360.27	49.0	12.016	0.00125	0.420
CCSD(T)/cc-pV6Z	1.23254	2360.25	49.3	12.019	0.00125	0.419
CCSD(T)/cc-pCVDZ	1.25415	2342.10	48.7	11.608	0.00114	0.392
CCSD(T)/cc-pCVTZ	1.23321	2357.37	48.9	12.005	0.00125	0.420
CCSD(T)/cc-pCVQZ	1.23017	2368.23	49.1	12.065	0.00125	0.421
CCSD(T)/cc-pCV5Z	1.22946	2370.30	49.3	12.079	0.00125	0.422
Extrapolation						
CCSD(T)/cc-pCV(Q5)Z[a]	1.22899	2371.25	49.5	12.088	0.00128	0.423
Δ_{FCI}[b]	+0.00018	-2.07	+0.2	-0.003	0.00000	+0.001
$\Delta_{Relativistic}$[c]	+0.00001	-0.59	0.0	0.000	0.00000	0.000
Best BO	1.22917	2368.59	49.6	12.085	0.00126	0.424
Δ_{DBOC}[d]	+0.00066	-2.25		-0.013	0.00000	
Best Adiabatic	1.22983	2366.34		12.072	0.00126	
$\Delta_{Nonadiabatic}$[e]	+0.0025					
Best Nonadiabatic	1.2323					
Error[BO vs. Expt(BO)][f]	0.0003					
Error[BO vs. Expt][g]	-0.00300	1.86	0.3	0.059	0.00003	0.001
Error[Adiabatic vs. Expt(Adiab)][h]	0.0001					
Error[Adiabatic vs. Expt][g]	-0.00234	-0.39		0.046	0.00003	
Error[Nonadiabatic vs. Expt][h]	-0.0001					
Expt(BO)[e]	1.2295					
Expt(Adiab)[e]	1.2297					
Expt[i]	1.23217	2366.73	49.3	12.026	0.00123	0.422

[a] $E = E^5_{SCF} + E^{Q5}_{\rm corr}$, where $E^{Q5}_{\rm corr}$ is given by Eqn. (61). [b] FCI/cc-pCVTZ - CCSD(T)/cc-pCVTZ. [c] CCSD/ccpCV5Z level with unrelaxed densities. [d] CISD/cc-pVTZ DBOC values not sufficiently converged to give reliable higher order derivatives; $\omega_e x_e$ and α_e not reported. [e] Computed by Martin[7]. [f] Compared with BO values derived from experiment [Expt(BO)] by Martin[7]. [g] Compared with raw experimental values including effective adiabatic and nonadiabatic effects [Expt]. [h] Compared with adiabatic result derived from experiment [Expt(Adiab)] by Martin[7]. [i] Fernando *et al.*[35].

Table 4: Spectroscopic constants of the $\tilde{X}\ ^1\Sigma^+$ state of CH^+

Level of theory	r_e	ω_e	$\omega_e x_e$	B_e	$\overline{D}_e$	α_e
FCI/cc-pVDZ	1.14598	2892.15	64.6	13.807	0.00126	0.492
FCI/cc-pVTZ	1.13132	2846.66	57.4	14.167	0.00140	0.491
FCI/cc-pVQZ	1.12999	2853.02	58.8	14.200	0.00141	0.494
FCI/cc-pV5Z	1.12953	2855.30	59.9	14.211	0.00141	0.496
FCI/cc-pCVDZ	1.14540	2892.91	64.5	13.820	0.00126	0.490
FCI/cc-pCVTZ	1.13047	2853.11	57.0	14.188	0.00140	0.489
CCSD(T)/cc-pVDZ	1.14580	2894.61	64.4	13.811	0.00126	0.490
CCSD(T)/cc-pVTZ	1.13109	2849.66	57.2	14.172	0.00140	0.490
CCSD(T)/cc-pVQZ	1.12977	2855.91	58.4	14.206	0.00141	0.493
CCSD(T)/cc-pV5Z	1.12932	2858.07	59.5	14.217	0.00141	0.493
CCSD(T)/cc-pV6Z	1.12933	2857.59	59.3	14.217	0.00141	0.493
CCSD(T)/cc-pCVDZ	1.14524	2895.35	64.5	13.824	0.00126	0.489
CCSD(T)/cc-pCVTZ	1.13025	2856.05	57.8	14.193	0.00140	0.488
CCSD(T)/cc-pCVQZ	1.12824	2861.29	58.8	14.244	0.00141	0.495
CCSD(T)/cc-pCV5Z	1.12770	2863.70	59.3	14.258	0.00141	0.496
Extrapolation						
CCSD(T)/cc-pCV(Q5)Z[a]	1.12732	2864.56	59.4	14.267	0.00142	0.497
Δ_{FCI}[b]	+0.00021	-2.92	+0.2	-0.005	0.00000	+0.001
$\Delta_{Relativistic}$[c]	-0.00002	-0.74	0.0	0.000	0.00000	0.000
Best BO	1.12751	2860.90	59.6	14.262	0.00142	0.498
Δ_{DBOC}[d]	+0.00063	-2.81		-0.016	0.00000	
Best Adiabatic	1.12815	2858.09		14.246	0.00142	
Error[BO vs. Expt][e]	-0.00339	2.90	0.3	0.086	0.00005	0.005
Error[Adiabatic vs. Expt][e]	-0.00275	0.09		0.070	0.00005	
Expt[f]	1.1309	2858	59.300	14.176	0.00137	0.493

[a] $E = E^5_{SCF} + E^{Q5}_{\rm corr}$, where $E^{Q5}_{\rm corr}$ is given by Eqn. (61). [b] FCI/cc-pCVTZ - CCSD(T)/cc-pCVTZ. [c] CCSD/cc-pCV5Z level with unrelaxed densities. [d] CISD/cc-pVTZ DBOC values not sufficiently converged to give reliable higher order derivatives; $\omega_e x_e$ and α_e not reported. [e] Compared with raw experimental values including effective adiabatic and nonadiabatic effects [Expt]. [f] Carrington *et al.*[36].

Table 5: Spectroscopic constants of the $\tilde{X}\ ^3\Sigma^-$ state of NH

Level of theory	r_e	ω_e	$\omega_e x_e$	B_e	$\overline{D}_e$	α_e
FCI-cc-pVDZ	1.05647	3188.20	81.7	16.065	0.00163	0.656
FCI-cc-pVTZ	1.03970	3259.19	79.3	16.587	0.00172	0.656
FCI/cc-pCVDZ	1.05547	3191.49	81.8	16.096	0.00164	0.657
CCSD(T)/cc-pVDZ	1.05588	3196.93	80.9	16.083	0.00163	0.652
CCSD(T)/cc-pVTZ	1.03921	3267.77	78.4	16.603	0.00172	0.653
CCSD(T)/cc-pVQZ	1.03716	3282.12	78.4	16.669	0.00172	0.650
CCSD(T)/cc-pV5Z	1.03685	3285.58	78.8	16.679	0.00172	0.648
CCSD(T)/cc-pCVDZ	1.05488	3200.33	80.9	16.113	0.00163	0.652
CCSD(T)/cc-pCVTZ	1.03788	3268.24	78.5	16.646	0.00173	0.657
CCSD(T)/cc-pCVQZ	1.03607	3288.74	78.2	16.704	0.00172	0.650
CSD(T)/cc-pCV5Z	1.03558	3292.67	78.6	16.720	0.00172	0.649
Extrapolation						
CCSD(T)/cc-pCV(Q5)Z[a]	1.03527	3294.23	78.2	16.730	0.00173	0.649
Δ_{FCI}[b]	+0.00052	-8.05	+0.6	-0.017	0.00000	+0.004
$\Delta_{relativistic}$[c]	+0.00003	-1.75	0.0	-0.001	0.00000	0.000
Best BO	1.03582	3284.43	78.9	16.712	0.00173	0.653
Δ_{DBOC}[d]	+0.00027	-1.38		-0.009	0.00000	
Best Adiabatic	1.03609	3283.05		16.703	0.00173	
Error[BO vs. Expt(BO)][e]	-0.00073					
Error[BO vs. Expt(Adiab)][f]	-0.00093					
Error[BO vs. Expt][f]	-0.00093	1.85	0.0	0.013	0.00002	0.004
Error[Adiabatic vs. Expt(Adiab)][f]	-0.00066					
Error[Adiabatic vs. Expt][f]	-0.00066	0.47		0.004	0.00002	
Expt(BO)[g]	1.03655					
Expt(Ad)[h]	1.03675					
Expt[i]	1.03675	3282.583	78.915	16.700	0.00171	0.649

[a] $E = E^5_{SCF} + E^{Q5}_{\rm corr}$, where $E^{Q5}_{\rm corr}$ is given by Eqn. (61). [b] FCI/cc-pCVTZ - CCSD(T)/cc-pCVTZ [c] CCSD/cc-pCV5Z level with unrelaxed densities [d] CISD/cc-pVTZ DBOC values not sufficiently converged to give reliable higher order derivatives; $\omega_e x_e$ and α_e not reported. [e] Compared with BO values derived from experiment [Expt(BO)]. See Reference [7]. [f] Compared with raw experimental nonadiabatic($\approx$ adiabatic) values [Expt]. [g] Martin[8]. [h] According to Martin,[8] nonadiabatic effects in $\tilde{X}\ ^3\Sigma^-$ state of NH are very small, so $r_e^{ad} \approx r_e^{nonad}$. [i] Bernath *et al.*[37, 38].

has been used by Martin[7, 8] to derive BO bond lengths from experimental values for BH and NH. Rigorous discussion of adiabatic and nonadiabatic effects in rovibrational spectra of diatomics is given by Watson[40] and Tiemann and Ogilvie[39] and a more qualitative discussion is given in References [41, 7, 8].

2.3.1 Convergence of the One-particle Space

Figure 1 illustrates how the CCSD(T) predictions of r_e and ω_e monotonically converge towards the cc-pVNZ-derived complete basis set limit as the size of the cc-pVNZ (valence-only) basis increases. On the scale of these graphs, the errors for the cc-pVDZ basis are much larger than those for other basis sets, suggesting that this basis set is too small to be used reliably in extrapolation schemes for molecular properties.[42] The cc-pVQZ basis appears sufficient to converge r_e to 0.001 Å, but a cc-pV5Z basis is required to converge ω_e to 1 cm^{-1}.

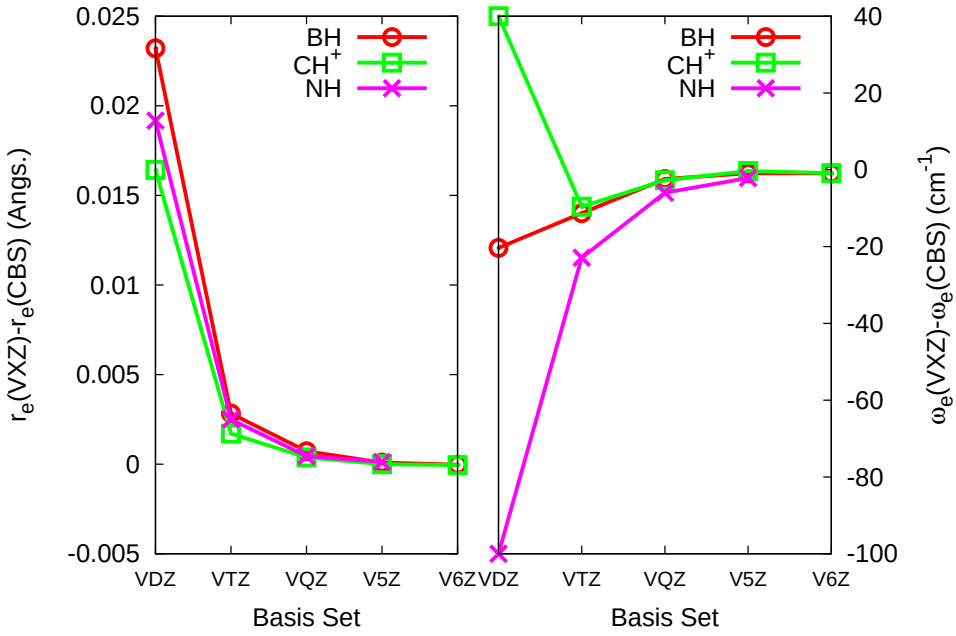

Figure 1: Convergence of CCSD(T) r_e and ω_e towards the complete basis set limit derived for valence-only (cc-pVNZ)

Similarly, Figure 2 shows the convergence of r_e and ω_e towards the CBS limit derived using cc-pCVNZ basis sets. Errors in r_e go from approximately 0.02 Å for the cc-pCVDZ basis to under 0.005 Å for cc-pCVTZ and under 0.001 Å for cc-pCVQZ. Again, however,

cc-pCVQZ does not appear sufficient to converge ω_e within 1 cm^{-1}. When the cc-pV5Z basis is increased to cc-pCV5Z and core electrons are correlated, bond lengths are shortened by 0.001-0.003 Å and vibrational frequencies are increased by 6-10 cm^{-1}. These changes demonstrate that direct comparison of valence-only results with experiment is not justified if spectroscopic accuracy is desired. We note that the difference between all-electron cc-pCVNZ and frozen-core cc-pVNZ values for r_e and ω_e grows with basis set size.

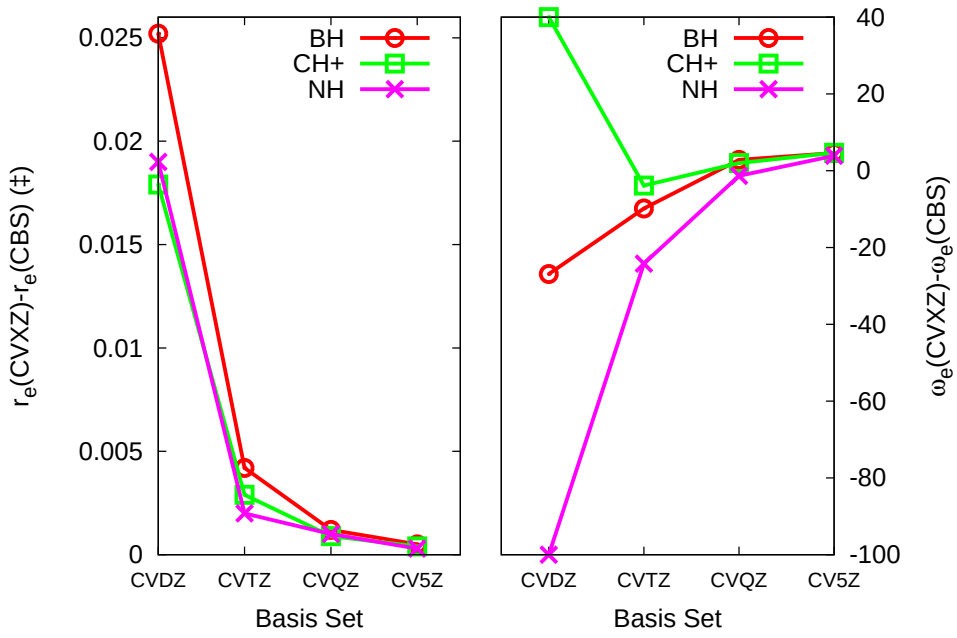

Figure 2: Convergence of CCSD(T) r_e towards the complete basis set limit derived for core-valence (cc-pCVNZ) basis sets.

Similarly to r_e and ω_e, the other spectroscopic constants tend to change significantly on going from a double-ζ to a triple-ζ basis set, but the changes become smaller with subsequent expansion of the basis. However, the convergence is more erratic and not monotonic for α_e and $\omega_e x_e$, which depend on the third and fourth derivatives, respectively, of the potential. These two terms appear to be rather insensitive to core correlation. The centrifugal distortion constant $\overline{D}_e$ converges for triple-ζ basis sets and beyond and is not sensitive to core correlation.

As mentioned earlier, significant effort [18, 10, 19, 11] has gone into understanding the systematic convergence of different properties towards the complete basis set limit. In this

study, we use the two-point linear extrapolation scheme of Helgaker *et al.* for correlation energies [19] to estimate the complete basis set limit. Results of this extrapolation using the cc-pCVQZ and cc-pCV5Z basis sets are denoted cc-pCV(Q5)Z, as indicated in the lower half of Tables 3-5. As expected, both increasing the size of the basis and the CBS extrapolation result in smaller predicted bond lengths.

Compared to the experimentally derived Born-Oppenheimer values for BH,[7] the cc-pCV(Q5)Z estimated complete basis set limit for CCSD(T) differs by -0.0005 Å for r_e. For NH, the extrapolated CCSD(T)/cc-pCV(Q5)Z value for r_e deviates by -0.00128 Å from the experimentally deduced BO value.[8] This error demonstrates that even estimates of the CBS CCSD(T) limit are not always able to come within 0.001 Å of experimentally deduced Born-Oppenheimer bond lengths without additional correction for small effects.

2.3.2 Importance of Higher-Order Excitations: n-particle Convergence

The n-particle calibration has been done to determine the remaining error in spectroscopic constants due to the incomplete treatment of electron correlation in the popular CCSD(T) model. Full CI provides a complete treatment of electron correlation within the given one-particle basis set, and Table 6 shows that the error in the CCSD(T) spectroscopic constants due to the incomplete treatment of electron correlation is around 0.0002-0.0006 Å for r_e, 2-9 cm^{-1} for ω_e, 0-1 cm^{-1} for $\omega_e x_e$, 0.003-0.018 cm^{-1} for B_e, and 0.001-0.004 cm^{-1} for α_e. The correction to the centrifugal distortion constant $\overline{D}_e$ is zero to the digits reported. The FCI corrections to CCSD(T) are very similar for the isoelectronic BH and CH^+ molecules, but they are around 2-4 times as large for NH.

It is immediately clear from Table 6 that the difference between CCSD(T) and FCI spectroscopic constants is almost insensitive to changes in the one-particle basis set. This weak coupling between the one-particle and n-particle spaces is advantageous because it allows one to approximate large-basis FCI potential energy curves by computing much less expensive CCSD(T) energies using a large basis and adjusting these values with a FCI correction computed using a smaller basis. Thus, the large-basis FCI energies are estimated

Table 6: Difference between FCI and CCSD(T) spectroscopic constants for BH, CH^+ and NH

Basis Set	r_e	ω_e	$\omega_e x_e$	B_e	$\overline{D}_e$	α_e
BH						
cc-pVDZ	0.00019	-1.93	0.2	-0.0035	0.00000	0.0012
cc-pVTZ	0.00020	-2.13	0.1	-0.0038	0.00000	0.0011
cc-pVQZ	0.00019	-2.13	0.2	-0.0030	0.00000	0.0011
cc-pV5Z	0.00019	-2.06	0.2	-0.0036	0.00000	0.0011
cc-pCVDZ	0.00019	-1.98	0.2	-0.0035	0.00000	0.0013
cc-pCVTZ	0.00018	-2.10	0.2	-0.0036	0.00000	0.0011
CH^+						
cc-pVDZ	0.00018	-2.46	0.2	-0.0047	0.00000	0.0012
cc-pVTZ	0.00023	-3.00	0.2	-0.0059	0.00000	0.0013
cc-pVQZ	0.00022	-2.89	0.4	-0.0055	0.00000	0.0013
cc-pV5Z	0.00018	-2.77	0.5	-0.0052	0.00000	0.0016
cc-pCVDZ	0.00016	-2.44	0.0	-0.0046	0.00000	0.0010
cc-pCVTZ	0.00022	-2.94	-0.8	-0.0054	0.00000	0.0012
NH						
cc-pVDZ	0.00058	-8.73	0.9	-0.0177	0.00000	0.0043
cc-pVTZ	0.00049	-7.59	0.9	-0.0156	0.00000	0.0038
cc-pCVDZ	0.00059	-8.84	0.9	-0.0178	0.00000	0.0044

by:

$$E_{\mathrm{FCI/VXZ}} \approx E_{\mathrm{CCSD(T)/VXZ}} + [E_{\mathrm{FCI/VYZ}} - E_{\mathrm{CCSD(T)/VYZ}}] \tag{72}$$

where cardinal number $Y < X$. According to Table 6, even a polarized double-ζ basis is sufficient to obtain a reliable estimate of the higher-order correlation correction.

Tables 3-5 give the Δ_{FCI} correction to the spectroscopic constants for BH, CH^+, and NH obtained in this fashion when the extrapolated CBS CCSD(T) energies at each point are adjusted according to the FCI correction in the above equation. For BH and CH^+, the FCI correction was obtained using the cc-pCVTZ basis, while for NH we could only afford a FCI calculation with the cc-pCVDZ basis. Generally, CCSD(T) tends to overestimate ω_e and shrink r_e. Δ_{FCI} for our best computed values of r_e and ω_e are 0.00018 Å and -2.07 cm^{-1} for BH, 0.00021 Å and -2.92 cm^{-1} for CH^+, and 0.00052 Å and -8.05 cm^{-1} for NH. A recent study by Hirata *et al.* [43] indicates that the full treatment of triple excitations in coupled-cluster theory via the CCSDT model is nearly converged with respect to electron correlation, because spectroscopic constants hardly change upon going to coupled-cluster theory with full quadruples, CCSDTQ. Comparing our CCSD(T) values to the CCSDT results of Feller and Sordo[10], we find that much of the error in CCSD(T) is indeed recovered by CCSDT, but the effect of higher-order excitations is not completely negligible. For example, the changes in spectroscopic constants going from CCSD(T) to CCSDT for NH in a cc-pVTZ basis are 0.0003 Å (r_e) and -6.6 cm^{-1} (ω_e) compared to the complete FCI corrections of 0.0006 Å (r_e) and -7.6 cm^{-1}. As indicated by Table 7, the corrections for correlation effects beyond CCSD(T) are of roughly the same order as the corrections due to basis set extrapolation considered above. They are somewhat smaller for r_e and larger for ω_e compared to CBS extrapolation.

2.3.3 Importance of Relativistic Corrections

Even though relativistic effects are usually considered insignificant for first row diatomics, they are indispensable for the level of spectroscopic accuracy we are trying to achieve. The importance of scalar relativistic effects to achieving high accuracy has been evident in recent literature.[20, 21, 22] There exist rigorous relativistic treatments like the full four-component

Dirac-Hartree-Fock theory, but it has been shown that a simple one-component scalar relativisitic Hamiltonian gives excellent results for systems consisting of light atoms.[44] Furthermore, Bauschlicher's work[45] indicated that scalar relativistic corrections computed via first-order perturbation theory using correlated wavefunctions give nearly identical results to those calculated using the Douglas-Kroll[46] formalism for small molecules. However, it should also be pointed out that for very high rovibrational levels of water, Quiney *et al.* [47] found that more complete treatments of relativistic effects could be significant.

Scalar relativistic effects are considerably smaller in light diatomics than in molecules containing heavy atoms. Nevertheless, for BH, CH^+ and NH, these corrections are not necessarily negligible compared to the intrinsic errors in our methods. We find that the relativistic corrections to r_e are very small indeed (no more than 0.00003 Å), but for ω_e they are -0.59 cm^{-1} (BH), -0.74 cm^{-1} (CH^+), and -1.75 cm^{-1} (NH). However, relativistic effects seem to have a very minimal impact on other spectroscopic constants like $\omega_e x_e$, α_e, B_e and $\overline{D}_e$.

2.3.4 Importance of Adiabatic and Nonadiabatic Effects

Relative corrections to spectroscopic constants due to deviations from the Born-Oppenheimer approximation are assumed to be on the order of the electron/nuclear mass ratio ($\sim 1/2000$ for H atom). However, our test cases indicate that both adiabatic and nonadiabatic effects could be more significant. After computing our best results within the framework of the Born-Oppenheimer approximation and determining adiabatic effects using the DBOC,[25] we assume the majority of the remaining deviation from experimental values is attributable to nonadiabatic effects.[39]

We calculated first-order adiabatic corrections using the DBOC scheme and a correlated wavefunction, namely configuration interaction with single and double excitations (CISD) with a cc-pVTZ basis. Our previous study on the DBOC indicates that it converges relatively quickly with respect to the one- and n-particle expansions.[25] CISD/cc-pVTZ results were very close to the CISD CBS limit for the cases considered, and electron correlation

beyond CISD did not have a significant effect on the DBOC correction to the barrier to linearity in H_2O. In an earlier work, Handy and Lee[34] showed that the RHF/6-31G* DBOC corrections to bond lengths of diatomics decrease with mass in the order H_2 > HF > N_2 > F_2. The largest effect was seen for H_2, for which the DBOC correction to r_e was about 0.0002 Å.

The effect of the DBOC on the BH molecule is surprisingly large — 0.00066 Å for r_e, and -2.25 cm^{-1} for ω_e. This change is greater than that due to basis set incompleteness (0.00047 Å and -0.95 cm^{-1}) or to correlation effects beyond CCSD(T) (0.00018 Å and -2.07 cm^{-1}). Despite the trend that the DBOC should decrease with increasing mass,[34] the effect on r_e of BH is more than three times larger than that of H_2 (0.0002 Å).[25] The adiabatic contribution to CH^+ is similar to that in BH: 0.00063 Å for r_e and -2.81 cm^{-1} for ω_e. Table 7 indicates that adiabatic corrections become disproportionately smaller in the heavier NH molecule, changing r_e and ω_e by 0.00027 Å and -1.38 cm^{-1}, respectively.

Only small errors remain in the present adiabatic theoretical treatment: residual basis set incompleteness in CCSD(T) energies, the use of finite basis sets in the FCI corrections, the truncation of the one- and n-particle spaces in the DBOC correction, and the use of only one-electron terms in the computation of relativistic effects. The preceding discussion indicates the very small size of these remaining uncertainties, and our final spectroscopic constants should be nearly exact in the adiabatic limit. Hence, we attribute most of the remaining difference from experiment to nonadiabatic effects. For BH, then, r_e changes by 0.00234 Å due to nonadiabatic effects. This change is larger than any of the small corrections considered in the present work, but it is consistent with Martin's estimate [7] of 0.0025 Å computed according to equation (70); the rotational g_J factor is found to be unusually large in BH.[7] If we add Martin's nonadiabatic correction of 0.0025 Å to our best adiabatic bond length of 1.22983 Å, the resulting theoretical nonadiabatic r_e of 1.2323 Å is nearly identical to the experimental r_e of 1.2322Å.

The difference between our best calculated adiabatic results and experiment for CH^+ indicate that the nonadiabatic contribution to r_e should be 0.00275 Å, similar to the isoelectronic BH molecule. Unfortunately, adiabatic or BO-corrected experimental data are not

available for CH^+ for comparison. Finally, our results for NH indicate that nonadiabatic effects are much smaller in that case (less than 0.0007 Å for r_e). This agrees qualitatively with the very small difference in experimental measurements of r_e for NH and ND (difference of 0.0001 Å).[37, 38] Nevertheless, nonadiabatic effects in NH may still be comparable to some of the small effects presently studied.

2.3.5 Comparison of Small Effects on Spectroscopic Constants

Table 7 summarizes the effects on r_e and ω_e of the small contributions considered in the present adiabatic theoretical treatment, and these effects are displayed graphically in Figures 3 (r_e) and 4 (ω_e).

Table 7: Effect of different corrections to r_e and ω_e of BH, CH^+ and NH

	r_e			ω_e		
	BH	CH^+	NH	BH	CH^+	NH
ΔExtrapolation[a]	-0.00047	-0.00038	-0.00031	0.95	0.86	1.56
ΔFCI[b]	0.00018	0.00021	0.00052	-2.07	-2.92	-8.05
ΔREL[c]	-0.00001	-0.00002	0.00003	-0.59	-0.74	-1.75
ΔDBOC[d]	0.00066	0.00063	0.00027	-2.25	-2.81	-1.38
Total	0.00036	0.00045	0.00051	-3.95	-5.61	-9.62

[a]CCSD(T)/cc-pCV(Q5)Z CBS extrapolation - CCSD(T)/cc-pCV5Z. [b]FCI/cc-pCVTZ - CCSD(T)/cc-pCVTZ for BH and CH^+ and FCI/cc-pCVDZ - CCSD(T)/cc-pCVDZ for NH. [c]At CCSD/cc-pCV5Z level with unrelaxed densities. [d]At CISD/cc-pVTZ level.

As pointed out previously, all of these contributions are less important than going to core-valence basis sets and correlating the core electrons. For BH and CH^+, the most significant of the small effects on r_e is due to the adiabatic correction (DBOC), lengthening bonds by 0.0006 - 0.0007 Å. As discussed previously, this effect is unusually large in these molecules, and for NH we find that it becomes much smaller (0.0003 Å) and less important than basis set extrapolation or higher-order correlation effects (FCI correction). Basis set extrapolation beyond cc-pCV5Z is usually more important than the FCI correction for r_e, although the two effects are of a similar size (magnitude of 0.0002 - 0.0005 Å). The relativistic correction to r_e is negligible. Core correlation and basis set extrapolation

consistently decrease bond lengths, while the full CI and adiabatic corrections consistently increase them. Because of these different signs, the net effect of all these contributions is only 0.0004 - 0.0005 Å. These results thus demonstrate that, as long as core correlation is included, the error in very large basis (e.g., cc-pCV5Z) CCSD(T) computations is probably under 0.001 Å compared to the relativistic-corrected adiabatic limit for first-row hydrides.

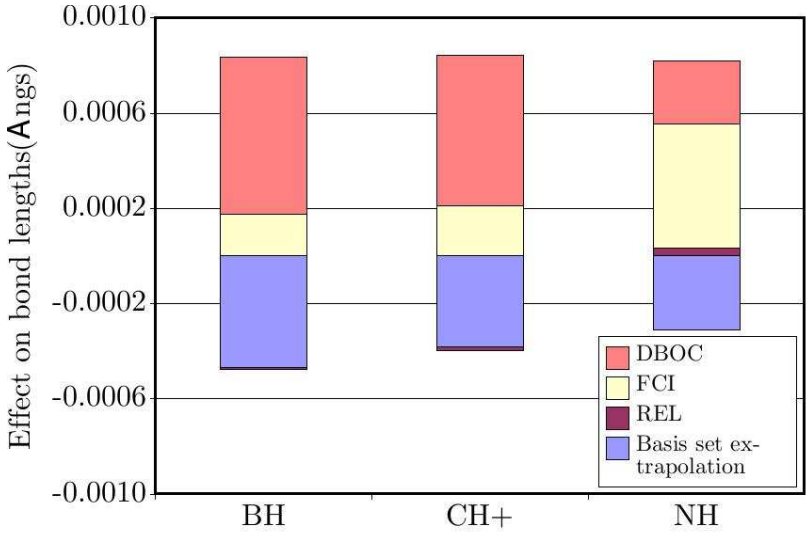

Figure 3: Effect of FCI, relativistic and adiabatic corrections on r_e

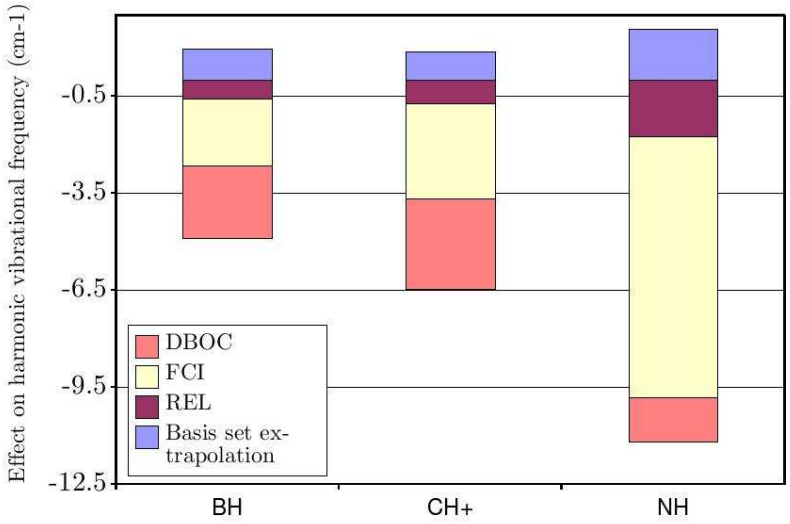

Figure 4: Effect of FCI, relativistic and adiabatic corrections on ω_e

For BH and CH^+, the adiabatic and FCI corrections to ω_e are similar in magnitude (2-3 cm^{-1}), while for NH the FCI correction is much larger (8 cm^{-1} vs. 1 cm^{-1}). For ω_e,

the basis set extrapolation correction is similar to but consistently smaller than the FCI correction. Although relativistic corrections to r_e were negligible, ω_e is changed by 1-2 cm^{-1}, which is relevant on the scale of spectroscopic accuracy. The relativistic correction to ω_e is larger than the adiabatic correction for NH. The net effect of all the small effects on ω_e is 4-6 cm^{-1}, suggesting that the inherent errors of large-basis CCSD(T) computations of harmonic vibrational frequencies are of this order.

2.3.6 What is the Limit of *ab initio* Methods?

Previous sections have focused primarily on the relative contributions of the small effects considered in this work. In this section, we will consider how our best computed spectroscopic constants compare to experiment. By accounting for one-particle space convergence by extrapolation of the correlation energy with cc-pCVQZ and cc-pCV5Z basis sets,[19] ensuring completeness of the n-particle space by correcting the CCSD(T) energies with full CI corrections, and adding one-electron relativistic terms, our theoretical spectroscopic constants should be near the exact relativity-corrected Born-Oppenheimer limit. After adding adiabatic corrections via the CISD/cc-pVTZ DBOC, our theoretical results should approach experiment very closely when nonadiabatic effects are small.

Perhaps the most direct comparison to experimentally deduced values can be made for the BH molecule, where Martin [7] used a theoretical value of g_J along with equations (70) and (71) to estimate adiabatic and BO results for r_e. Our best adiabatic result for r_e is 1.2298 Å, which is nearly identical to Martin's value of 1.2297 Å. The difference between our best Born-Oppenheimer r_e (1.2292 Å) and Martin's experimentally deduced estimate (1.2295 Å) is slightly larger, but we note that Martin's estimate of the adiabatic effect used to obtain r_e^{BO}, 0.0002 Å, is significantly smaller than our computed adiabatic shift of 0.00066 Å. As noted previously, if we add Martin's computed nonadiabatic correction (0.0025 Å) to our best adiabatic estimate, we obtain 1.2323 Å for r_e, in excellent agreement with the experimental value of 1.2322 Å. Comparing our adiabatic results directly to the unmodified experimental values, we find that the theoretical ω_e, 2366.34 cm^{-1}, matches very well with the experimental value of 2366.73 cm^{-1}.

Pure Born-Oppenheimer constants have not been estimated from the experimental data for CH^+, so we compare to the experimental effective constants which include nonadiabatic effects. Our adiabatic-corrected results are r_e = 1.12815 Å and ω_e = 2858.09 cm^{-1}. Comparing these values with effective nonadiabatic experimental values of r_e = 1.1309 Å and ω_e = 2858 cm^{-1}, we find errors of -0.00275 Å and 0.09 cm^{-1}, respectively. We can once again attribute most of this error to the large nonadiabatic effects in CH^+ (which is isoelectronic with BH).

As discussed above and pointed out by Martin,[8] nonadiabatic effects are expected to be small in NH. To the extent that this is true, our adiabatic-corrected constants may be compared directly to the experimental results. Our adiabatic results of r_e = 1.03609 Å and ω_e = 3283.05 cm^{-1} match the effective experimental values of 1.03675 Å and 3282.58 cm^{-1} rather well, although the agreement is not quite as good as that seen for adiabatic results for the BH molecule (perhaps because the nonadiabatic terms are not completely negligible in NH).

For BH and CH^+, adiabatic or Born-Oppenheimer corrected experimental results are not available for the higher-order spectroscopic constants, but for NH the unadjusted experimental results are comparable to our Born-Oppenheimer results to the extent that adiabatic and nonadiabatic effects might be neglected.

2.4 Conclusions

Small effects usually neglected in quantum chemistry may become significant as higher accuracy is desired. The importance of the completeness of one- and n-particle basis sets, as well as that of relativistic and adiabatic corrections, has been quantified for three first row hydrides, BH, CH^+, and NH. Full CI potential energies have been estimated at the complete basis set limit and corrected via scalar relativistic terms and the Born-Oppenheimer diagonal correction. One-particle basis set extrapolation, corrections for electron correlation beyond the CCSD(T) model, and adiabatic corrections are of roughly similar importance for the species studied. Scalar relativistic effects are negligible for bond lengths but are significant for predicting harmonic vibrational frequencies to spectroscopic accuracy. When compared

to experimentally deduced adiabatic values, our best results for r_e are accurate within 0.0007 Å. Harmonic vibrational frequencies are accurate to 0.5 cm^{-1} or less, even when compared to experimental values which have not been adjusted to remove nonadiabatic contributions.

The material of this chapter was published as a paper in the *Journal of Physical Chemistry A*[48].

CHAPTER III

HIGH ACCURACY *AB INITIO* STUDIES OF LI_6^+, LI_6^- AND THREE ISOMERS OF LI_6

The structures and energetics of Li_6^+, Li_6^- and three isomers of Li_6 are investigated using the coupled-cluster singles, doubles and perturbative triples [CCSD(T)] method with valence and core-valence correlation consistent basis sets of double- to quadruple-ζ quality (cc-pVXZ and cc-pCVXZ, where X=D-Q). These results are compared with qualitatively different predictions by less reliable methods. Our results conclusively show that the D_{4h} isomer is the global minimum structure for Li_6. It is energetically favored over the C_{5v} and D_{3h} structures by about 5.1 and 7.1 kcal mol^{-1}, respectively, after the inclusion of the zero-point vibrational energy (ZPVE) correction. Our most accurate total atomization energies are 123.2, 117.6 and 115.7 kcal mol^{-1} for the D_{4h}, C_{5v} and D_{3h} isomers, respectively. Comparison of experimental optical absorption spectra with our computed electronic spectra also indicate that the D_{4h} isomer is indeed the most stable structure. The cation, anion, and some higher spin states are investigated using the less expensive cc-pCVDZ basis set. Adiabatic ionization energies and electron affinities are reported and compared with experimental values. Predictions of molecular properties are found to be sensitive to the basis set used and to the treatment of electron correlation.[1]

3.1 Introduction

There has been great interest in metal clusters over the past few decades due to the need to understand and explore the evolution of molecular properties with size[49, 50]. Fascinating concepts like quantum confinement and surface effects in nanoclusters have captured the attention of scientists from all disciplines. Initially, the difficulties of producing clusters and characterizing them spectroscopically made computational and theoretical studies of these

[1]Prevously published as B. Temelso, and C.D. Sherrill, J. Chem. Phys. 122 (2005) 064315.

systems indispensable. Even as the experimental techniques have advanced, the role of computational studies in providing reliable geometries and energy levels for use in interpreting spectroscopic data has remained very significant[51, 49, 50, 52, 53, 54]. Lithium clusters have been of special value in this endeavor due to their small number of electrons and the ease with which they can be studied using high-level computational methods[55, 56, 57, 58, 59, 60]. The ultimate goal of these works is to understand the unique properties of these clusters as well as the evolution of their electronic structure as one starts with a single atom, builds clusters and nanoclusters, and finally reaches the bulk solid[51, 58].

Simple spherical shell models[61, 51], which assume that the valence electrons are independent and move in a spherically symmetric potential, have been very useful in gaining a qualitative understanding of the electronic structure of alkali metal clusters. The "jellium" model[62, 50] improves upon this description by allowing the electrons to interact self-consistently within a local density approach. While this model has been applied successfully to sodium clusters[63, 50], it did not work as well for lithium clusters[64, 65]. For example, the patterns in the sawtooth behavior of vertical ionization energies of lithium clusters with increasing size predicted by the jellium model diverged significantly from experiment[64], and contrary to experimental results, the jellium model predicts lithium clusters to have more pronounced shell effects on dissociation energies than corresponding sodium clusters[65]. Some of the failures in the spherical jellium model have been attributed to the assumption of spherical electron density and subsequent theories including deviations from spherical symmetry have given more accurate predictions[66, 67]. Also, these approaches do not treat core electrons explicitly and therefore may have difficulty when there is a small core-valence energy gap, as is the case with lithium. Additionally, deviations between density functional computations of bulk lithium using the local density approximation and experimental results for conductivity and Fermi surface-related properties[68, 69] suggest that more sophisticated treatments of electron correlation may be important in describing lithium clusters reliably.

Lithium clusters of 2 to 40 atoms have been studied with density-functional theory

(DFT) using both local density approximation (LDA)[70, 64] as well as nonlocal gradient-corrected functionals[58, 59, 71, 64]. Koutecký *et al.* have used conventional *ab initio* electronic structure methods like Hartree-Fock (HF) and various types of configuration interaction (CI) [55, 56, 57, 72, 59], while others have used second-order Møller-Plesset perturbation theory (MP2) [59, 73]. coupled-cluster methods [59, 60], and complete active space self-consistent field theory (CASSCF) [59]. McAdon and Goddard[74, 75, 76] used generalized valence bond (GVB) method to study metallic bonding in lithium clusters and proposed that valence electron density localizes in triangular sites for planar clusters and tetrahedral sites for three-dimensional species. *Ab initio* molecular dynamics[77], *ab initio* path integral methods[59, 78, 79], and variational quantum Monte Carlo[80] were among many other techniques[81, 82] used to study these small clusters computationally.

The case of homonuclear metallic hexamers is a particularly rich and interesting one in that it is a transition point where planar and non-planar isomers are competitive in energy. Clusters with less than 5-6 atoms generally prefer a planar conformation while those with six or more atoms take on three-dimensional structures[54, 52]. This can be explained in terms of the minimization principle for the cluster surface area. While planar structures have less surface area for smaller clusters, a more compact 3-D structure has less surface area for larger clusters. In the case of hexamers, the surface areas of the planar and 3-D structures are competitive. The prominent structures for metal hexamers include a planar isomer with a triangular (D_{3h}) symmetry and two non-planar isomers with pentagonal pyramidal (C_{5v}) and axially-compressed octahedral (D_{4h}) shapes. Looking at different metallic hexamers, the global minimum structure varies quite substantially. Additionally, different experimental and computational methods often indicate different structures. For example, geometric information on Au_6 derived from the vibrational auto-detachment spectrum of Au_6^- initially suggested a ring structure of D_{6h} symmetry as a minimum[83] but it was later claimed that the C_{5v} isomer is the most stable structure[84]. More in-depth studies using theoretical methods like CASSCF, first- and second-order configuration interaction (FOCI and SOCI), and multireference diexcited configuration interaction (MRD-CI) concluded that the optimal structure of the gold hexamer is a capped pentagonal structure of C_{5v}

symmetry[85]. Recent DFT studies have, however, predicted a planar triangular structure of D_{3h} symmetry[86, 87]. Similar controversies have occured for Cu_6[85, 88, 89], Ag_6,[85] and Na_6[53, 82, 90].

For alkali-metal clusters, the presence of only an s-electron in the valence leads to two interesting phenomena. First, the bonding is not prone to directionality as is normally seen for clusters of atoms containing p- and d-electrons in their valence. Second, the potential energy surface becomes very flat and numerous shallow local minima appear. Both the absence of directional bonding as well as flat potential energy surfaces and shallow minima present challenges for experimentalists and theoreticians alike[71]. It thus comes as no surprise that there is a high level of ambiguity involving the optimal structure of Li_6.

For the case of Li_6, Hartree-Fock (HF) based *ab initio* molecular dynamics simulations showed that in three different 100 ps simulations, all three of the D_{4h}, C_{5v}, and D_{3h} isomers were sampled[77]. This is indicative of the flatness of the potential energy surface and the shallow nature of the minima. The D_{3h} isomer has received considerably more attention in earlier computational studies[72, 56, 57]. mainly because preceding works on the similar alkali metal cluster, Na_6, indicated that the D_{3h} structure was energetically favored over the other two isomers and because optical absorption spectroscopy on Na_6 gave results consistent with what would be expected from a D_{3h} cluster[53]. However, for Li_6, optical absorption spectra collected using depletion spectroscopy in the 400-700nm range[54, 52], combined with minimal basis set MRD-CI[57] computations, indicated a C_{2v} isomer. More recent theoretical studies using larger basis sets have found a more symmetric D_{4h} isomer but not the C_{2v} isomer[58, 59]. The most reliable theoretical approach previously used to study Li_6 is quadratic configuration interaction with single and double excitations (QCISD), using a 6-311G* basis[59].

There has been little experimental or theoretical work on the structures and properties of anionic and cationic lithium hexamers. Li_6^+ has been observed after lithium vapor aggregates into clusters and the product is ionized by a powerful laser[54, 52]. Some theoretical work on the cationic and anionic lithium hexamer has been performed by using the SCF and MRD-CI methods[72], but only a minimal basis set was used.

In this work, we present highly accurate geometries, zero-point vibrational energies (ZPVE's), and binding energies in order to resolve the uncertainty concerning the relative stability and energetics of the three isomers of Li_6 (D_{4h}, C_{5v}, and D_{3h}), shown in Figures 6-8. Our best estimates of the binding energies use the very reliable coupled-cluster method with single, double, and perturbative triple substitutions [CCSD(T)][91] in conjunction with a very large basis set, the quadruple-ζ polarized core-valence basis set cc-pCVQZ. These results should closely approach the *ab initio* limit for these isomers. We also report the first high-level theoretical results for the lowest $^3B_1$ state of Li_6 (Figure 15) and the ground states of Li_6^+ (Figure 16) and Li_6^- (Figure 17). Due to the open-shell nature of these species, computations are more difficult, and so we use the more modest cc-pCVDZ basis. The effects of basis sets and electron correlation are also carefully investigated for these clusters.

3.2 Computational Approach

All computations were carried out using the ACES II [30] and MOLPRO [92] program packages running on a 72-processor IBM SP and a 48-processor IBM Pentium 4 Linux cluster. Geometry optimizations were done using analytic gradient methods employing the rational-function approximation (RFA) technique in ACES II. For geometric optimizations of the singlet state at the CCSD(T)/cc-pCVQZ level, numerical gradients with the RFA method were used, as implemented in MOLPRO. All frequencies and ZPVE's have been computed using ACES II at the CCSD(T)/cc-pCVDZ level of theory. Plots of Hartree-Fock valence orbitals were generated using the cc-pCVDZ basis with MOLDEN's[93] interface to MOLPRO. Vertical excitation spectra for the singlet states are computed using equation-of-motion (EOM) CCSD[94].

The unusual bonding in these clusters raises the question of whether single-reference methods, based upon the assumption of a single dominant electron configuration, are appropriate. Previous investigation[59] of the CASSCF one-particle density matrix indicated that single-reference approaches suffice for these clusters. It was found that the CASSCF wavefunction is built mostly (92% for Li_2 and 93% for Li_3^+) from the reference Hartree-Fock

determinant. We computed the T_1 diagnostic[95, 96] at the CCSD(T)/cc-pCVQZ level and obtained 0.013, 0.012 and 0.011 for the D_{4h}, C_{5v} and D_{3h} structures, respectively. These values are all below the recommended 0.020 threshold above which multireference character and nondynamical correlation often become significant. Additionally, the magnitudes of the largest T_2 amplitudes for these isomers (0.065, 0.074, and 0.062 for D_{4h}, C_{5v}, and D_{3h}) compare favorably with the largest T_2 amplitudes for systems like H_2O and BH which contain very little multireference character (e.g., the largest T_2 for CCSD/6-31G* H_2O is 0.052). For Li_6^+ and Li_6^-, the largest T_2 amplitudes at the CCSD(T)/cc-pCVDZ level of theory had magnitudes of 0.072 and 0.077, respectively. We therefore expect the CCSD(T) method to yield accurate results for these systems.

We use the correlation consistent basis sets of Dunning and co-workers[13, 14, 15, 16, 17] because they yield energies and properties that converge systematically towards the complete basis set (CBS) limit. These basis sets include polarization functions which can be critical in describing systems with significantly delocalized electron densities[72]. Because the 1s and 2s electrons in lithium atom are similar in energy, core correlation can be important also, and thus all electrons need to be correlated. However, standard split-valence basis sets lack tight core functions appropriate to describe core correlation, and this can be particularly problematic for alkali earth metals such as lithium[97]. Indeed, for the standard cc-pVXZ basis sets, we observed significant jumps in predicted geometries and energies as progressively larger basis sets were used. For this reason, we have also employed the core-valence correlation consistent basis sets (cc-pCVXZ) of Dunning and co-workers[14], the related "core-valence weighted" (cc-pwCVXZ) [98, 60] basis sets. These basis sets are compared in Section 3.3.1. For the anionic lithium hexamer, Li_6^-, diffuse functions may also be important. However, there are no correlation consistent basis sets with diffuse functions for alkali and alkaline clusters. To circumvent that problem, we added the diffuse s and p functions from the 6-311++G** basis set[99] to the standard core-valence correlations consistent basis sets (cc-pCVXZ).

The *ab initio* atomization energy or binding energy per atom is indicative of the "static

stability" of the clusters, while the "dynamic stability," which is not computed here, corresponds to the relative stability of clusters of different sizes and is thus useful in determining fragmentation and dissociation pathways, cascading to an ultra-stable cluster with a "magic number" of atoms[52, 100]. The binding energies per atom (E_b^6, E_b^{6+} and E_b^{6-}) can be computed from the energy of the hexamer (E_6, E_6^+ and E_6^-) and the energies for the neutral (E_1), cationic (E_1^+) and anionic (E_1^-) lithium atom as follows:

$$E_b^6 = (6E_1 - E_6)/6 \tag{73}$$

$$E_b^{6+} = (5E_1 + E_1^+ - E_6^+)/6 \tag{74}$$

$$E_b^{6-} = (5E_1 + E_1^- - E_6^-)/6 \tag{75}$$

Due to the closeness in energy between the three isomers in this study, it is essential to include a zero-point vibrational energy (ZPVE) correction to the Born-Oppenheimer energies. We have computed ZVPE's at the CCSD(T)/cc-pCVDZ level of theory. Using larger basis sets for ZPVE's becomes very difficult because of the large computational expense involved in obtaining second derivatives. Second derivatives were also used to perform vibrational frequency analysis to verify the character of optimized geometries as minima or saddle points. Adiabatic ionization energies have been calculated for the neutral clusters at the CCSD(T)/cc-pCVDZ level. The equation-of-motion CCSD (EOM-CCSD)[94] method, as implemented in ACES II[30], is currently the state-of-the-art technique for predicting electronic excited state properties and it is used here to determine vertical excitation energies and oscillator strengths. The theoretical spectra predicted by EOM-CCSD are qualitatively compared with experimental spectra[54, 52] to determine which isomer is observed experimentally at low temperatures.

3.3 Results and Discussion

3.3.1 Basis Set Effects

As discussed previously, finding a good correlation consistent basis set for lithium is critical for predicting properties reliably. The conventional valence-only correlation consistent basis sets (cc-pVXZ), which are designed for frozen-core calculations, are not convenient for

systems containing atoms with a small core-valence energy separation. Instead, it is important to use basis sets including core correlating functions, such as the correlation consistent core-valence (cc-pCVXZ) sets. In order to check the reliability of the different correlation consistent basis sets, we performed tests to see which basis sets yield a monotonic and smooth convergence for different properties, particularly geometries and binding energies. Table 8 and Figure 5 compare the change in predicted geometries and energies for the D_{4h} isomer as we use the cc-pVXZ, cc-pCVXZ and cc-pwCVXZ basis sets of increasing cardinal numbers X.

Table 8: Changes to energies and bond lengths with respect to changes in basis set for the D_{4h} isomer

Level of theory	Bond Length (Å)		Binding Energy[a]
	D_1	D_2	Per Atom
Basis Set Effects			
cc-pVXZ			
VTZ-VDZ	-0.131	-0.080	1.96
VQZ-VTZ	-0.033	-0.066	1.72
cc-pCVXZ			
CVTZ-CVDZ	-0.055	-0.029	0.77
CVQZ-CVTZ	-0.007	-0.006	0.19
cc-pwCVXZ			
wCVTZ-wCVDZ	-0.053	-0.029	-0.75
Correlation Effects			
$[CCSD(T) - CCSD]$/VDZ	0.053	-0.002	0.95
$[CCSD(T) - CCSD]$/VTZ	0.039	-0.007	1.14
$[CCSD(T) - CCSD]$/CVDZ	0.046	-0.004	1.02

[a] In kcal mol^{-1}.

The bond lengths, D_1 and D_2, are defined in Figures 6-8. For the case of the valence-only (cc-pVXZ) basis sets, there is a large change in predicted geometry (-0.131 Å for D_1 and -0.080 Å for D_2) and binding energy per atom (1.96 kcal mol^{-1}) upon going from cc-pVDZ to cc-pVTZ. The change for cc-pVTZ to cc-pVQZ is still large but a little less pronounced both in terms of geometries and binding energies. In contrast, the core-valence basis sets (cc-pCVXZ) show a much smaller jump in geometries (-0.055 Å for D_1 and -0.029 Å for D_2) and binding energies (0.77 kcal mol^{-1}) for a change from cc-pCVDZ to cc-pCVTZ. The difference is even smaller, as it should be, for a change from cc-pCVTZ to

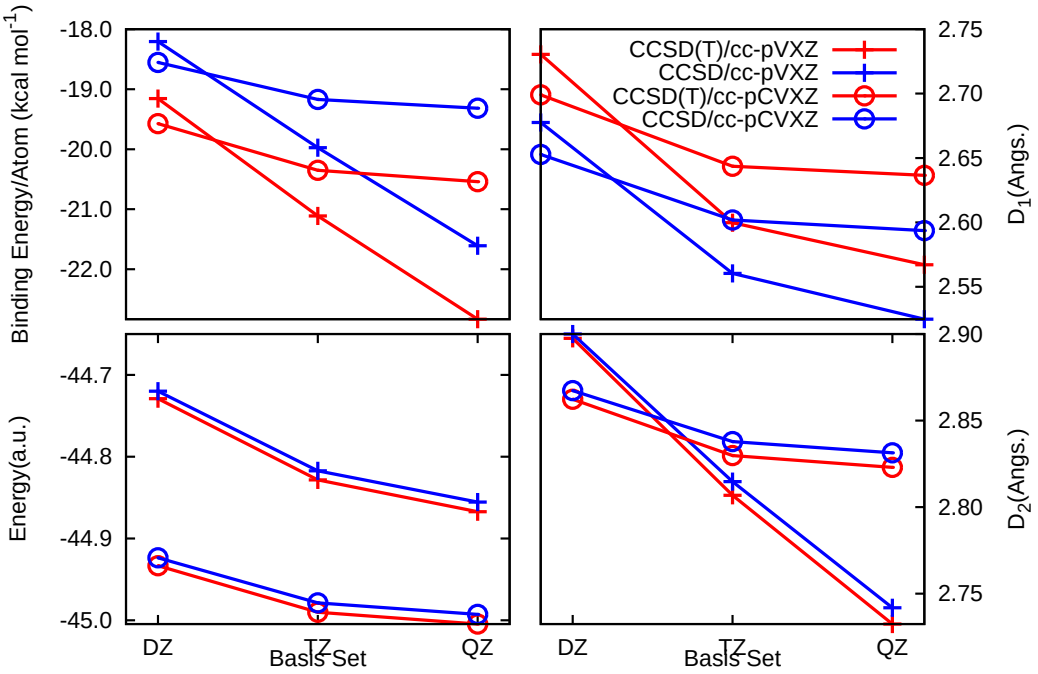

Figure 5: Comparison of correlation and basis set effects for the D_{4h} isomer of Li_6

cc-pCVQZ: -0.007 Å for D_1, -0.006 Å for D_2, and 0.19 kcal mol^{-1} for the binding energy. The significant change in the geometry and binding energies computed using the cc-pVXZ basis sets demonstrates that the one-particle space it represents is converging slowly while the much smaller change for the cc-pCVXZ basis sets is indicative of a representation that is approaching completeness at a faster rate. We performed a similar analysis of the core-valence weighted correlation consistent basis sets (cc-pwCVNZ), which are designed to more rapidly converge the core-valence correlation energy at the expense of the core-core correlation energy[98]. For Li_6, we found very little difference between the cc-pCVXZ and cc-pwCVXZ basis sets, and thus we used the former in the remainder of the study.

3.3.2 Electron Correlation Effects

One of the challenges of *ab initio* electronic structure theory is to find a highly accurate yet computationally feasible compromise between the level of electron correlation (n-particle space, where n is the number of electrons) and the size of the basis set (one-particle space)[101], Table 8 compares the effect of changing the correlation treatment from CCSD

to CCSD(T) with that of increasing the size of basis set for the D_{4h} isomer. This information is also displayed in Figure 5, which demonstrates that basis set incompleteness, core correlation, and triple excitations can *all* be important in obtaining accurate results. Therefore, we employ CCSD(T), core electrons being correlated, with the largest basis set feasible at each stage of our predictions. Our best energies for Li_6 are computed with the large cc-pCVQZ basis. More expensive computations of frequencies and of open-shell Li_6^+ and Li_6^- employ the cc-pCVDZ basis.

3.3.3 Singlet State of Li_6

As noted previously, the singlet state of Li_6 has three energetically close isomers: D_{4h}, C_{5v}, and D_{3h}[77]. Each one of these isomers corresponds to a local minimum on the potential energy hypersurface, as verified here by normal mode analysis. To check for the existence of other local minima, we performed calculations using a much lower spatial symmetry (C_s), but all those attempts led back to a structure matching one of the three isomers discussed here. It has been suggested that D_{5h} and C_{2v} isomers exist; however, optimizations starting from a D_{5h} configuration lead back to the quasi-planar C_{5v} isomer, and the C_{2v} structure changes to a more symmetric D_{4h} isomer upon using a larger basis set and a more complete correlation method.

One of the first treatments is a minimal basis HF computation which predicts a D_{3h} global minimum. Multireference diexcited configuration interaction, with and without Davidson correction (MRD-CI-Dav and MRD-CI, respectively), suggest a C_{5v} isomer as the most stable species[72]. These discrepancies are indicative of the sensitivity of Li_6 geometries and energies to the basis set and correlation method used. Other computations by Rousseau *et al.* [59] using a triple-ζ basis set and a variety of correlated methods predict a D_{4h} global minimum even though the relative energies vary quite significantly and the ordering of the other two isomers differs depending on the methods used. For example, while the QCISD method suggests a more stable D_{3h} structure than a C_{5v} one, MP2 and B3LYP predict otherwise. It is also worth noting that the HF method using minimal basis gives completely different results from HF/6-311G*, once again showing the importance of

basis set effects in these systems.

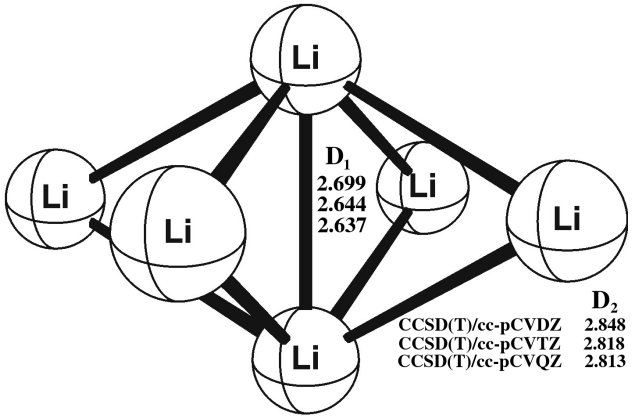

Figure 6: D_{4h} isomer of Li_6

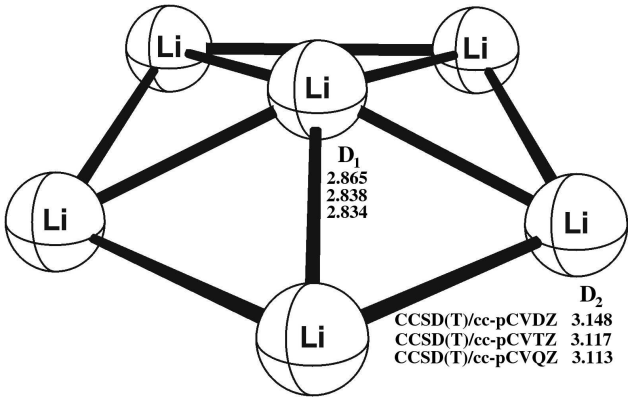

Figure 7: C_{5v} isomer of Li_6

A brief synopsis of relative energies predicted in previous literature for the three isomers is given in Table 9.

3.3.3.1 D_{4h} Isomer

Early works in the literature[72, 55, 56, 57] have claimed that a minimum of C_{2v} symmetry exists, while more advanced methods have later shown that the C_{2v} isomer in fact is an axially-compressed octahedral structure of D_{4h} symmetry[58, 59]. It has two types of bonds, namely a shortened axial bond, designated as D_1 in Figure 6, and another slightly longer bond, labeled as D_2. As shown in Table 10, the most accurate bond lengths for D_1 and D_2 are 2.637 Å and 2.813 Å at the CCSD(T)/cc-pCVQZ level. These values are well-converged, as can be seen by the small changes (-0.007 Å and -0.006 Å in D_1 and D_2, respectively),

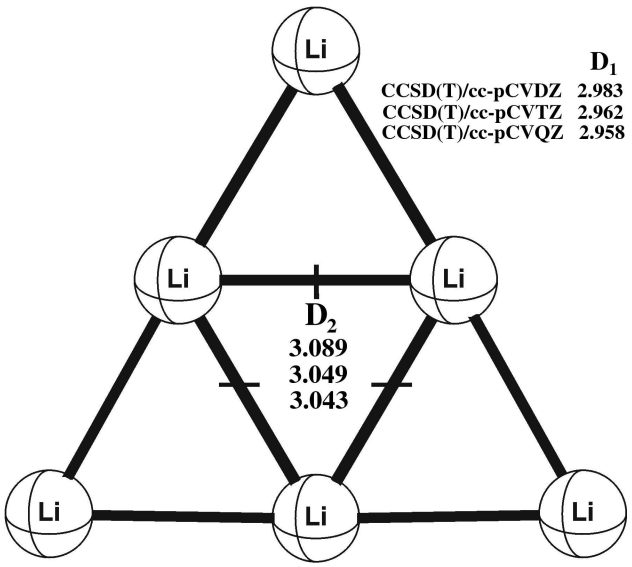

Figure 8: D_{3h} isomer of Li_6

Table 9: Comparison of different methods from previous literature

Method	Relative Energy (kcal mol^{-1})		
	D_{4h}/C_{2v}	C_{5v}	D_{3h}
HF/MB[a,b]	5.40	4.32	0.00
HF/6-311G*[d]	0.00	2.62	1.31
MRD-CI/MB[a,b]	1.74	0.00	0.30
MRD-CI-Dav/MB[a,b,c]	2.10	0.00	0.24
QCISD/6-311G*[d]	0.00	3.82	2.81
B3LYP/6-311G*[d]	0.00	3.72	5.32
MP2/6-311G*[d]	0.00	5.03	7.66

[a] Minimal basis - see Reference [72] for details. [b] Calculated from binding energies provided in Reference [72]. [c] MRD-CI with Davidson correction - see Reference [72] for details. [d] See Reference [59].

upon going from the cc-pCVTZ to the cc-pCVQZ basis. Binding energies also appear well-converged at the CCSD(T)/cc-pCVQZ level, which predicts 123.24 kcal mol^{-1} (total) and 20.54 kcal mol^{-1} (per atom). (Table 10 also includes total energies for easier reproducibility for our theoretical results.)

We can guage the level of oblateness in the D_{4h} isomer by taking the ratio of its rotational constant with respect to the compressed axis (0.097 cm^{-1}) with that along the uncompressed axes (0.152 cm^{-1}). While this ratio should be 1.00 for an octahedron, the value for our D_{4h}

Table 10: Singlet state isomers of Li_6

Level of theory	Energy (a.u.)	Bond Length (Å)		ZPVE[a]	Binding Energy[a]		Relative Energy[a,b]
		D_1	D_2		Total	Per Atom	
D_{4h}							
CCSD(T)/cc-pVDZ	-44.778989	2.730	2.879	3.60	114.94	19.16	0.00(0.00)
CCSD(T)/cc-pVTZ	-44.878263	2.600	2.798	3.85	126.67	21.11	0.00(0.00)
CCSD(T)/cc-pVQZ	-44.917279	2.567	2.732		137.00	22.83	0.00(0.00)
CCSD(T)/cc-pCVDZ	-44.983317	2.699	2.848	3.71	117.45	19.58	0.00(0.00)
CCSD(T)/cc-pCVTZ	-45.040081	2.644	2.819		122.11	20.35	0.00(0.00)
CCSD(T)/cc-pCVQZ	-45.054531	2.637	2.813		123.24	20.54	0.00(0.00)
C_{5v}							
CCSD(T)/cc-pVDZ	-44.772879	2.898	3.169	3.18	111.10	18.52	3.83(3.42)
CCSD(T)/cc-pVTZ	-44.867203	2.819	3.095	3.19	119.73	19.96	6.94(6.27)
CCSD(T)/cc-pCVDZ	-44.976566	2.865	3.148	3.23	113.21	18.87	4.24(3.75)
CCSD(T)/cc-pCVTZ	-45.031248	2.838	3.117		116.57	19.43	5.54(5.06)
CCSD(T)/cc-pCVQZ	-45.045571	2.834	3.113		117.62	19.60	5.62(5.14)
D_{3h}							
CCSD(T)/cc-pVDZ	-44.770865	3.016	3.130	3.16	109.84	18.31	5.10(4.66)
CCSD(T)/cc-pVTZ	-44.863290	2.950	3.029	3.20	117.28	19.55	9.40(8.75)
CCSD(T)/cc-pCVDZ	-44.974510	2.983	3.089	3.21	111.92	18.65	5.53(5.03)
CCSD(T)/cc-pCVTZ	-45.028196	2.962	3.049		114.65	19.11	7.46(7.96)
CCSD(T)/cc-pCVQZ	-45.042434	2.958	3.043		115.65	19.28	7.59(7.09)

[a] In kcal mol^{-1}. [b] ZPVE corrected results given in parenthesis.

isomer at the CCSD(T)/cc-pCVQZ level is 1.567. The energetic advantage of this distortion away from O_h symmetry is assessed by comparing the energy of a cluster constrained to be perfectly octahedral with that allowed to relax into a D_{4h} minimum. Accordingly, at the CCSD(T)/cc-pCVDZ level of theory, we find that a cluster constrained to an O_h symmetry is 12.4 kcal mol^{-1} higher in energy than that allowed to distort to D_{4h} symmetry.

3.3.3.2 C_{5v} Isomer

The C_{5v} structure has a pentagonal pyramidal shape with a short C_5 axis. The distance between the base of the pentagon and the out-of-plane lithium atom is small (∼1.0 Å), indicating the quasiplanar nature of this isomer. There is a very small energy separation [1.95 kcal mol^{-1} at the CCSD(T)/cc-pCVQZ level, with CCSD(T)/cc-pCVDZ ZPVE correction] between the quasiplanar C_{5v} isomer and the planar D_{3h} structure, the C_{5v} isomer being more stable.

The geometric parameters reported for this isomer are the distance between any atom

in the pentagonal base and the out-of-plane lithium atom, designated as D_1, and the other bond between any two adjacent lithium atoms on the pentagonal base, designated as D_2. Our most accurate predictions at the CCSD(T)/cc-pCVQZ level of theory are D_1=2.833 Å and D_2=3.113 Å. The total and per-atom binding energies at this level are 117.62 kcal mol^{-1} and 19.60 kcal mol^{-1}, respectively, and this isomer lies 5.14 kcal mol^{-1} above the D_{4h} isomer after ZPVE correction. The rotational constant with respect to the two equivalent axes on the pentagonal base are 0.131 cm^{-1}, in contrast to 0.069 cm^{-1} along the short C_5 axis.

3.3.3.3 D_{3h} Isomer

Hexamers composed of larger atoms, notably Na_6[53, 90, 55, 102], Cu_6[85, 88, 89], Ag_6[85], and Au_6[86], have been found to have planar D_{3h}-type structures as their most stable form, and the case of the lithium hexamer is considered peculiar for that reason. The main reason why the D_{3h} isomer is energetically favorable in hexamers of larger atoms as opposed to the case of lithium hexamers is under investigation.

The D_{3h} isomer is not perfectly triangular as the inner triangular structure exhibits a slightly different three-center bonding than do the outer bonds. As a result, the outer bonds, designated as D_1, are slightly smaller than the inner three-center bonds labeled as D_2. Similar geometries have been predicted in previous studies of this isomer[54, 59]. Our CCSD(T)/cc-pCVQZ computations give 2.958 Å and 3.043 Å for D_1 and D_2, respectively. The total and per-atom binding energies at this level are 115.65 and 19.28 kcal mol^{-1}, respectively. The corresponding rotational constants are 0.109 cm^{-1} with respect to the two equivalent axes in the plane on the molecule and 0.054 cm^{-1} with respect to the C_3 axis perpendicular to the plane of the molecule.

3.3.3.4 Comparison and Analysis

As noted earlier, the presence of only one valence s electron in alkali metal atoms gives birth to non-directional bonding in clusters. A more in-depth study of bonding in lithium clusters has been performed by Rousseau and co-workers[58, 59], who used density-functional theory (DFT) and electron localization functions (ELF). It was found that electrons in lithium

clusters localize in interstitial regions, leading to multicenter bonding. For smaller clusters, this multicenter bonding leads to "bond alternation" in the range of 2.45 Å- 3.15 Å. The bond alternation occurs between a "short" two-center two-electron (2c-2e) type, characteristic of Li_2, the "long" three-center two-electron (3c-2e) bond prototypical of triangular Li_3^+ and other multicenter n-electron bonds. The "short" bond has a length that ranges from 2.45 Å to 2.85 Å while the "long" three/four-center type of bond has a length of 2.85-3.15 Å[59, 58]. As shown in Table 10, the D_{4h} isomer exhibits a short axial bond (2.637 Å) and long axial-to-equatorial bonds (2.813 Å) at the most complete level of theory. The C_{5v} structure exhibits long bonds (3.113 Å) between adjacent atoms in the pentagonal base and intermediate bond lengths (2.834 Å) between the cap and the pentagonal base. The D_{3h} structure exhibits only the three-center two-electron bonding with Li-Li bond lengths of 2.958-3.043 Å.

The stability of the clusters can be studied by examining the binding energies (atomization energies) as well as the relative energies of the different isomers with respect to the most energetically favorable isomer, D_{4h}. As shown in Table 10, the binding energy per atom at the CCSD(T)/cc-pCVQZ level is 20.54 kcal mol^{-1} (0.89 eV), 19.60 kcal mol^{-1} (0.85 eV) and 19.28 kcal mol^{-1} (0.84 eV) for the D_{4h}, C_{5v}, and D_{3h} isomers, respectively. Relative to the D_{4h} isomer, the C_{5v} and D_{3h} isomers lie 5.14 kcal mol^{-1} and 7.09 kcal mol^{-1} higher in energy, respectively, after ZPVE correction. This level of theory should be sufficient to predict these energies very accurately. Based on the observed convergence of results and the typical reliability of the methods employed, we expect errors within ± 0.5 kcal mol^{-1} for relative energies and ± 0.1 eV for binding energies. Thus we expect that the present results are sufficiently accurate to definitively determine the energetic ordering of the three isomers. However, it is also interesting to compare our predictions to the available experimental data. Bréchignac et al.[65] have combined their experimental ionization potential of Li_6 [IP(Li_6)] and Li [IP(Li)][103], with the binding energy of Li_6^+ [$E_b(Li_n^+)$], determined using unimolecular dissociation of ionized clusters to give an experimental atomization energy of 0.88 eV for Li_6:

$$E_b(\mathrm{Li}_6) = E_b(\mathrm{Li}_6^+) + IP(\mathrm{Li}_6) - IP(\mathrm{Li}). \tag{76}$$

The binding energy of 0.89 eV we predicted for the D_{4h} isomer agrees with the experimental value best, but given our estimated error bars of about ± 0.1 eV and those entailed in the indirect determination of the experimental atomization energy, the comparison is inconclusive.

Rousseau[58] has suggested that the D_{4h} isomer is more stable because the axial lithium atoms contain two orthogonal p orbitals which can produce π-type interactions. Looking at the plots of the valence orbitals for these isomers in Figures 9-11 elucidates some of the predicted structural features.

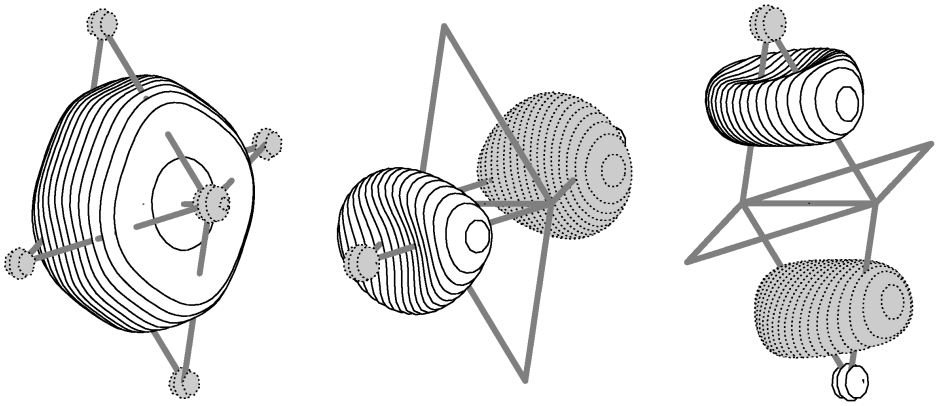

Figure 9: HOMO-2, HOMO-1, and HOMO for D_{4h} isomer of Li_6

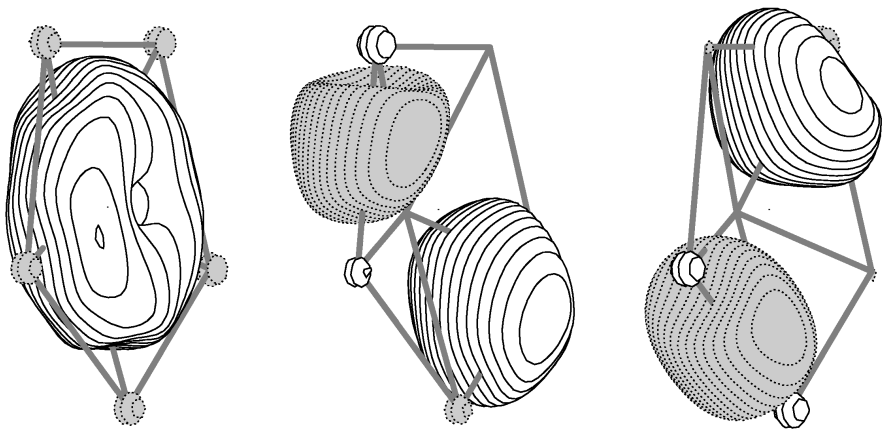

Figure 10: HOMO-2, HOMO-1, and HOMO for C_{5v} isomer of Li_6

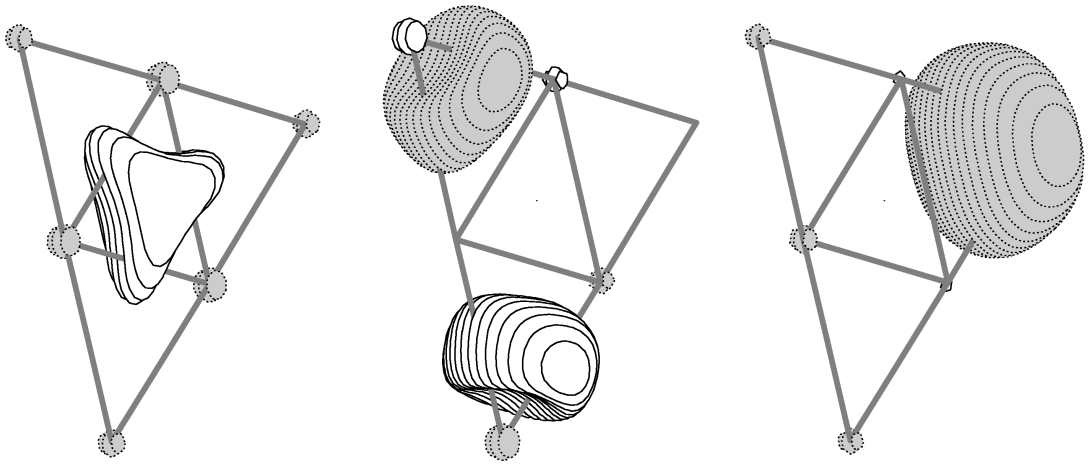

Figure 11: HOMO-2, HOMO-1, and HOMO for D_{3h} isomer of Li_6

As shown in Figure 9, the HOMO-2 orbital for the D_{4h} isomer has most of its electron density along the compressed axis and the HOMO-1 and HOMO orbitals effectively contribute to give the compressed bond a conventional "triple bond" character. Equally insightful are the valence orbital plots for the other two isomers, where we see the localization of most of the valence electron density over the interstitial regions. The similarity in the electron density of the D_{3h} and C_{5v} isomers can explain previous studies[52] which suggested that while there is a small energy barrier separating the non-planar D_{4h} isomer from the D_{3h} isomer, the quasiplanar C_{5v} converts to the D_{3h} structure without a barrier by displacing its out-of-plane atom into the pentagonal base. The energy difference between the D_{3h} and C_{5v} isomers is only 1.95 kcal mol^{-1}.

While there are no direct experimental determination of geometrical parameters like bond lengths and angles for comparison with our theoretical values, optical absorption spectra[54, 52] combined with *ab initio* vertical excitation spectra can yield qualitative understanding of the structure of these clusters. Depletion spectroscopy in the range of 400-700 nm has been used to produce the spectrum given in Figure 12.

It is dominated by two features, namely a small peak at 1.8 eV and a more intense peak at 2.5 eV. The clusters produced in these experiments undergo cooling coexpansions in vacuum with 1-5 bars of argon gas, achieving low internal vibrational tempeatures: 70 K for Li_2, 25 K for Li_3, and much lower temperatures for larger clusters with significantly more degrees

of freedom[54, 52]. Previous investigations[78, 79] on structural changes of lithium clusters due to quantum and thermal fluctuations have concluded that while such fluctuations do lead to the disappearance of bond alternation, they do not lead to isomerization reactions at these temperatures. Therefore, qualitative comparisions between the above-mentioned optical absorption spectra and calculated vertical excitation spectra from static *ab initio* techniques are justified.

To investigate which isomer gives an electronic spectrum containing similar features, we calculated vertical electronic excitation energies and oscillator strengths for each isomer at the EOM-CCSD/cc-pCVDZ level of theory. The results are displayed in Figure 13, in which the lines have been broadened artificially using Lorentzian functions centered about intense peaks to simulate a real spectrum and simplify the comparison with the experimental spectrum (no actual computations of linewidths were performed). The figures indicate that, within the errors of the EOM-CCSD (typically ± 0.3 eV for excitation energies), the features in the spectrum of the D_{4h} isomer match the experimental spectra best. The pronounced peaks in the D_{4h} spectrum appear at 1.7 and 2.6 eV, compared to 1.8 and 2.5 eV in the experimental spectrum. In contrast, the C_{5v} spectrum has only one sharp peak at 2.2 eV, while the D_{3h} isomer has two small peaks at 1.7 and 1.8 eV and a pronounced one at 2.2 eV. Thus the experimental spectrum appears to match best the computed spectrum of the D_{4h} isomer, consistent with our very accurate results for the energetics which demonstrate that this isomer is the most stable and should be the most heavily populated at the low temperatures of the experiment[54]. However, we can not rule out the possibility that other isomers contributed to the observed optical absorption spectrum. We note that previous computations of the absorption spectrum using the MR-CISD method provided similar results[54, 52], although those computations yielded additional peaks which have very small oscillator strengths according to our computations.

If we compare the previous, lower-level theoretical results in Table 9 to our present high-level results, we see that all of the minimal basis set results, even those with extensive electron correlation, predict the wrong energetic ordering of the isomers. As for the 6-311G* predictions of Rousseau and Marx[59], Hartree-Fock and QCISD give the wrong energetic

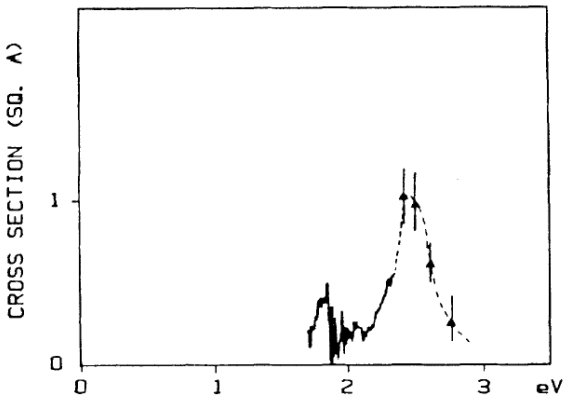

Figure 12: Optical absorption spectrum of Li_6 (References [54, 52]) with peaks at 1.8 and 2.5 eV. Reprinted figure with permission from Dugourd, *et al.*, Phys. Rev. Lett. **67**, 2638 (1991). Copyright 1991 by the American Physical Society.

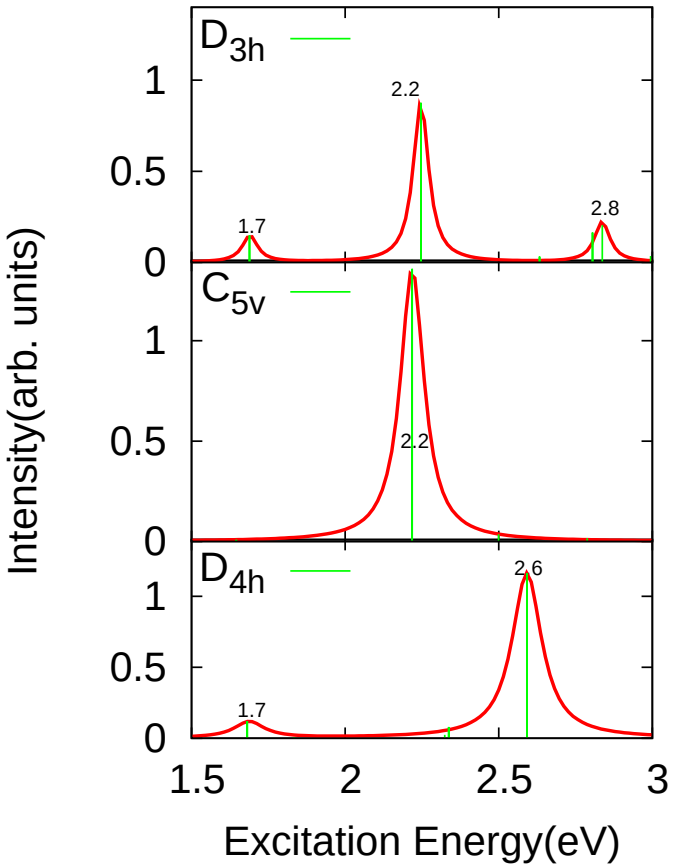

Figure 13: Calculated vertical absorption spectra for three isomers of Li_6 (lines broadened artificially to facilitate comparison)

ordering, while B3LYP and MP2 give the correct energetic ordering of the isomers. The MP2/6-311G* relative energies are quite close (within 0.7 kcal mol^{-1}) to the best present coupled-cluster results. Given the significant correlation and basis set dependence of the energetics (as seen in Tables 8 and 10), this agreement is clearly fortuitous. In general, the QCISD/6-311G* geometries reported by Rousseau[59] compare favorably with the present CCSD(T)/cc-pCVQZ geometries, which usually exhibit slightly longer (ca. 0.02-0.03 Å) bonds. The greatest difference is seen for the C_{5v} isomer, where the QCISD/6-311G* bond lengths (D_1=2.867 Å, D_2=3.151 Å) differ significantly from those at the more complete CCSD(T)/cc-pCVQZ level (D_1=2.834 Å, D_2=3.113 Å).

3.3.4 Higher-Spin States

Although it is understood that the ground state of Li_6 is a singlet, we investigated the possible presence of low-lying minima with higher spin multiplicities. We attempted first to locate higher-spin states with the same point group symmetries observed for the ground state minima: D_{4h}, C_{5v}, and D_{3h}. Table 11 summarizes the results. Vibrational frequency analysis indicates that none of the stationary points obtained for these higher-spin states are potential energy minima; in each case, the number of imaginary vibrational frequencies (the Hessian index) is at least one, indicating a saddle point on the potential energy surface. Although we attempted to follow the imaginary frequency modes downhill to locate true minima, the high-spin computations in lower symmetries were plagued with convergence difficulties; as these states were not of prime interest for our current purposes, we did not pursue optimization further except for a triplet state discussed below.

Several of the stationary points in Table 11 are fairly close in energy to the singlet states. For the D_{4h} configuration, the next triplet state is 8 kcal mol^{-1} higher in energy at the CCSD(T)/cc-pCVDZ level of theory. The lowest triplet surface remains within 20 and 27 kcal mol^{-1} for the C_{5v} and D_{3h} configurations, respectively, at this level. Quintet states are somewhat higher in energy (27-51 kcal mol^{-1}), and septets are higher still. As indicated in the table, the geometrical parameters for these higher-spin stationary points can change substantially (e.g., by 2.057 Å for D_1 in the D_{4h} triplet). Unfortunately, our

Table 11: Higher-spin states of the neutral Li_6

Level of theory	2S+1	Energy(a.u.)	Bond Length(Å)		ZPVE[a]	Relative Energy[a,b]	Hessian Index[c] (Imag. Freqs.)
			D_1	D_2			
D_{4h}							
CCSD(T)/cc-pCVDZ	1	-44.983317	2.699	2.848	3.71	0.00	0
CCSD(T)/cc-pCVDZ	3	-44.971288	4.756	2.893	3.05	7.55	2(117,117)
CCSD(T)/cc-pCVDZ	5	-44.939902	3.996	2.951	3.16	27.24	3(365,217,217)
C_{5v}							
CCSD(T)/cc-pCVDZ	1	-44.976566	2.865	3.148	3.23	0.00	0
CCSD(T)/cc-pCVDZ	3	-44.946166	3.055	2.920	3.00	19.62	2(99,99)
CCSD(T)/cc-pCVDZ	5	-44.921427	3.130	2.933	2.66	34.60	8[d]
D_{3h}							
CCSD(T)/cc-pCVDZ	1	-44.974510	2.983	3.089	3.21	0.00	0
CCSD(T)/cc-pCVDZ	3	-44.931200	3.096	2.957	2.56	27.18	2(761,88)
CCSD(T)/cc-pCVDZ	5	-44.893733	3.048	2.778	3.20	50.69	2(46,46)
C_{2v} Minimum							
CCSD(T)/cc-pCVDZ	3	-44.975617	2.957	2.929-3.023	3.73	4.83	0

[a] In kcal mol^{-1}. [b] Energy relative to the singlet state with the same point-group symmetry at the same level of theory (neglecting ZPVE). [c] Number of imaginary frequencies, with the magnitude of those frequencies (cm^{-1}) in parentheses. [d] Imaginary frequencies not listed.

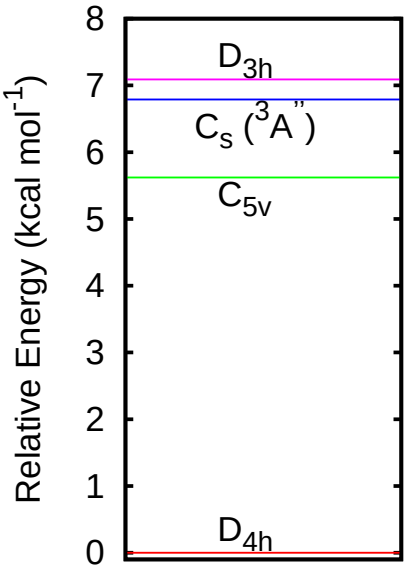

Figure 14: Relative energy scale for isomers of Li_6

limited investigations of lower-symmetry geometries for these higher spin states yielded only a $^3B_1$ minimum structure of C_{2v} symmetry. This triplet was also predicted by Boustani *et al.* [72] who used SCF and MRD-CI methods with 6-31G basis to locate this structure and characterize it as a minimum using normal mode analysis. The geometric parameters for this triplet state are given in Figure 15.

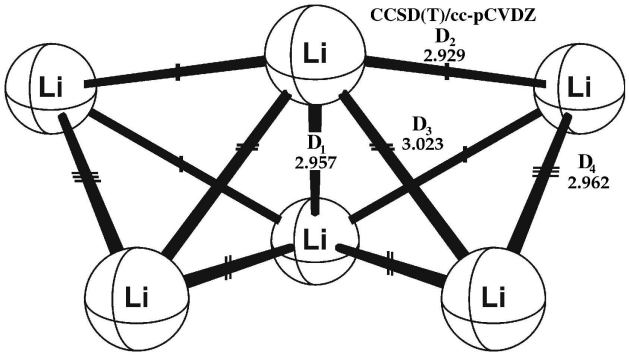

Figure 15: The structure of $^3B_1$ state of Li_6 (C_{2v} symmetry)

Compared to the singlet D_{4h} isomer, the C_{2v} triplet has a significantly longer axial bond length of 2.957 Å, and the bonds extending from the atoms on the axis to those on the central plane are also considerably longer (2.929-3.023 Å) than the 2.848 Å predicted for the D_{4h} singlet at the CCSD(T)/cc-pCVDZ level. This C_{2v} triplet is only 4.83 and 0.60 kcal mol^{-1} above the D_{4h} and C_{5v} singlet isomers, respectively, and 0.69 kcal mol^{-1} below the singlet D_{3h} isomer at the CCSD(T)/cc-pCVDZ level. Boustani *et al.*[72] also found triplet structures of C_{5v} ($^3E_1$) and D_{3h} ($^3E'$) symmetries lying only 4-5 kcal mol^{-1} above the singlets using the SCF and MRD-CI methods with minimal basis set, but normal mode analysis was not done to confirm if they were actual minima.

3.3.5 Li_6^+

Unlike the neutral hexamer, only one structure has been reported for the cation. Minimal basis set SCF and MRD-CI computations by Boustani *et al.*[72] found a D_{2h} structure with binding energies per atom of 12.24 kcal mol^{-1} (SCF) and 19.41 kcal mol^{-1} (Davidson-corrected MRD-CI). Our CCSD(T)/cc-pCVDZ indicate a less symmetric structure with C_{2v} symmetry. Figure 16 and Table 12 describe the geometric parameters and properties of Li_6^+.

The structure is perhaps best thought of as a distortion which eliminates the C_4 axis of the the axially-compressed D_{4h} isomer of the neutral. The axial bond is shortened by a modest amount, 0.079 Å at the CCSD(T)/cc-pCVDZ level, while the other bonds change dramatically as a result of the ionization: bonds extending from the axial atoms to the atoms

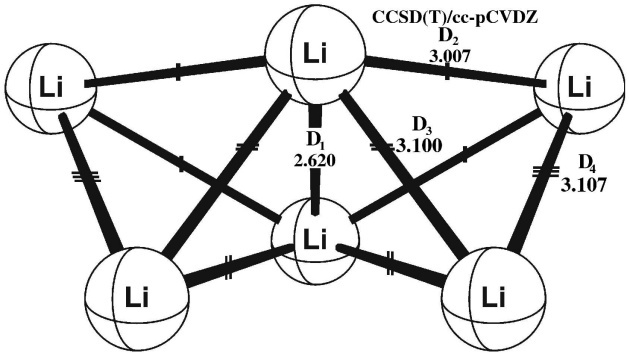

Figure 16: The structure of Li_6^+ (C_{2v} symmetry)

Table 12: Geometries and properties of Li_6^+ and Li_6^-

Molecule/Symmetry	Level of Theory	Energy(a.u.)	Binding Energy[a]		ZPVE[a]
			Total	Per Atom	
Li_6^+/C_s	CCSD(T)/cc-pCVDZ	-44.826482	142.55	23.76	3.60
Li_6^-/D_{4h}	CCSD(T)/cc-pCVDZ	-45.015643	126.81	21.14	3.73
Li_6^-/D_{4h}	CCSD(T)/cc-pCVDZ+diff[b]	-45.016307	124.14	20.69	3.73

[a] In kcal mol^{-1}. [b] cc-pCVDZ with s and p diffuse functions from 6-311++G** basis.

in the central plane change from ∼2.8 Å for Li_6 to ∼3.0-3.1 Å for Li_6^+. The distortion is a manifestation of the Jahn-Teller effect; in the D_{4h} geometry, Li_6^+ contains doubly degenerate HOMO orbitals which are not both doubly occupied, and the energy may be lowered by a distortion of the structure which breaks that degeneracy. We note that the cation is more stable to atomization (to 5 Li + Li^+) than any of the neutral isomers (to 6 Li). Its atomization energy of 1.03 eV (23.76 kcal mol^{-1}) agrees well with the experimental value of 1.08 eV found by Bréchignac et al[65].

The adiabatic ionization energies at the CCSD(T)/cc-pCVDZ level are 4.27, 4.08 and 4.03 eV for the D_{4h}, C_{5v} and D_{3h} isomers, respectively. Experimental ionization potential (IP) for Li_6[103, 104, 64] have been determined by linear extrapolation of photoionization efficiency curves, yielding an IP that is lies between the adiabatic and vertical limits. Nevertheless, the experimental IP of 4.20 eV compares favorably with the calculated adiabatic IP for the D_{4h} isomer, even though the estimated error of ±0.1 eV in our values, as well as the absence of pure adiabatic IP from experiment, makes the comparison less robust.

3.3.6 Li_6^-

The anion, like the cation, has not been studied extensively. Minimal basis SCF and MRD-CI computations indicate a single structure of D_{4h} symmetry[72]. Our CCSD(T)/cc-pCVDZ computations also yield a D_{4h} structure. Figure 17 and Table 12 present our results for the geometry and energetics of Li_6^-. As mentioned previously, diffuse functions can be critical for anions, and so we have compared results with the cc-pCVDZ basis to the cc-pCVDZ+diff basis described above. In this case, geometries and binding energies do not change dramatically upon the addition of diffuse functions.

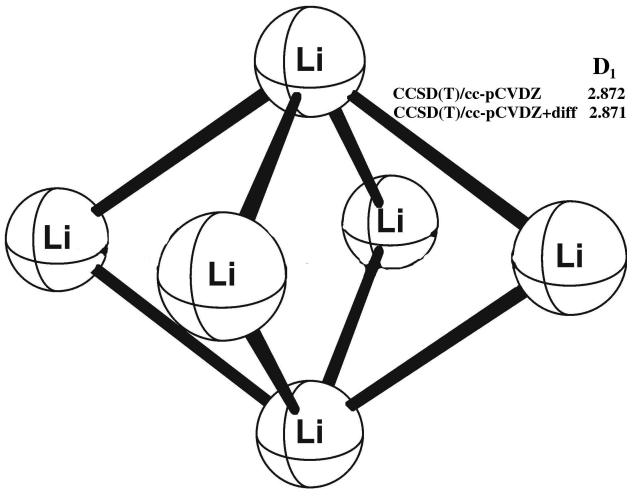

Figure 17: The structure of Li_6^- (D_{4h} symmetry)

Relative to the D_{4h} isomer of the neutral Li_6, the anion is less oblate; the ratio of its rotational constant with respect to the nondegenerate axis (0.108 cm^{-1}) to the degenerate axes (0.146 cm^{-1}) is only 1.352 at the CCSD(T)/cc-pCVDZ+diff level of theory, compared to a CCSD(T)/cc-pCVDZ value of 1.542 for the neutral cluster. The axial bond length is significantly larger (3.259 Å vs. 2.699 Å) compared to the neutral cluster. On the other hand, the bonds extending from from the axial atoms to the equatorial atoms change very sightly from the neutral D_{4h} structure — from 2.813 Å for Li_6 to 2.872 Å for Li_6^-. The anionic cluster is more stable against dissociation (to 5 Li + Li^-) than the neutral cluster (to 6 Li), by a difference of 6.69 kcal mol^{-1} using the CCSD(T)/cc-pCVDZ+diff binding energy for Li_6^-. The adiabatic electron affinities for the D_{4h}, C_{5v}, and D_{3h} structures of

Li_6 are estimated as 0.89, 1.07, and 1.13 eV at the CCSD(T)/cc-pCVDZ+diff level without ZPVE correction.

3.4 Conclusions

The Li_6^+, Li_6^- clusters and three isomers of Li_6 have been studied using CCSD(T) with large basis sets and their optimum geometries and energetics have been reported. For the neutral cluster, the D_{4h} isomer is the most stable structure with a total atomization energy of 123.24 kcal mol^{-1}, as compared to 117.62 kcal mol^{-1} and 115.65 kcal mol^{-1} for the C_{5v} and D_{3h} isomers, respectively. This contrasts with other metal hexamers such as Na_6 and Au_6 which are thought to have a D_{3h} global minimum. Spectral features from an experimental optical absorption spectra of Li_6 compare well with those from our EOM-CCSD vertical excitation spectra for the D_{4h} isomer, but not as well for the D_{3h} and C_{5v} isomers. There exist some low-lying states of higher spin multiplicity but none have a minimum structure of D_{4v}, C_{5v} or D_{3h} symmetry. A $^3B_1$ minimum of C_{2v} symmetry was found, lying 0.7 kcal mol^{-1} below the D_{3h} singlet minimum. For Li_6^+, the global minimum corresponds to a structure of C_{2v} symmetry, resulting from a stabilizing Jahn-Teller distortion. Its atomization energy is 142.55 kcal mol^{-1} at the CCSD(T)/cc-pCVDZ level. The anion, Li_6^-, has a D_{4h} structure and a total binding energy of 124.14 kcal mol^{-1} at the CCSD(T)/cc-pCVDZ+diff level of theory. Theoretical predictions for these clusters were found to be sensitive both to the basis set used and to electron correlation, including core correlation. The present, high-accuracy coupled-cluster results should help guide the interpretation of experiments on these clusters, which are at the size where 2D and 3D structures are energetically competitive.

The material of this chapter was published as a paper in the *Journal of Chemical Physics* [105]

CHAPTER IV

HIGH-LEVEL AB INITIO STUDIES OF HYDROGEN ABSTRACTION FROM PROTOTYPE HYDROCARBON SYSTEMS

Symmetric and non-symmetric hydrogen abstraction reactions are studied using state-of-the-art *ab initio* electronic structure methods. Second-order Møller-Plesset perturbation theory (MP2) and the coupled-cluster singles, doubles and perturbative triples [CCSD(T)] methods with large correlation consistent basis sets (cc-pVXZ, where X = D,T,Q) are used in determining the transition-state geometries, activation barriers, and thermodynamic properties of several representative hydrogen abstraction reactions. The importance of basis set, electron correlation, and choice of zeroth-order reference wavefunction in the accurate prediction of activation barriers and reaction enthalpies are also investigated. The ethynyl radical (·CCH), which has a very high affinity for hydrogen atoms, is studied as a prototype hydrogen abstraction agent. Our high-level quantum mechanical computations indicate that hydrogen abstraction using the ethynyl radical has an activation energy of less than 3 kcal mol^{-1} for hydrogens bonded to an sp^2 or sp^3 carbon. These low activation barriers further corroborate previous studies suggesting that ethynyl-type radicals would make good tooltips for abstracting hydrogens from diamondoid surfaces during mechanosynthesis. Modeling the diamond C(111) surface with isobutane and treating the ethynyl radical as a tooltip, hydrogen abstraction in this reaction is predicted to be barrierless.[1]

4.1 Introduction

Hydrogen transfer and abstraction reactions are ubiquitous, occurring in such diverse environments as enzymatic reactions[106], DNA strand breaking[107], catalysis[108], and all facets of organic chemistry. They also play a critical role in the making of diamond films via low-pressure chemical vapor deposition [109] (CVD). The artificial synthesis of diamond, whether by CVD or other techniques such as high-temperature high-pressure [110]

[1]Previously published as B. Temelso, C. D. Sherrill, R. C. Merkle, and R. A. Freitas Jr. J. Phys. Chem. A 110 (2006) 11160.

(HTHP) crystallization of metal-solvated carbon, has attracted increasing interest in recent years. It is hoped that more economical ways to obtain diamond may unlock its scientific and technological potential, as it has many possible applications resulting from its unparalleled hardness, thermal and electrical conductivity, transparency in large regions of the electromagnetic spectrum, and wide band gap. In the CVD synthesis of diamond, a precursor hydrocarbon gas like methane enters a plasma/thermal/electric activation chamber in excess hydrogen gas. The activation process leads to the formation of atomic hydrogen, which abstracts hydrogen from the gas-phase hydrocarbons to yield very reactive carbon-containing radicals. These radicals deposit on the substrate and form carbon-carbon bonds leading to diamond growth. Atomic hydrogens also abstract hydrogen from the diamond surface, thereby creating nucleation sites for further diamond growth. They promote the preferential growth of diamond over graphite by etching graphite at a higher rate than diamond. This process, however, is guided by random diffusion of hydrocarbon radicals onto a substrate and subsequent hydrogen abstraction and donation reactions. The randomness in diamond CVD leads to the introduction of impurities and crystal lattice deformities that degrade the quality of the diamond films.

Some shortcomings of CVD have prompted the discussion of new approaches for diamond synthesis which might provide more control over the deposition of carbon-rich precursor molecules as well as the hydrogen abstraction/donation reactions. Mechanosynthesis is one new paradigm which proposes to attach a molecular tooltip to a scanning probe microscope (SPM) to perform elementary synthetic operations such as carbon deposition or hydrogen abstraction/donation at a specific location on the substrate [111, 112, 113, 114, 115, 116, 117, 118, 119, 120]. Such an approach has already been demonstrated theoretically and experimentally for the abstraction of hydrogen from a Si(100) surface and the selective manipulation of silicon atoms[121]. Ethynyl radical has been suggested as a hydrogen abstraction tool because it can easily and rapidly abstract hydrogens from most hydrocarbons [122, 111, 123, 124]. To explore the feasibility of mechanosynthesis of diamond, an understanding of the thermochemistry and kinetics involved in the elementary processes becomes imperative, and modern theoretical methods are very useful in this endeavor.

Quantum chemical methods are capable of providing very accurate estimates of reaction thermodynamics. Indeed, the so-called Gaussian-1 (G1)[125], Gaussian-2 (G2)[126, 127] and Gaussian-3 (G3)[128, 129, 130] composite methods and their variants are capable of providing reaction enthalpies typically within 1-2 kcal mol^{-1} of experiment. These Gn approaches combine a series of lower-level quantum computations to estimate the result of high-level correlated computations; the final values are then adjusted by additional empirical corrections. The similar Weizmann-1 (W1) and Weizmann-2 (W2) theories [131] achieve comparable accuracies with only one molecule-independent empirical parameter, while the newer W3 formalism promises to provide accuracies in the order of 0.2 kcal mol^{-1} at a reasonable computational cost for small systems[132]. Alternatively, the recent HEAT (high accuracy extrapolated *ab initio* thermochemistry) [133] method provides similar accuracy in several test cases while avoiding any empirical corrections. Although these theoretical approaches are rather expensive computationally and applicable only to small molecular systems, they demonstrate that truly high-quality energetics are possible using modern *ab initio* methods.

Several theoretical studies have examined hydrogen transfer reactions between small alkanes. Truhlar and co-workers have presented a comprehensive study of bond energies and classical activation barriers using semi-classical and semi-empirical methods[134]. In other work considering purely *ab initio* methods, they examined the challenges presented by radical-molecule reactions due to spin contamination and electron correlation in different methods[135]. Litwinowicz *et al.*[136] evaluated the role of tunneling in simple hydrogen transfer reactions and also used spin projection techniques to remove spin contaminants and compare the resulting activation barriers with experimental values. Skokov and Wheeler and co-workers[137] performed a similar study using density functional theory (DFT). Significant work to reconcile experimentally observed rates[138, 139] with theoretical values for the reactions of ethynyl radical with other small molecules has been done by Nguyen and co-workers [140, 141, 142].

While numerous experimental and theoretical databases exist for the computation of heats of formation of simple hydrogen abstraction reactions, systematic and comprehensive

high-accuracy studies of the reaction *barriers* (especially for reactions involving the ethynyl radical) are rare. Hence, a goal of the present work is to provide reliable benchmark activation barriers for such reactions. Here we consider several hydrogen abstraction reactions for simple hydrocarbons, focusing primarily on the ethynyl radical as the abstraction agent. Of particular interest is the reaction in which ethynyl radical abstracts hydrogen from isobutane, which serves as a good model[143] of the diamond(111) surface. This model may shed light on the thermodynamic and kinetic feasibility of the hydrogen abstraction step in the mechanosynthesis of diamond[144, 145, 116, 117, 118, 119].

4.2 Theoretical Methodology

The symmetric hydrogen abstraction/transfer reactions considered in this study are given in reactions (77)-(79), along with the point-group symmetry considered for the reaction (and the corresponding Abelian computational subgroup).

$$\mathrm{H}\cdot + \mathrm{H_2} \rightarrow \mathrm{H_2} + \cdot\mathrm{H} \qquad D_{\infty h}/D_{2h} \tag{77}$$

$$\mathrm{CH_3}\cdot + \mathrm{CH_4} \rightarrow \mathrm{CH_4} + \cdot\mathrm{CH_3} \qquad D_{3d}/C_{2h} \tag{78}$$

$$\mathrm{HCC}\cdot + \mathrm{HCCH} \rightarrow \mathrm{HCCH} + \cdot\mathrm{CCH} \qquad D_{\infty h}/D_{2h} \tag{79}$$

The non-symmetric reactions considered are those in (80)-(84).

$$\mathrm{HCC}\cdot + \mathrm{H_2} \rightarrow \mathrm{HCCH} + \cdot\mathrm{H} \qquad C_{\infty v}/C_{2v} \tag{80}$$

$$\mathrm{HCC}\cdot + \mathrm{CH_4} \rightarrow \mathrm{HCCH} + \cdot\mathrm{CH_3} \qquad C_{3v}/C_s \tag{81}$$

$$\mathrm{HCC}\cdot + \mathrm{C_2H_4} \rightarrow \mathrm{HCCH} + \cdot\mathrm{C_2H_3} \qquad C_s/C_s \tag{82}$$

$$\mathrm{HCC}\cdot + \mathrm{HC(CH_3)_3} \rightarrow \mathrm{HCCH} + \cdot\mathrm{C(CH_3)_3} \qquad C_{3v}/C_s \tag{83}$$

$$\mathrm{HCC}\cdot + \mathrm{C_6H_6} \rightarrow \mathrm{HCCH} + \cdot\mathrm{C_6H_5} \qquad C_{2v}/C_{2v} \tag{84}$$

These systems are studied using Dunning's correlation consistent basis sets (cc-pVXZ, X=D,T,Q)[13, 16], which provide a systematic convergence of energies and properties toward the complete basis set (CBS) limit. For the sake of brevity, we will occasionally refer to these basis sets simply as DZ, TZ, and QZ in the tables. Electron correlation is accounted for using second-order Møller-Plesset perturbation theory (MP2) and coupled-cluster theory with single, double, and perturbative triple substitutions [CCSD(T)][146].

In order to gauge the reliability of density-functional methods for hydrogen abstraction reactions, we also employed the B3LYP [147] and BHLYP [148] (also called BH&HLYP) functionals as implemented in MOLPRO[92]. As discussed below, we found that the B3LYP/cc-pVDZ level of theory incorrectly predicts a bent geometry for the ground state of the ethynyl radical (although this is corrected with the larger cc-pVTZ basis) and it also gives unusually low barriers to the hydrogen abstraction reactions studied. Similar problems have also been observed for larger alkylethynyl radicals, but the use of hybrid functionals containing more Hartree-Fock (HF) exchange gives linear geometries for these radicals and more accurate abstraction barriers[149, 150]. One such functional is BHLYP[148], which uses 50% Hartree-Fock exchange (compared to 20% in B3LYP) and 50% Becke88 exchange [151] in conjunction with the LYP correlation functional[152]. (Of the many other exchange-correlation functionals designed to predict improved hydrogen abstraction barriers, the MPW1K[153] functional has had some success[140].)

For open-shell systems, we have considered both unrestricted and restricted open-shell orbitals. We will denote computations using unrestricted orbitals with a 'U' prefix, and those using restricted orbitals with an 'R' prefix (e.g., UMP2 or RMP2). Unrestricted orbitals are frequently easier to converge, and the extra flexibility they provide often improves results for bond-breaking and bond-making reactions when electronic near-degeneracy effects are strong. On the other hand, unrestricted orbitals can lead to poorer results in less severe cases of electronic near-degeneracies (e.g., in the spin-recoupling region of unimolecular dissociation reactions)[154, 155, 156, 157]. Additionally, the use of unrestricted orbitals means that the wavefunction is no longer an eigenfunction of the $\hat{S}^2$ operator, and is contaminated by states with higher spin multiplicities. A comparison of restricted and

unrestricted orbitals and a discussion of spin contamination are presented below.

All DFT computations employed the MOLPRO 2002.6 program[92]. UMP2 and UCCSD(T) computations were performed using ACES II[30]. Open-shell RMP2[158] and RCCSD(T)[159, 160] computations using restricted orbitals were performed using MOLPRO. Optimizations, transition state searches, and vibrational frequency analyses were performed using analytic energy gradients as implemented in ACES II. For MOLPRO 2002.6, which generally lacks analytic gradients, energies were differentiated numerically; this numerical differentiation process occasionally caused translational or rotational degrees of freedom to have frequencies deviating slightly from zero (values were real or imaginary and less than 50 cm^{-1} in magnitude). Although tightening the convergence criteria should remove these difficulties in principle, in practice we found that even tight convergence (10^{-12} on energies and 10^{-5} on gradients) had little effect due to limitations in the 2002 version of the program we used. We therefore attempted to identify and suppress these numerical artifacts in our subsequent analysis.

Because electronic near-degeneracies may become important as bonds are formed or broken[161, 162, 163], we performed full configuration interaction (full CI) computations for selected reactions to determine the effect of higher-order electron correlations beyond those included in the CCSD(T) method. For a given basis set, full CI includes a complete treatment of all many-body electron correlation effects, as it yields the exact solution to the time-independent, non-relativistic Schrödinger equation within the space spanned by the one-particle orbital basis set. Full CI computations were performed using the DETCI module[28] of the PSI 3.2 package[29]. The equation-of-motion (EOM) CCSD [164] bending potentials for ethynyl radical were also generated using PSI 3.2[29], while all other EOM-CCSD excitation energies were computed with ACES II[30].

Experimental enthalpies of formation ΔH_f^o(298 K) for our reactants and products are readily available,[165] and they entail relatively small uncertainties. These values have been used to obtain heats of reaction, ΔH(298 K), for the reactions considered. In order to compare more directly with the experimental thermochemical data, we have converted our *ab initio* bare energy differences, ΔE, into 0 K enthalpy differences, ΔH(0 K), by adding

the zero-point vibrational energy correction (ΔZPVE), estimated simply as one-half of the sum of the (unscaled) vibrational frequencies. We also obtain 298 K enthalpy differences, ΔH(298 K), by adding finite temperature corrections using the usual vibrational, rotational, and translational partition functions in conjunction with the harmonic oscillator, rigid rotator, and particle-in-a-box models.

The phenomenological activation barriers, E_a, are determined from experiment by an indirect process in which the reaction rate, k, is obtained at a series of temperatures, T. Fitting the temperature-dependent rate to a simple Arrhenius form, $k(T)$=$Ae^{-E_a/RT}$, the physical activation barrier can be determined. The problem with this approach is that most rate-vs-temperature relations do not fit the Arrhenius form for all temperature regimes due to effects like hydrogen tunneling and the strong temperature dependence of the vibrational partition function when there are low-frequency bending modes, and these phenomena have been observed for most hydrogen abstraction reactions using the ethynyl radical[166]. We used experimental activation barriers obtained from rate-vs-temperature data over a temperature range of about 150 K – 350 K for which the simple Arrhenius form was suitable and for which reaction rates were available[167, 168, 169, 141, 170, 140, 171]. It must be stressed that these experimentally deduced activation barriers depend on the temperature range used for the Arrhenius fit[169], and that this complicates a direct comparison with reaction barriers computed quantum mechanically.

To compare our "classical" activation barriers, $\Delta E^{\ddagger}$ with these experimentally deduced activation energies, E_a, we first add zero-point vibrational corrections and finite-temperature corrections (as discussed above) to obtain $\Delta H^{\ddagger}$(T). Next, it follows from transition state theory [172] that for a reaction which undergoes a change of $\Delta n^{\ddagger}$ in the number of molecules while going from reactants to a transition state, the experimental $E_a(T)$ is related to $\Delta H^{\ddagger}$(T) by

$$E_a(T) = \Delta H^{\ddagger}(T) + (1 - \Delta n^{\ddagger})RT. \tag{85}$$

$\Delta n^{\ddagger}$ for these bimolecular hydrogen abstraction reactions is -1 since the two reactants form one complex in the transition state. One possible cause for a deviation from Arrhenius

behavior is quantum mechanical tunneling of hydrogen atoms through classical barriers. The simplest approach to assess the role of quantum tunneling is the Wigner correction to the reaction rate[173, 174]. Given the magnitude ν_t of the imaginary frequency along the reaction coordinate at the transition state, the rate is enhanced by a factor of

$$K_W(T) = 1 + \frac{1}{24}\left(\frac{h\nu_t}{k_b T}\right)^2. \tag{86}$$

Note that this correction predicts tunneling to be faster through thin barriers (with large ν_t) than through wide barriers (small ν_t), as one would expect. Because we are comparing activation energies rather than rates, we may incorporate this correction into our theoretical results as an effective barrier height lowering by evaluating

$$\Delta E_a = -k_b \frac{dlnK_W}{d(1/T)} = -2k_b T \frac{y(T)}{1+y(T)}, \tag{87}$$

where $y(T) = \frac{1}{24}\left(h\nu_t/k_b T\right)^2$. As discussed below, this correction amounts to a few tenths of one kcal mol^{-1} for the systems studied. Wigner-corrected activation energies will be denoted E_a-W.

4.3 Results and Discussion

4.3.1 Transition State Geometries

Vibrational normal mode analyses were performed to determine whether optimized structures corresponded to minima, transition states, or higher-order saddle points. For simplicity and for easier comparison among different levels of theory, only direct collinear C–H–C reaction coordinates were considered and symmetries were constrained as given in reactions (77)-(84). However, for some reactions at certain levels of theory, the true transition state (having exactly one imaginary vibrational frequency) may occur for lower-symmetry geometries than those considered. Table 13 reports those cases where the nominal (symmetry-constrained) transition states have a Hessian index (number of imaginary vibrational frequencies) greater than one. In these cases, the smaller additional imaginary frequencies correspond primarily to bending motions of the ethynyl radical (in some cases symmetry requires this bend to be doubly-degenerate). The CCH bends may be weakly coupled to rotation-like motions of the other reactant. For example, in the case of HCC· + C_2H_4,

there are actually three extra imaginary frequencies at the RMP2/cc-pVDZ level of theory: one in-plane CCH bend and two out-of-plane vibrations corresponding to symmetric and antisymmetric combinations of the CCH bend coupled with a rotation of C_2H_4 relative to the CCH.

For the reactions HCC· + H_2 → HCCH + ·H and HCC· + HCCH → HCCH + ·CCH, these extra imaginary frequencies appear to be artifactual because they tend to disappear upon using a larger basis set or a more robust level of theory. For reactions of ethynyl with CH_4, C_2H_4, $(CH_3)_3CH$, and C_6H_5, the lower symmetry and/or larger size of the system made it difficult to pursue vibrational frequency analysis with the larger cc-pVTZ basis or the more reliable CCSD(T) method, and we were not always able to obtain these data. In these cases, it is not clear whether the extra imaginary frequencies are artifactual or not. However, given that they may indeed be artifactual, and also to ease comparisons among different levels of theory, we did not pursue computationally expensive transition state searches in lower symmetries, and any extra imaginary frequencies were ignored in subsequent analysis. In cases where the Hessian index was found to be greater than one, this means that our computed classical barrier $\Delta E^{\ddagger}$ will be an upper bound for that level of theory. For the reaction HCC· + H_2 → HCCH + ·H only, at the RMP2/cc-pVDZ level of theory, we followed one of the degenerate 80i frequencies downhill to a bent transition state which lies 0.4 kcal mol^{-1} lower in energy, giving a classical barrier $\Delta E^{\ddagger}$ of 2.8 instead of 3.2 kcal mol^{-1}. We expect that lower-symmetry transition state searches in other cases would yield similarly small energy lowerings but would not significantly affect our analysis (indeed, for our purposes, it would only complicate comparisons between different levels of theory).

Most of the non-symmetric reactions have very small activation barriers and large negative enthalpies of reaction (see below), so Hammond's postulate[175] would suggest an "early" transition state with a geometry similar to that of the reactants. Our theoretical results in Table 14 for the cc-pVDZ basis set support this prediction.

Using the MP2 or CCSD(T) methods, non-symmetric reactions feature a transition state geometry with only a modest (0.03–0.06 Å) stretch in the breaking bond and a fairly

Table 13: Nominal transition states having more than one imaginary vibrational frequency[a]

level of theory	Hessian index	imag. freqs	comment
HCC· + HCCH → HCCH + ·CCH[b]			
RMP2/DZ	3	1640i,59i,59i	basis set effect
RMP2/TZ	1	1659i	
RB3LYP/DZ	3	1293i,88i,88i	
RB3LYP/TZ	3	1428i,56i,56i	
UB3LYP/DZ	3	1205i,35i,35i	
UB3LYP/TZ	3	1342i,12i,12i	
HCC· + H_2 → HCCH + ·H[c]			
RMP2/DZ	3	640i,80i,80i	basis set effect
RMP2/TZ	1	606i	
RCCSD(T)/DZ	3	571i,92i,92i	basis set effect
RCCSD(T)/TZ	1	527i	
UCCSD(T)/DZ	3	587i,68i,68i	basis set effect
UCCSD(T)/TZ	1	540i	
HCC· + CH_4 → HCCH + ·CH_3			
RMP2/DZ	3	257i,63i,63i	
RMP2/TZ	3	224i	
RCCSD(T)/DZ	3	247i,74i,74i	
UMP2/DZ	3	282i,34i,34i	basis set effect
UMP2/TZ	3	257i	
UCCSD(T)/DZ	3	259i,50i,50i	
UBHLYP/DZ	1	96i	
UBHLYP/TZ	1	140i	
HCC· + C_2H_4 → HCCH + ·C_2H_3			
RMP2/DZ	4	281i,143i,51i,20i	
RMP2/TZ	4	251i,105i,72i,36i	
RCCSD(T)/DZ	2	265i,95i,44i	
UMP2/DZ	2	487i,45i	
UCCSD(T)/DZ	2	291i,65i	
HCC· + $HC(CH_3)_3$ → HCCH + ·$C(CH_3)_3$			
RMP2/DZ	3	45i,35i,22i	
UMP2/DZ	3	77i,32i,32i	
HCC· + C_6H_6 → HCCH + ·C_6H_5			
RMP2/DZ	3	190i,113i,45i	
UMP2/DZ	2	241i,62i	

[a]At least in some cases, the additional imaginary frequencies tend to disappear at more reliable levels of theory and are considered artifactual; see text. [b]Only one imaginary frequency for RMP2/TZ, UMP2/DZ, RCCSD(T)/DZ, UCCSD(T)/DZ, RBHLYP/DZ, RBHLYP/TZ, UBHLYP/DZ, and UBHLYP/TZ. [c]Only one imaginary frequency for MP2/TZ, UMP2/DZ, UMP2/TZ, RCCSD(T)/TZ, UCCSD(T)/TZ, RBHLYP/DZ, RBHLYP/TZ, UBHLYP/DZ, UBHLYP/TZ, UBHLYP/QZ.

Table 14: Transition state geometries (Å) of the type R_1–H–R_2, using the cc-pVDZ basis set[a]

	MP2		B3LYP		BHLYP		CCSD(T)	
transition state	R(R_1–H)	R(H–R_2)	R(R_1–H)	R(H–R_2)	R(R_1–H)	R(H–R_2)	R(R_1–H)	R(H–R_2)
				UHF REFERENCE				
H–H–H	0.932	0.932	0.947	0.947	0.939	0.939	0.943	0.943
CH_3–H–CH_3	1.330	1.330	1.350	1.349	1.340	1.341	1.344	1.344
HCC–H–CCH	1.269	1.269	1.282	1.282	1.273	1.273	1.281	1.281
H–H–CCH	0.783	1.740	0.762	2.866	0.767	1.950	0.793	1.722
CH_3–H–CCH	1.135	1.724	1.100	3.504	1.112	1.907	1.148	1.678
C_2H_3–H–CCH	1.152	1.580					1.155	1.610
$(CH_3)_3C$–H–CCH	1.117	2.093					1.117	2.205
C_6H_5–H–CCH	1.145	1.613					1.150	1.625
				ROHF REFERENCE				
H–H–H	0.984	0.886	0.942	0.942	0.930	0.930	0.943	0.943
CH_3–H–CH_3	1.416	1.266	1.347	1.347	1.334	1.334	1.344	1.344
HCC–H–CCH	1.392	1.187	1.280	1.280	1.269	1.269	1.282	1.282
H–H–CCH	0.782	1.760	0.764	2.564	0.777	1.777	0.792	1.729
CH_3–H–CCH	1.128	1.770					1.147	1.684
C_2H_3–H–CCH	1.129	1.713					1.151	1.627
$(CH_3)_3C$–H–CCH	1.112	2.254					1.117	2.235
C_6H_5–H–CCH	1.125	1.736					1.146	1.642

[a]R(R_1–H) and R(H–R_2) bond distances can be compared with R(H–H) $\sim$ 0.74 Å and R(C–H) $\sim$ 1.09 Å for the reactants and products.

long distance (1.6–2.3 Å) for the forming bond. The symmetric reactions, on the other hand, are expected to feature symmetric transition states with equal bond lengths for the forming and breaking bonds. This is what is observed except for the RMP2 method, where non-symmetric transition states are discovered. Figure 22 displays a contour diagram of the potential energy surface for H· + H_2 → H_2 + H· at the RMP2/cc-pVDZ level of theory. The surface features a shallow local minimum at symmetric geometries, with two symmetry-equivalent, non-symmetric transition states on either side. We view this curious result as purely artifactual, and we note that ROHF references have led to other cases of unphysical results in the literature, including the classic example of the allyl radical[176, 177]. The more robust CCSD(T) method yields symmetric transition states for ROHF orbitals.

Except for the anomalous asymmetric transition states predicted by RMP2, the transition state geometries for the symmetric reactions are fairly similar (within 0.02 Å for bonds to the abstracted hydrogen) no matter which theoretical method is used. Computed transition state geometries for the non-symmetric reactions, however, differ significantly depending on the theoretical method and whether restricted or unrestricted orbitals are used,

except for CCSD(T), which is generally insensitive to the choice of orbitals. UB3LYP and RB3LYP, which suffer from significant self-interaction errors at non-equilibrium geometries, yield geometries that greatly differ from the other theoretical estimates. Overall, the results from Table 14 underscore the need to exercise caution in choosing theoretical methods to study bond-breaking reactions, and they indicate that the robust CCSD(T) method appears (not surprisingly) to be the most reliable of those considered here for computing accurate transition state geometries of hydrogen abstraction reactions. Of course even CCSD(T) may break down for more difficult bond-breaking reactions[161], and the effect of electron correlation beyond CCSD(T) is explored below.

4.3.2 Symmetric Reactions

Barrier heights for the symmetric hydrogen transfer reactions are presented in Table 15 for several theoretical methods and basis sets. Basis set effects are fairly small for MP2 and CCSD(T), with barrier heights typically decreasing by a few tenths of one kcal mol^{-1} upon improvement of the basis set. UMP2 results for HCC$\cdot$ + HCCH are out of line with this general trend and show a larger basis set effect of $\sim$ 3 kcal mol^{-1}. Surprisingly, basis set effects in the symmetric reactions are larger for DFT, which is typically rather insensitive to basis set improvements. In contrast to the *ab initio* results, the DFT barriers tend to increase as larger basis sets are used.

Comparing the theoretical methods to each other, we see that UMP2 significantly overestimates barrier heights, and UB3LYP and UBHLYP significantly underestimate them, compared to the more reliable UCCSD(T) results; the differences are several kcal mol^{-1}. The difference among theoretical predictions is particularly surprising for the reaction H_2 + $\cdot$H $\rightarrow$ H$\cdot$ + H_2, given that this is only a three-electron system. Large basis set UCCSD(T) computations should be nearly exact for this problem (see comparison to full CI below), and they yield values for $\Delta E^{\ddagger}$ around 10 kcal mol^{-1}. The UMP2 values, on the other hand, are around 13 kcal mol^{-1}, while UB3LYP/cc-pVQZ and UBHLYP/cc-pVQZ predict a mere 4.1 kcal mol^{-1} and 6.5 kcal mol^{-1}, respectively. New density functionals that are designed to predict better hydrogen abstraction barriers do improve on B3LYP at least. In a study

Table 15: Barrier heights (kcal mol^{-1}) for symmetric reactions using UHF and ROHF references.

	MP2			B3LYP			BHLYP			CCSD(T)			
	DZ	TZ	QZ	DZ	TZ	QZ	DZ	TZ	QZ	DZ	TZ	QZ	Expt.
UHF REFERENCE													
H_2+H→ H+H_2													
$\Delta E^{\ddagger}$	13.3	13.2	13.0	3.0	4.1	4.1	5.5	6.5	6.5	10.3	10.0	9.8	
$\Delta H^{\ddagger}(0)$	12.6	12.5	12.2	2.0	3.1	3.1	4.7	5.6	5.7	9.6	9.3	9.0	
$\Delta H^{\ddagger}(298)$	11.8	11.7	11.4	1.1	2.3	2.3	3.9	4.8	4.8	8.8	8.4	8.2	
$E_a(298)$	13.0	12.8	12.6	2.3	3.5	3.5	5.1	6.0	6.0	10.0	9.6	9.3	9.7[a]
$E_a(298)$-W	12.0	11.9	11.7	2.1	3.0	3.1	4.5	5.4	5.4	9.2	8.8	8.5	9.7[a]
$CH_3\cdot$ + CH_4 →CH_4 + $\cdot CH_3$													
$\Delta E^{\ddagger}$	18.9	18.8		13.7	17.1		17.8	19.5		18.1	17.8		
$\Delta H^{\ddagger}(0)$	18.6	18.4		13.2	16.6		17.4	19.0		17.7	17.4[b]		
$\Delta H^{\ddagger}(298)$	17.9	17.8		12.6	16.1		16.8	18.5		17.1	16.7[b]		
$E_a(298)$	19.1	19.0		13.8	17.3		18.0	19.6		18.2	17.9[b]		14.3[c]
$E_a(298)$-W	18.1	18.0		13.0	16.4		17.0	18.7		17.3	17.0[b]		14.3[c]
$HCC\cdot$ + HCCH → HCCH + $\cdot CCH$													
$\Delta E^{\ddagger}$	20.2	17.0		7.4	11.3		11.8	13.3		13.1	11.7		
$\Delta H^{\ddagger}(0)$	20.2	17.1		5.0	8.2		8.7	10.2		10.5	9.1[b]		
$\Delta H^{\ddagger}(298)$	20.2	17.0		4.8	7.4		8.9	10.4		10.6	9.3[b]		
$E_a(298)$	21.4	18.2		5.9	8.6		10.1	11.6		11.8	10.4[b]		N/A
$E_a(298)$-W	20.4	17.2		5.2	7.8		9.3	10.7		11.0	9.6[b]		N/A
ROHF REFERENCE													
H_2+H→ H+H_2													
$\Delta E^{\ddagger}$	13.1	12.8	12.5	4.8	5.9	5.9	8.5	9.4	9.5	10.4	10.1	9.8	
$\Delta H^{\ddagger}(0)$	12.5	12.1	11.8	3.8	4.9	5.0	7.8	8.7	8.7	9.7	9.3	9.0	
$\Delta H^{\ddagger}(298)$	11.7	11.3	11.0	3.0	4.1	4.1	7.0	7.8	7.9	8.9	8.5	8.2	
$E_a(298)$	12.9	12.5	12.2	4.2	5.3	5.3	8.2	9.0	9.1	10.0	9.7	9.5	9.7[a]
$E_a(298)$-W	11.9	11.5	11.2	3.6	4.6	4.6	7.3	9.9	8.2	9.2	8.9	8.6	9.7[a]
$CH_3\cdot$ + CH_4 →CH_4 + $\cdot CH_3$													
$\Delta E^{\ddagger}$	16.1	15.9		14.2	16.1		19.4	21.1		18.2	17.9		
$\Delta H^{\ddagger}(0)$	15.7	15.4		13.8	15.6		19.1	20.8		17.8	17.5[b]		
$\Delta H^{\ddagger}(298)$	15.0	14.8		13.2	15.1		18.5	20.1		17.2	16.9[b]		
$E_a(298)$	16.2	16.0		14.4	16.2		19.6	21.3		18.4	18.1[b]		14.3[c]
$E_a(298)$-W	15.3	15.1		13.5	15.4		18.7	20.3		17.5	17.2[b]		14.3[c]
$HCC\cdot$ + HCCH → HCCH + $\cdot CCH$													
$\Delta E^{\ddagger}$	9.9	8.7		8.1	9.8		13.7	15.2		12.6	11.5		
$\Delta H^{\ddagger}(0)$	7.1	6.1		5.6	7.6		10.8	12.2		10.2	9.0[b]		
$\Delta H^{\ddagger}(298)$	6.1	6.2		5.4	7.3		11.0	12.5		10.1	8.9[b]		
$E_a(298)$	7.3	7.4		6.6	8.5		12.2	13.6		11.3	10.1[b]		N/A
$E_a(298)$-W	6.5	6.6		7.1	7.9		11.3	12.7		10.7	9.5[b]		N/A

[a]Reference [167]. [b]ΔZPVE, thermal, and Wigner tunneling corrections evaluated at CCSD(T)/cc-pVDZ level. [c]Reference [168].

by Truhlar and co-workers[153], two such functionals MPW1K and MPW1PW91, using the 6-31+G(d,p) basis set, predict $\Delta E^{\ddagger}$ of 7.2 and 5.9 kcal mol^{-1}, respectively.

For the reaction HCC· + HCCH → HCCH + ·CCH, in the cc-pVDZ basis, UMP2 overestimates and UB3LYP underestimates the UCCSD(T) classical barrier $\Delta E^{\ddagger}$ by as much as 7 and 5 kcal mol^{-1}, respectively. On the other hand, these UMP2 and UB3LYP errors become significantly smaller (5.3 and 0.4 kcal mol^{-1}, respectively) in the cc-pVTZ basis set. Our UCCSD(T)/cc-pVTZ value of 11.7 kcal mol^{-1} for $\Delta E^{\ddagger}(0)$ compares well with the result of 12.1 obtained by Nguyen and co-workers [140] using at the MPW1K/6-311++G(3df,2p)//MPW1K/6-311++G(d,p) level of theory. On the other hand, there is a somewhat larger discrepancy than one might expect with Nguyen's result [142] of 13.9 kcal mol^{-1} at the CCSD(T)-fc/6-311++G(d,p)//B3LYP/6-311++G(d,p) level of theory. Our preliminary investigations suggest that around half of this difference arises because Nguyen frozen core electrons, whereas we correlated all electrons because some of our computations employed software without frozen-core gradient capabilities; it is generally preferable to freeze core electrons when possible in studies using basis sets like cc-pVTZ, which lack core correlating functions. This frozen core effect appears to be larger than one might have expected, and indeed our exploratory computations indicate it is significantly smaller (a few tenths of one kcal mol^{-1}) for other reactions and levels of theory considered here. The remaining difference is between our value and Nguyen's is likely due to the differences in the basis set and small differences in geometries. Compared to the reactions of H_2 + ·H or HCC· + HCCH, discrepancies between theoretical results are much less pronounced for CH_4 + ·CH_3, on the order of 1-2 kcal mol^{-1} for the triple-ζ basis set [although the UB3LYP value remains 4 kcal mol^{-1} below UCCSD(T) for the cc-pVDZ basis set].

The overestimation of barrier heights by UMP2 is not surprising given that it will have difficulty describing the transition state, which features stretched bonds and a larger degree of nondynamical electron correlation (electronic near-degeneracies) than the reactants. The underestimation of barrier heights by DFT is a well-known phenomenon related to the errors in the self-interaction energy[178, 179, 180]. Self-interaction errors become large for

structures away from equilibrium like transition states. An increase in the exact Hartree-Fock exchange from 0% in pure DFT to 20% in B3LYP to 50% in BHLYP leads to better error cancellation between the reactants and transition states for the computation of barrier heights[179, 181, 182].

Using restricted orbitals causes most of the DFT barrier heights $\Delta E^{\ddagger}$ to increase. This significantly improves results for the reaction of H_2 with H, but for the other two symmetric reactions the RBHLYP barriers are overestimated compared to RCCSD(T). As we found above for transition state geometries, the CCSD(T) results are not very sensitive to the choice of UHF or ROHF reference, but the UMP2 and RMP2 barriers differ by as much as 10 kcal mol^{-1} for the reaction of HCC· with HCCH, the RMP2 results being closer to those from CCSD(T). We find that UMP2 suffers greatly from spin contamination for this reaction, as discussed in more detail below.

Zero-point vibrational energy corrections and thermal corrections are typically similar for different levels of theory for the symmetric reactions, although there are some significant differences for the reaction of HCC· with HCCH. In that case, UMP2 predicts anomalously small ΔZPVE and thermal corrections; the other methods are in general agreement with each other, but ΔZPVE can range from 2.2 kcal mol^{-1} (RB3LYP/cc-pVTZ) to 3.1 kcal mol^{-1} (UBHLYP/cc-pVTZ). As mentioned in the next section, the ethynyl radical has a challenging electronic structure, making the accurate prediction of geometries and vibrational frequencies more difficult than normal.

We may compare the theoretical results to experimentally-deduced activation energies, E_a, obtained by fitting reaction rates to an assumed Arrhenius form, although it must be kept in mind that these experimental values are subject to some uncertainty. These difficulties notwithstanding, we observe that the UCCSD(T)/cc-pVQZ value for $E_a(298)$ is within 0.4 kcal mol^{-1} of experiment for the H_2 + H· reaction, which represents excellent agreement for a barrier height. Indeed, this agreement may be partially fortuitous, because the Wigner tunneling correction reduces the effective computed barrier and increases the error at this level of theory by 0.8 kcal mol^{-1}. Because UCCSD(T)/cc-pVQZ computations will closely approach the Born-Oppenheimer limit for a three electron system, we ascribe

the majority of this error to the approximate nature of the Wigner tunneling correction and to the inherent difficulties in comparing quantum barrier heights to phenomenologically deduced experimental E_a values, as discussed previously. We conclude that more accurate comparisons between theory and experiment would appear to require going beyond simple transition state theory to more sophisticated dynamical treatments (including tunneling corrections), which could be used to compute reaction rates which may be compared directly with experiment.

For the reaction of methane with methyl radical, there is a larger disagreement of about 3.6 kcal mol^{-1} between experiment and UCCSD(T)/cc-pVTZ for E_a. In this case, the theoretical results are in general agreement with each other, and they also agree with previous theoretical estimates in the literature[183, 122, 136, 184]. For example, robust composite methods like W1, G3X and CBS-QB3 predict $\Delta H^{\ddagger}(0)$ to be 17.5, 18.4 and 17.3 kcal mol^{-1}, respectively[183], compared to our UCCSD(T)/cc-pVTZ result for of 17.4 kcal mol^{-1}. The Wigner tunneling correction reduces the discrepancy between experiment and our UCCSD(T)/cc-pVTZ result for E_a to 2.7 kcal mol^{-1} (or 2.9 kcal mol^{-1} when restricted orbitals are used). Given that improvements in the basis set tend to decrease the CCSD(T) activation energies, this disagreement would likely be reduced by an additional few tenths of a kcal mol^{-1} by larger basis set computations. The remaining disagreement is likely due to the unavoidable difficulties in comparing experimental and theoretical E_a values, non-Arrhenius behavior of the reaction, errors in the Wigner tunneling correction, and/or possibly some uncertainty in the experimental value.

4.3.3 Non-symmetric Reactions

All the non-symmetric reactions we have studied involve ethynyl radical abstracting a hydrogen from representative hydrocarbon systems, namely H_2, CH_4, C_2H_4, $HC(CH_3)_3$ and C_6H_6. As the electronic structure of the ethynyl radical is a challenging subject of its own, we will begin our discussion of non-symmetric abstraction reactions with an overview of literature on the ethynyl radical.

Table 16: Thermodynamic quantities (kcal mol^{-1}) for non-symmetric reactions using UHF references.[a]

	MP2		B3LYP		BHLYP		CCSD(T)		
	DZ	TZ	DZ	TZ	DZ	TZ	DZ	TZ	expt
HCC· + H_2 → HCCH + ·H									
$\Delta E^{\ddagger}$	3.5	2.5	-	-	0.6	1.0	3.4	2.0	
$\Delta H^{\ddagger}(0)$	3.8	3.3	-	-	1.0	1.5	3.7	3.0	
$\Delta H^{\ddagger}(298)$	3.7	2.9	-	-	1.2	1.4	2.4	2.6	
$E_a(298)$	4.9	4.1	-	-	2.4	2.6	3.6	3.8	2.0[b]
$E_a(298)$-W	4.5	3.8	-	-	2.3	2.5	3.3	3.5	2.0[b]
ΔE	-46.7	-46.8	-30.7	-30.0	-31.4	-30.8	-29.4	-31.5	
$\Delta H(0)$	-47.5	-47.6	-28.3	-28.4	-29.9	-29.5	-28.0	-30.4	
$\Delta H(298)$	-47.8	-48.0	-28.6	-29.3	-30.5	-30.1	-28.7	-31.0	-28.9[c]
HCC· + CH_4 → HCCH + ·CH_3									
$\Delta E^{\ddagger}$	2.6	1.4	-	-	0.3	0.8	2.4		
$\Delta H^{\ddagger}(0)$	1.6	1.0	-	-	0.3	0.5	1.7		
$\Delta H^{\ddagger}(298)$	1.4	1.1	-	-	0.5	0.7	1.8		
$E_a(298)$	2.6	2.3	-	-	1.7	1.9	2.9		1.0[d]
$E_a(298)$-W	2.5	2.2	-	-	1.7	1.8	2.9		1.0[d]
ΔE	-37.9	-39.1	-27.8	-29.1	-28.6	-29.9	-24.8	-27.8[e]	
$\Delta H(0)$	-41.9	-43.0	-28.3	-30.4	-30.4	-31.9	-26.8	-29.8[e]	
$\Delta H(298)$	-41.5	-42.6	-27.8	-30.5	-30.3	-31.7	-26.7	-29.8[e]	-28.2[c]
HCC· + C_2H_4 → HCCH + ·C_2H_3									
$\Delta E^{\ddagger}$	6.0	3.5	-	-	0.9	1.6	3.1		
$\Delta H^{\ddagger}(0)$	5.7	3.2[f]	-	-	0.1	0.4	1.7		
$\Delta H^{\ddagger}(298)$	6.1	3.6[f]	-	-	0.4	0.6	1.5		
$E_a(298)$	7.2	4.8[f]	-	-	1.6	1.8	2.6		N/A
$E_a(298)$-W	7.0	4.6[f]	-	-	1.6	1.8	2.6		N/A
ΔE	-26.8	-28.2	-23.3	-24.4	-23.0	-23.9	-19.2	-21.8	
$\Delta H(0)$	-29.4	-30.8	-23.5	-25.4	-24.4	-25.5	-20.4	-23.5	
$\Delta H(298)$	-29.1	-30.5	-23.2	-25.6	-24.3	-25.4	-20.6	-23.4	-21.8[c]
HCC· + $HC(CH_3)_3$ → HCCH + ·$C(CH_3)_3$									
$\Delta E^{\ddagger}$	-0.4	0.0	-	-	-	-	-0.6		
$\Delta H^{\ddagger}(0)$	-0.7	-0.4[f]	-	-	-	-	-1.0[f]		
$\Delta H^{\ddagger}(298)$	-1.1	-0.7[f]	-	-	-	-	-1.3[f]		
$E_a(298)$	0.1	0.5[f]	-	-	-	-	-0.2[f]		-0.1[h]
$E_a(298)$-W	0.1	0.4[f]	-	-	-	-	-0.2[f]		-0.1[h]
ΔE	-44.5	-45.5	-39.3	-40.7	-37.1	-39.7	-32.3		
$\Delta H(0)$	-48.1	-49.1[f]	-39.9	-41.2[g]	-38.9	-41.5[g]	-35.9[f]		
$\Delta H(298)$	-47.5	-48.5[f]	-39.1	-40.5[g]	-38.4	-41.1[g]	-35.2[f]		-36.6[c]
HCC· + C_6H_6 → HCCH + ·C_6H_5									
$\Delta E^{\ddagger}$	3.1	1.6	-	-	-	-	2.3		
$\Delta H^{\ddagger}(0)$	1.1	-0.4[f]	-	-	-	-	0.2[f]		
$\Delta H^{\ddagger}(298)$	1.2	-0.3[f]	-	-	-	-	0.4[f]		
$E_a(298)$	2.4	0.9[f]	-	-	-	-	1.6[f]		0[i]
$E_a(298)$-W	2.3	0.8[f]	-	-	-	-	1.5[f]		0[i]
ΔE	-7.7	-11.0	-21.8	-23.0	-21.0	-22.1	-15.8		
$\Delta H(0)$	-7.3	-10.6[f]	-21.2	-22.4[g]	-21.6	-22.7[g]	-15.4[f]		
$\Delta H(298)$	-7.3	-10.7[f]	-20.9	-22.1[g]	-21.6	-22.7[g]	-15.5[f]		-21.9[c]

[a] "-" indicates the absence of a transition state (barrier) corresponding to a collinear hydrogen abstraction. [b]Reference [169]. [c]Reference [165]. [d]Reference [170]. [e]ΔZPVE, thermal, and Wigner tunneling corrections evaluated at UCCSD(T)/cc-pVDZ level. [f]ΔZPVE, thermal, and Wigner tunneling corrections evaluated at UMP2/cc-pVDZ level. [g]ΔZPVE and thermal corrections evaluated using the cc-pVDZ basis set. [h]Reference [171]. [i]Reference [185].

Table 17: Thermodynamic quantities (kcal mol^{-1}) for non-symmetric reactions using ROHF references.[a]

	MP2		B3LYP		BHLYP		CCSD(T)		
	DZ	TZ	DZ	TZ	DZ	TZ	DZ	TZ	expt
HCC· + H_2 → HCCH + ·H									
$\Delta E^{\ddagger}$	3.2	2.1	-	-	1.4	1.8	3.5	2.3	
$\Delta H^{\ddagger}(0)$	3.8	3.1	-	-	2.0	2.4	4.3	3.3	
$\Delta H^{\ddagger}(298)$	2.3	2.7	-	-	1.9	2.2	2.7	2.9	
$E_a(298)$	3.5	3.9	-	-	3.1	3.4	3.9	4.0	2.0[b]
$E_a(298)$-W	3.2	3.6	-	-	2.9	3.2	3.6	3.8	2.0[b]
ΔE	-35.5	-36.9	-32.1	-31.4	-33.3	-32.8	-28.6	-30.9	
$\Delta H(0)$	-33.6	-35.7	-29.8	-29.0	-31.7	-31.4	-26.6	-29.5	
$\Delta H(298)$	-34.6	-36.4	-30.1	-29.3	-32.4	-32.0	-27.7	-30.2	-28.9[c]
HCC· + CH_4 → HCCH + ·CH_3									
$\Delta E^{\ddagger}$	1.8	0.7	-	-	1.0	1.6	2.6	2.2	
$\Delta H^{\ddagger}(0)$	1.5	0.4	-	-	1.0	1.2	2.2	1.7[d]	
$\Delta H^{\ddagger}(298)$	0.5	-0.6	-	-	1.3	1.5	0.9	0.5[d]	
$E_a(298)$	1.7	0.6	-	-	2.5	2.6	2.1	1.7[d]	1.0[e]
$E_a(298)$-W	1.6	0.5	-	-	2.4	2.6	2.0	1.6[d]	1.0[e]
ΔE	-26.7	-29.5	-28.3	-29.5	-29.3	-30.6	-24.1	-27.2	
$\Delta H(0)$	-28.0	-31.2	-28.8	-30.0	-31.1	-32.5	-25.4	-29.0	
$\Delta H(298)$	-28.3	-31.2	-28.4	-29.6	-31.0	-32.3	-25.8	-29.0	-28.2[c]
HCC· + C_2H_4 → HCCH + ·C_2H_3									
$\Delta E^{\ddagger}$	2.3	1.0	-	-	1.9	2.7	2.7		
$\Delta H^{\ddagger}(0)$	1.3	-0.1[f]	-	-	0.7	1.1	1.7		
$\Delta H^{\ddagger}(298)$	-0.1	-1.4[f]	-	-	0.9	1.3	0.5		
$E_a(298)$	1.1	-0.2[f]	-	-	2.1	2.5	1.7		N/A
$E_a(298)$-W	1.0	-0.3[f]	-	-	2.0	2.5	1.7		N/A
ΔE	-20.5	-22.7	-23.8	-24.8	-23.6	-24.5	-18.8	-21.5	
$\Delta H(0)$	-21.2	-24.7	-24.0	-24.8	-24.7	-25.8	-19.5	-22.6	
$\Delta H(298)$	-21.6	-24.5	-23.6	-24.5	-24.8	-25.8	-20.0	-22.7	-21.8[c]
HCC· + $HC(CH_3)_3$ → HCCH + ·$C(CH_3)_3$									
$\Delta E^{\ddagger}$	-0.8		-	-	-	-	-0.4		
$\Delta H^{\ddagger}(0)$	-0.8		-	-	-	-	-0.4[f]		
$\Delta H^{\ddagger}(298)$	-1.3		-	-	-	-	-0.9[f]		
$E_a(298)$	-0.1		-	-	-	-	0.3[f]		-0.1[h]
$E_a(298)$-W	-0.2		-	-	-	-	0.2[f]		-0.1[h]
ΔE	-33.6	-36.2	-39.8	-41.1	-39.0	-40.2	-31.5		
$\Delta H(0)$	-34.7	-37.3[f]	-40.3	-41.6[g]	-40.5	-41.7[g]	-32.6[f]		
$\Delta H(298)$	-34.7	-37.3[f]	-39.6	-40.9[g]	-40.2	-41.3[g]	-32.6[f]		-36.6[c]
HCC· + C_6H_6 → HCCH + ·C_6H_5									
$\Delta E^{\ddagger}$	1.6	0.0	-	-	-	-	2.0		
$\Delta H^{\ddagger}(0)$	0.7	-0.9[f]	-	-	-	-	1.1[f]		
$\Delta H^{\ddagger}(298)$	-0.1	-1.6[f]	-	-	-	-	0.4[f]		
$E_a(298)$	1.1	-0.4[f]	-	-	-	-	1.6[f]		0[i]
$E_a(298)$-W	1.0	-0.5[f]	-	-	-	-	1.5[f]		0[i]
ΔE	-18.7	-20.8	-22.4	-23.6	-21.9	-22.8	-17.4		
$\Delta H(0)$	-18.8	-20.9[f]	-21.8	-22.9[g]	-22.2	-23.2[g]	-17.5[f]		
$\Delta H(298)$	-17.7	-19.9[f]	-22.1	-23.2[g]	-22.2	-23.1[g]	-16.5[f]		-21.9[c]

[a] "-" indicates the absence of a transition state (barrier) corresponding to a collinear hydrogen abstraction. [b]Reference [169]. [c]Reference [165]. [d]ΔZPVE, thermal, and Wigner tunneling corrections evaluated at RCCSD(T)/cc-pVDZ level. [e]Reference [170]. [f]ΔZPVE, thermal, and Wigner tunneling corrections evaluated at RMP2/cc-pVDZ level. [g]ΔZPVE and thermal corrections evaluated using the cc-pVDZ basis set. [h]Reference [171]. [i]Reference [185].

4.3.3.1 Ethynyl Radical (·CCH)

The ethynyl radical has been the subject of numerous theoretical and experimental studies mainly because of its abundance in interstellar space [186, 187] and importance in combustion chemistry[188]. The non-trivial electronic spectrum[189, 190, 191] and hyperfine structure[192] have been explored extensively. One of the notable features of the ethynyl radical is that the A $^2\Pi$ excited electronic state lies only 3692 cm^{-1} (0.458 eV) above the ground X $^2\Sigma^+$ state[193, 194]. This state arises from the promotion of one of the electrons in the filled π orbitals to the half-filled carbon sigma radical orbital, $\cdots 1\pi^4 5\sigma^1 \rightarrow \cdots 1\pi^3 5\sigma^2$. Previous theoretical studies have examined potential energy surfaces of some of the low-lying electronic states of CCH[195, 196, 191, 197], including the conical intersection between the X $^2\Sigma^+$ and A $^2\Pi$ states which occurs for stretched C–H bond lengths[198]. Figure 18 shows the bending potentials of some of the low-lying doublet states of CCH computed using equation-of-motion (EOM) CCSD [164] in conjunction with the large cc-pVQZ basis set. Note that the A $^2\Pi$ state exhibits Renner-Teller splitting along the bending coordinate into $^2A'$ and $^2A''$ components[191, 196]. However, the minimum-energy configuration of the A $^2\Pi$ state, like that of the X $^2\Sigma^+$ state, is linear. The close proximity of the X $^2\Sigma^+$ and A

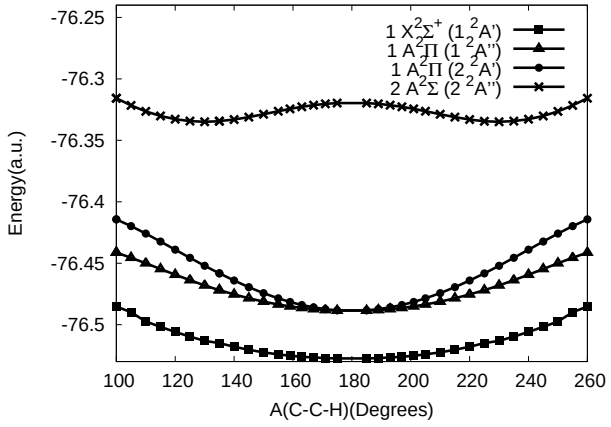

Figure 18: EOM-CCSD/cc-pVQZ bending potential for the four lowest-lying states of CCH. R(C-C)=1.200 Å, R(C-H)=1.060 Å.

$^2\Pi$ states in the ethynyl radical presents challenges for experimentalists and theoreticians alike. From an experimental standpoint, complex vibronic couplings have hampered efforts

to find a unique absorption peak to monitor the presence and concentration of the radical in, for example, kinetics experiments[166]. In theoretical studies, the strong vibronic coupling and conical intersection between the X $^2\Sigma^+$ and A $^2\Pi$ states can complicate the computation of spectra or reaction dynamics. In addition, although Hartree-Fock and post-Hartree-Fock methods correctly predict CCH to be linear, "pure" gradient-corrected functionals like BP86, BLYP and PWP86 predict a bent structure with a C-C-H angle of about $\sim 160^o$[199]. Hybrid functionals with minor fractions of Hartree-Fock exchange also yield a bent structure when small basis sets are used. We therefore choose BHLYP as a more reliable functional in this case. A highly accurate and conclusive *ab initio* study of the isolated ethynyl radical has been performed by Szalay *et al.*[200] using a variety of multi-reference and other highly-correlated methods in conjunction with very large basis sets. Our best CCSD(T) bond lengths for ·CCH are within a few thousandths of an angstrom of the benchmark results of Szalay *et al.*

4.3.3.2 Activation Energies

Due to the high hydrogen affinity of the ethynyl radical, one would expect that the barriers for abstracting hydrogen from most hydrocarbons would be rather low, and that the abstraction process would proceed very quickly. Indeed, that is exactly what our calculations yield; our best estimates of the activation energies are ≤ 4 kcal mol^{-1} for the five representative non-symmetric reactions we studied. Theoretical results using unrestricted and restricted references are presented in Tables 16 and 17, respectively. UB3LYP and UBHLYP continue the pattern of underestimating barriers, and in most non-symmetric reactions where the barriers are already very small, they predict a barrierless path to the products. The tables contain dashes in those cases where we were unable to find a transition state corresponding to a collinear hydrogen abstraction reaction.

The larger cc-pVTZ basis set generally lowers classical barriers $\Delta E^\ddagger$ by about 1 kcal mol^{-1} compared to cc-pVDZ for RMP2 and UMP2 for the reaction of ethynyl with H_2 or CH_4, but it has a smaller effect (a few tenths of 1 kcal mol^{-1}) for the DFT results. A more substantial basis set effect of 2.5 kcal mol^{-1} for $\Delta E^\ddagger$ is observed for UMP2 in the reaction

of ethynyl radical with ethylene. MP2 generally provides $\Delta E^{\ddagger}$ values within a few tenths of one kcal mol^{-1} of the more reliable CCSD(T) values, although larger discrepancies exist, particularly a difference of 2.9 kcal mol^{-1} for the reaction of ethynyl radical with ethylene when using unrestricted orbitals. Where DFT succeeds in finding a reaction barrier, the activation energies are underestimated compared to CCSD(T) but are generally in better agreement than for the symmetric reactions where the barriers are larger.

In a few instances for these non-symmetric reactions with very low barriers, ZPVE or temperature corrections to the classical barriers $\Delta E^{\ddagger}$ yield enthalpy changes $\Delta H^{\ddagger}$ which actually become negative. This occurs because we have located the transition states using the classical (Born-Oppenheimer) potential surface, with subsequent determination of enthalpy corrections. More sophisticated approaches may seek to find transition states on enthalpy or free-energy surfaces determined at the appropriate temperature[201]. For present purposes, such results simply confirm that the reaction barriers are very low, if they exist at all.

In the case of $\cdot$CCH + HC(CH$_3$)$_3$, we find the somewhat surprising result that even the classical barrier $\Delta E^{\ddagger}$ is negative (-0.4 at the UMP2/cc-pVDZ level of theory). When the reactants approach each other, they form a weakly bound van der Waals complex that is lower in energy than the separated reactants. As the reactants get even closer, they go over a barrier which has a higher energy than that of the van der Waals complex but a lower energy than that of the separated reactants; hence, the difference in energies between separated reactants and the transition state yields a "negative" barrier. This situation is illustrated schematically in Figure 19. At the UMP2/cc-pVDZ level of theory, a van der Waals complex with a well depth of 0.6 kcal mol^{-1} is formed when the ethynyl radical is 2.66 Å away from the active hydrogen, while the transition state (0.2 kcal mol^{-1} above the van der Waals minimum but 0.4 kcal mol^{-1} below the separated reactants) is observed at 2.09 Å. Our theoretical findings are in agreement with the experimentally measured negative temperature dependence of the rate of this reaction and the associated experimentally deduced negative barrier (-0.1 kcal mol^{-1})[171]. Based on similar observations for the reaction CN + C_2H_6, Sims *et al.*[202] suggest a mechanism involving the formation of a bound transient van der Waals complex. It is possible that similar van der Waals complexes

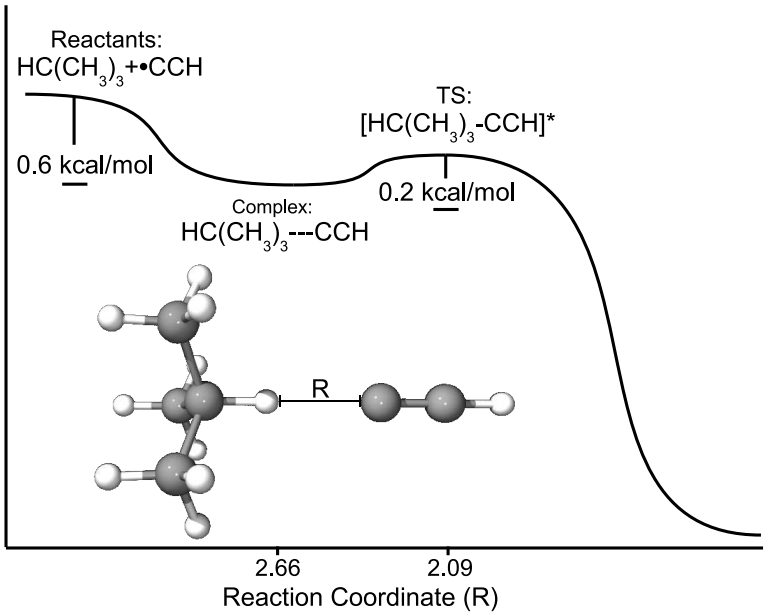

Figure 19: Schematic of the reaction of ethynyl radical with isobutane; quantities computed at the UMP2/cc-pVDZ level of theory.

may form in some of the other reactions we have studied, but that they are difficult to locate due to the very flat nature of the surface. Preliminary searches failed to locate a similar van der Waals complex in the reaction of ethynyl radical with methane, even when augmenting the basis set with diffuse functions (MP2/aug-cc-pVDZ). We do not rule out the possibility that these complexes may exist in some of the other reactions studied, but as they are not a focus of our study, we did not pursue them further.

For the reaction of ethynyl radical with H_2, activation energies $E_a(298)$-W predicted at the CCSD(T)/cc-pVTZ level (3.5 and 3.8 kcal mol^{-1} with unrestricted and restricted orbitals, respectively) are higher than the experimentally derived barrier[169] of 1.98 $\pm$ 0.11 kcal mol^{-1} for the temperature range of 178 - 359 K. Our UCCSD(T)/cc-pVTZ predicted $\Delta H^{\ddagger}(0)$ value of 3.0 kcal mol^{-1} compares well to other high level theoretical works reported in the literature. In particular, UCCSD(T)/aug-cc-pVTZ//UCCSD(T)/6-311++G(2df,2p), G2//UQCISD6-311+G(d,p), QCISD/cc-pVTZ predict $\Delta H^{\ddagger}(0)$ for this reaction to be 3.1 [141], 2.5 [203], and 2.9 [204], respectively.

For the reaction of ethynyl radical with CH_4, the tunneling corrected activation barrier, $E_a(298)$-W, computed at RCCSD(T)/cc-pVTZ level [with vibrational frequencies evaluated

at the RCCSD(T)/cc-pVDZ level] only differs by 0.6 kcal mol^{-1} from experiment. The corresponding value for $\Delta H^{\ddagger}(0)$, 1.7 kcal mol^{-1}, is somewhat smaller than the comparable literature value [205, 140] of 2.6 kcal mol^{-1} at the CCSD(T)/aug-cc-pVTZ//CCSD(T)/6-31G(d,p)+ZPVE[UMP2/6-311++G(3df,2p)] level of theory, and noticeably smaller than MPW1K/6-311++G(3df,2p)//MPW1K/6-311++G(d,p) value of 4.7 kcal mol^{-1}.

Hydrogen abstraction from isobutane by the ethynyl radical is of particular importance since isobutane has been used as a cluster model to represent diamond C(111) surface[143, 206, 207]. The absence of a hydrogen abstraction barrier for this reaction would thus indicate that ethynyl radical or any tool with an ethynyl radical tip should serve as a convenient abstraction tool[122].

Finally, the reaction of ethynyl radical with benzene can serve as a good model for hydrogen abstraction from delocalized π systems. For both restricted and unrestricted orbitals, MP2/cc-pVDZ and CCSD(T)/cc-pVDZ yield E_a(298)-W values in the range of 1.5 to 2.3 kcal mol^{-1}. However, using the larger cc-pVTZ basis for MP2 lowers E_a(298)-W to 0.8 kcal mol^{-1} for unrestricted orbitals, and it actually becomes negative (-0.5 kcal mol^{-1}) for restricted orbitals (the "negative" barrier here is, again, simply a consequence of locating the transition state on the Born-Oppenheimer surface, and the approximate nature of the Wigner tunneling correction). These rather small barriers are in general agreement with experimental work[185] suggesting that this reaction has no barrier.

4.3.3.3 Enthalpies of Reaction

So far, we have focused on activation energies, where direct comparison between theory and experiment is difficult. Let us now turn to enthalpies of reaction ΔH, where comparison with experiment is more straightforward. Here we will compare theoretical values of the reaction enthalpies at 298 K, $\Delta H(298)$, against the corresponding experimental values obtained from addition and subtraction of standard heats of formation, $\Delta H_f^o(298)$. For the symmetric reactions, of course the reaction enthalpies are zero by definition. For the non-symmetric reactions, results are presented in Tables 16 and 17.

As shown in the tables, B3LYP, BHLYP and CCSD(T) predict enthalpies of reaction

that agree reasonably well with experiment. For most reactions, $\Delta H(298)$ calculated using CCSD(T) matches experiment within about 2 kcal mol^{-1}. Larger differences are seen for the reaction of ethynyl radical with benzene, or for the reaction of ethynyl radical with isobutane (when using restricted orbitals). Our results confirm a previous observation[182] that the BHLYP functional, while improving on abstraction barriers predicted by B3LYP, leads to somewhat larger errors for the reaction enthalpies. In general, B3LYP enthalpies of reaction are in better agreement with experiment while the BHLYP predictions deviate from their B3LYP counterparts by up to 2.7 kcal mol^{-1}.

It is surprising to note that UMP2 gives estimates of $\Delta H(298)$ that are 8-20 kcal mol^{-1} lower than the corresponding experimental values (see Table 16); additionally, this anomaly does not disappear when the larger cc-pVTZ basis is used. However, when we employ a restricted reference via RMP2, as shown in Table 17, this significantly improves the $\Delta H(298)$ results compared to the UMP2 values. This observation highlights the problems of spin contamination when UHF references are used and underscores the need to carefully consider the choice of reference wavefunction in computations involving these radical-molecule reactions. In the next section, we examine the extent of spin contamination in the UHF-based results. We attribute most of the difference between UMP2 and experimental $\Delta H(298)$ values to the uneven effect of spin contamination between reactants and products. Apart from the MP2 method, the choice of restricted or unrestricted orbitals makes little difference in most of the theoretical reaction enthalpies, with most changes being 2 kcal mol^{-1} or less. Figures 20 and 21 display the differences between results obtained using restricted and unrestricted references for computations of barrier heights and reaction energies, respectively.

4.3.4 Spin Contamination

One potential problem with computations based upon unrestricted orbitals is that they can feature significant contamination by higher-multiplicity spin states. Although highly-correlated methods such as UCCSD(T) have been shown to be rather insensitive to spin contamination [208, 209], significant problems can arise for lower-order methods, including UMP2[210, 211, 212, 213]. Table 18 examines the degree of spin contamination for several

species considered here using the UMP2 and UCCSD(T) methods.

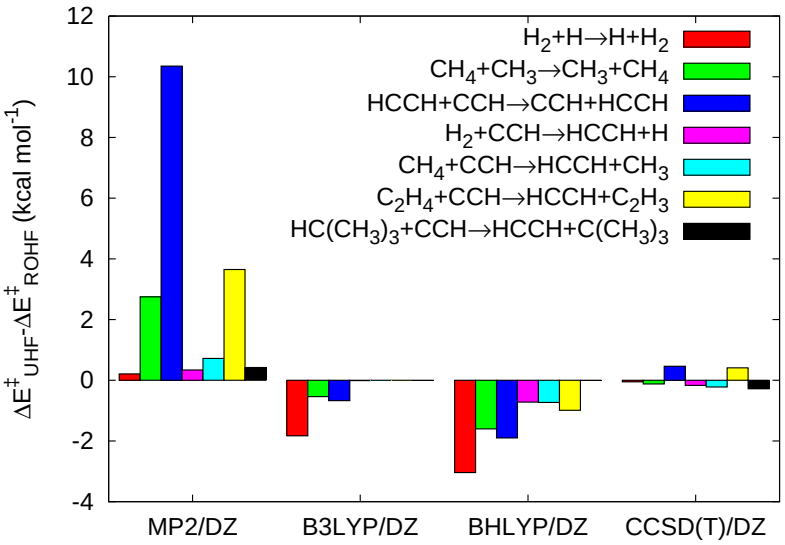

Figure 20: Effect of spin contamination on reaction barriers $\Delta E^{\ddagger}$.

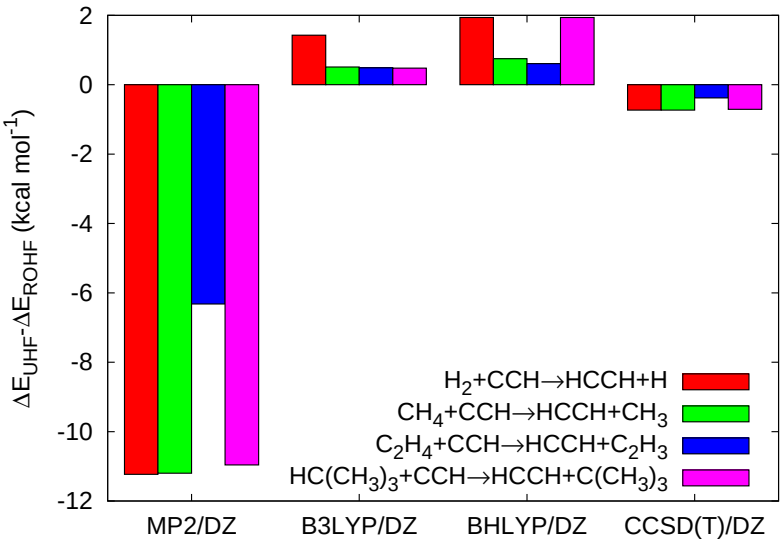

Figure 21: Effect of spin contamination on energies of reaction ΔE.

Spin contamination is considered to be a minimal problem in density-functional theory[214] and it is not well-defined[212]; nevertheless, Table 18 also includes UB3LYP and UBHLYP results for comparison. These DFT methods are not significantly affected by spin contamination, as indicated by expectation values of $< \hat{S}^2 >$ which are very close to the ideal 0.75 for a doublet radical.

Table 18: $< \hat{S}^2 >$ for selected species using a cc-pVDZ basis set[a]

	UMP2	UB3LYP	UBHLYP	UCCSD(T)
Reactants and Products				
$\cdot CH_3$	0.76	0.75	0.76	0.75
$\cdot CCH$	1.04	0.77	0.79	0.75
$\cdot C_2H_3$	0.91	0.76	0.78	0.75
$\cdot C(CH_3)_3$	0.76	0.75	0.76	0.75
$\cdot C_6H_5$	1.21	0.76	0.77	0.74
Transition States				
H-H-H	0.78	0.76	0.77	0.75
CH_3-H-CH_3	0.78	0.76	0.76	0.75
HCC-H-CCH	1.13	0.77	0.80	0.75
H-H-CCH	1.04		0.79	0.75
CH_3-H-CCH	1.03		0.75	0.75
C_2H_3-H-CCH	1.08			0.75
$C(CH_3)_3$-H-CCH	1.04			0.75
C_6H_5-H-CCH	1.04			0.75

[a]For a doublet state, $< S^2 >$ should be 0.75.

Although the spin contamination in the UMP2 wavefunction for some radicals like $\cdot C(CH_3)_3$ and $\cdot CH_3$ is fairly small, it is significant for the $\cdot CCH$, $\cdot C_2H_3$, and $\cdot C_6H_5$ radicals. Spin contamination in the ethynyl radical in particular is a well-known problem and it has been used to explain the inaccurate isotropic hyperfine couplings predicted by most *ab initio* methods using spin-unrestricted formalisms[199]. Note that significant spin contamination is also observed for the transition states considered. Because the degree of spin contamination is similar ($< \hat{S}^2 > \sim 1.05$) for $\cdot CCH$ and the transition states for reactions of $\cdot CCH$, the spin contamination errors largely cancel when computing activation barriers. However, in several of the reactions considered, there is less spin contamination in the products, leading to an erroneous lowering of the UMP2 enthalpies of reaction. In the case of the reaction HCC$\cdot$ + C_6H_6 $\rightarrow$ HCCH + $\cdot C_6H_5$, the highly spin contaminated phenyl radical product ($< \hat{S}^2 > = 1.21$) leads to a significant raising of the UMP2 value for $\Delta H(298)$.

Although using an ROHF reference conveniently alleviates spin contamination by quartets and larger multiplets from our doublet systems, it has been known to occasionally give artifactual results that have no physical basis[176, 177], and even in the present study, RMP2 predicts non-symmetric transition states for our three symmetric reactions (see Figure 22

and the previous discussion of transition state geometries). Fortunately, this unphysical result disappears for the more robust RCCSD(T) method.

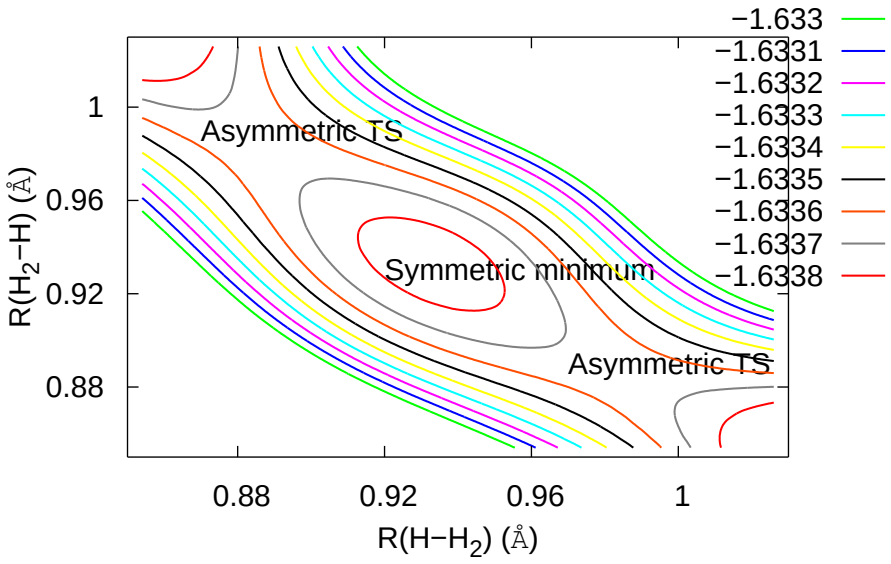

Figure 22: RMP2/cc-pVDZ potential energy surface (in a.u.) for H· + H_2 → H_2 + H·.

4.3.5 Electron Correlation Effects Beyond CCSD(T)

One would expect the reactants and products in the present study to be dominated by a single electron configuration, so that the single-reference methods employed here should give fairly reliable results. Indeed, our computations did not show signs of any severe electronic near-degeneracies in any of the reactant or product species. However, the transition states involve bonds which are in the process of being formed and broken, and additional electron configurations may contribute significantly to the zeroth-order wavefunction. In this case, the reliability of single-reference methods might be degraded, and it might be necessary to employ multi-reference methods to achieve high-accuracy results[161].

In order to test for the possible importance of electron correlation effects beyond those described by CCSD(T), where feasible we have performed full configuration interaction (FCI) computations which exactly solve the electronic Schrödinger equation within the given one-particle basis set.

Table 19: Effect of higher-order electron correlation beyond RCCSD(T) on barrier heights, $\Delta E^{\ddagger}$, and reaction energies, ΔE (kcal mol^{-1})[a]

	RCCSD(T)/6-31G	FCI[b]/6-31G	FCI-RCCSD(T)
H_2+H· → H·+H_2			
$\Delta E^{\ddagger}$	14.83	14.80	-0.03
HCC· + H_2 → HCCH + ·H			
$\Delta E^{\ddagger}$	5.99	6.02	0.03
ΔE	-26.19	-25.94	0.25
H· + CH_4 → H_2 + ·CH_3			
$\Delta E^{\ddagger}$	19.76	19.62	-0.14

[a]The core 1s orbitals on carbon are frozen for correlated calculations. [b]Full configuration interaction (FCI) constitutes an exact treatment of electron correlation within a given basis set.

Table 19 shows that, for the systems where we could afford the very expensive FCI computations, the CCSD(T) and FCI barriers are very similar (within 0.15 kcal mol^{-1}), indicating that CCSD(T) is sufficient to describe electron correlation effects in these systems. The difference between CCSD(T) and FCI for the reaction energies ΔE of the two non-symmetric reactions is 0.20-0.25 kcal mol^{-1}, somewhat larger than the differences observed for barrier heights. This correction remains, however, a very small fraction of the overall reaction energy. Analysis of the FCI wavefunctions for the species in Table 19 demonstrates that none of the leading coefficients, C_0, is below 0.91, and none of the second largest coefficients, C_1 is greater than 0.14. Additionally, T1 diagnostic[215, 216] for our RCCSD(T)/cc-pVDZ computations of transition states was never above the value of 0.02; Lee and co-workers argue that multi-reference systems typically feature values above this. Thus the similarity of CCSD(T) to FCI, the leading FCI coefficients, and the T1 diagnostics agree that these simple hydrogen abstraction reactions do not appear to have a large multi-reference character.

4.3.6 Abstraction Tool

For mechanosynthesis of diamond to be realized, it is imperative that the abstraction and deposition tools have favorable thermodynamics, facile kinetics, and good positional

control[111, 112, 113, 114, 115, 116]. The most natural tool for these purposes would be something like a scanning probe microscopy (SPM) tip[112], which has already been used for sub-nanometer manipulation of atoms[120]. Given its low barriers and high exothermicities for the hydrogen abstraction reactions discussed above, the ethynyl radical might be an excellent choice for attaching to an SPM tip to form a hydrogen abstraction tool [122, 111, 123, 124]. Assuming that the ethynyl moiety might be attached via a hydrocarbon connector, as a somewhat larger model system we have considered an ethynyl radical attached to a t-butyl group as shown in Figure 23.

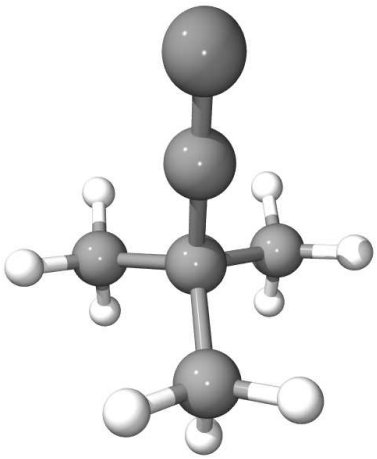

Figure 23: A generic abstraction tooltip modeled as an ethynyl radical moiety attached to a t-butyl base.

One interesting question to ask of this model is whether it exhibits any energetically accessible but undesirable alternative reactions which might hamper its function as a tool for abstracting hydrogens from a hydrocarbon surface. In particular, we considered the possibility that the tooltip might react with itself, with the radical tip forming bonds with carbon or hydrogen atoms of the t-butyl base. In a limited search for such reactions, we found only one relevant transition state, that of a hydrogen auto-abstraction, depicted in Figure 24. This transition state is 57 kcal mol^{-1} up in energy at the UMP2/cc-pVDZ level of theory and hence is not expected to be easily accessible at modest temperatures.

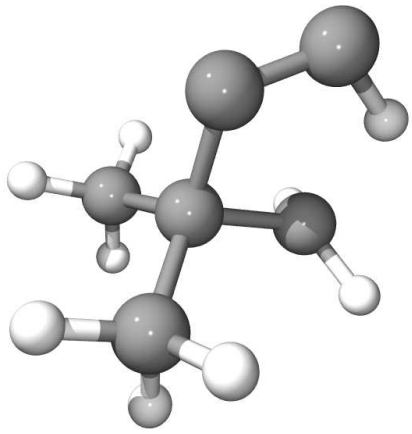

Figure 24: A transition state leading to hydrogen auto-abstraction.

Another important consideration in evaluating possible abstraction tools is their structural rigidity. If a candidate tool is too flexible, it may exhibit large-amplitude oscillations which could impair the positional selectivity of the abstraction process. In particular, if the bending frequencies of the radical tip are too low, then modest temperatures will be sufficient to populate highly excited vibrational levels of these bending modes. The isolated ethynyl radical, ·CCH, features an experimentally-determined[217] bending frequency of 372 cm^{-1}, which might be considered an intermediate value between high-energy and low-energy bending modes. We note that the theoretical computation of vibrational frequencies using UMP2, UB3LYP, UBHLYP or UCCSD(T) are typically accurate to a few percent, but the errors for radicals can be somewhat higher[218]. We see unusually large discrepancies between different theoretical methods or between theory and experiment for ethynyl-type radicals, and the UCCSD(T)/cc-pVDZ prediction for the degenerate bending frequency of ·CCH is 310 cm^{-1}, somewhat farther from experiment than one might expect for this high level of theory. Nevertheless, *ab initio* computations should provide at least reasonable estimates of these bending frequencies in related systems. We determined the bending frequency of the propynyl radical ($CH_3CC\cdot$) to be 169 cm^{-1} at the UCCSD(T)/cc-pVDZ level of theory, a somewhat lower frequency than that of ·CCH. For our model tooltip in Figure 23, with an ethynyl group attached to a t-butyl base, the UMP2/cc-pVDZ level of theory

predicts a value of 202 cm^{-1}, again an intermediate value, for the bending mode of the ethynyl group. These results suggest that precise positional control might become difficult at elevated temperatures unless modifications are made to introduce more rigidity into the system. At low temperatures, however, a bending frequency of around $\sim$ 200 cm^{-1} should be sufficient to prevent large uncertainties in the position of the radical tip. The C-C-C bending potential for the model tooltip (using the simple C-C-C internal coordinate, which is very similar to the corresponding normal mode) is shown in Figure 25. The fractional Boltzmann populations, f_n, for the evenly spaced energy levels n of a harmonic oscillator of frequency ν (in Hz) at temperature T are given by

$$f_n = (1 - e^{-h\nu/k_bT})e^{-nh\nu/k_bT}. \tag{88}$$

Using the value of 202 cm^{-1} and ignoring any coupling of the C-C-C bending mode with other modes, the Boltzmann populations of its n=0, n=1, n=2 and n=3 levels are 62%, 24%, 9% and 3%, respectively, at 298 K. Estimating the classical turning points from the

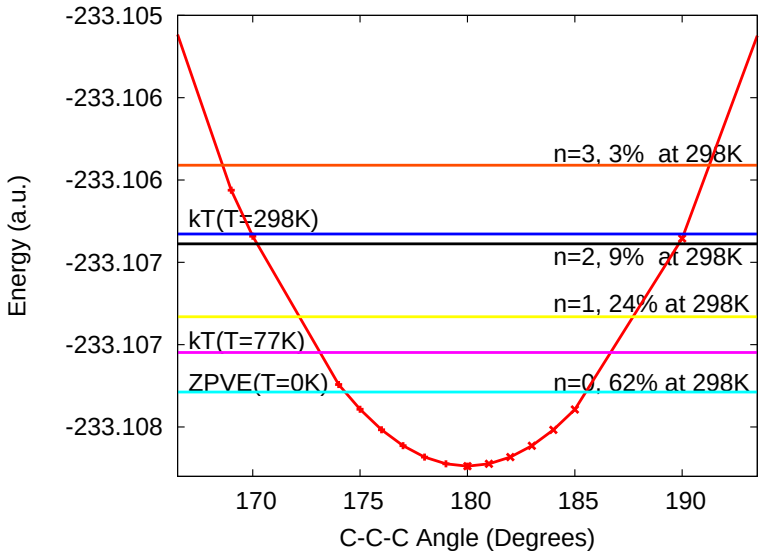

Figure 25: UMP2/cc-pVDZ -C-C-C bending potential for abstraction tooltip. All other internal coordinates of the tool were constrained to their UMP2/cc-pVDZ optimized values. The bending coordinate chosen keeps the ethynyl group co-planar with one of the C–C bonds of the t-butyl base.

bending potential in Figure 25, the positional uncertainties at the end of the tooltip for these vibrational levels are around 0.12, 0.15, 0.19, and 0.24 Å, respectively. Considering

the distance of 2.5 Å between two adjacent hydrogens on diamond C(111) surface terminated with hydrogens[122], the positional uncertainty even for a vibrationally excited tooltip is miniscule. On the basis of this analysis, the tool should have good positional selectivity at modest temperatures.

Finally, it is conceivable that the presence of unusually low-lying excited electronic states might affect the operation of radical tooltips if those excited states have unfavorable features in contrast to those noted for the ground state. As mentioned previously, the A $^2\Pi$ state lies only 0.458 eV above the ground state according to experiment[194]. Our computations suggest that this excited state is unreactive in collinear hydrogen abstraction reactions because it fills the sigma orbital which was singly occupied and reactive in the ground state. Although 0.458 eV is a small gap on the scale of electronic excitation energies, nevertheless, we do not expect it to significantly impair the operation of ethynyl-based tooltips at modest temperatures. First of all, this first excited state remains linear, like the ground state (see Figure 18), so that if this state were accessed, it should not by itself contribute to any positional uncertainty in the tooltip. Secondly, rovibrational energy levels within the A $^2\Pi$ electronic state are significantly perturbed by levels of the X $^2\Sigma^+$ electronic state[193, 219], meaning that nominally unreactive levels of the A state may borrow some reactive character due to their mixing with the X state. Thirdly, and most importantly, using the experimental energy gap of 0.458 eV yields a very small Boltzmann population for the A state — only $\sim 10^{-8}$ at 298 K. At liquid nitrogen temperature of 77 K, that ratio becomes truly negligible at $\sim 10^{-30}$. If, in spite of these small probabilities, the A $^2\Pi$ electronic state were to be accessed, it may not be long-lived. Unfortunately it is not possible based on current data to estimate the lifetime of all the potentially relevant vibronic levels of nominal A $^2\Pi$ character, but we note that a study by Wittig and co-workers[220] indicates spontaneous emission lifetimes of at least some of these levels to be on the order of 20-60 μs (the same order of magnitude one would expect by scaling spontaneous emission lifetimes of isoelectronic species[221, 222] by the cube of the ratio of the energy gaps between the ground and excited states)[223, 224].

Of course the electronic structure of actual tooltips will differ somewhat from that of

the simple ethynyl radical, and it is important to ask if the gap between the ground and first excited states might decrease for larger molecular systems. In partial exploration of this question, we computed the UCCSD(T) vertical and adiabatic excitation energies for the low-lying excited states of the ethynyl and propynyl radicals and for our model tooltip. Table 20 shows that both the vertical and adiabatic excitation energies for the

Table 20: Comparison of UCCSD(T) vertical (T_v) and adiabatic (T_e) excitation energies (in eV) for lowest-lying excited states

basis	$\cdot CCH$	T_v	T_e	$\cdot CCCH_3$	T_v	T_e	$\cdot CCC(CH_3)_3$	T_v	T_e
cc-pVDZ	$1\ ^2\Pi$	0.62	0.35	$1\ ^2E$	0.46	0.20	$1\ ^2E$	0.46	0.20
cc-pVTZ	$1\ ^2\Pi$	0.70	0.43	$1\ ^2E$	0.51	0.26			

X→A transitions are low for these species. For our proposed abstraction tool (Figure 23), using the UCCSD(T)/cc-pVDZ adiabatic excitation energy of 0.20 eV, we estimate the ratio of the Boltzmann population of the excited state to the ground state to be $\sim 10^{-4}$ at 298 K and $\sim 10^{-14}$ at 77 K. We therefore expect that the tooltip radical should remain in its ground electronic state at modest temperatures of operation. Regarding the contribution to reaction error rate caused by tooltip unreactivity in the excited state and the required transition time from excited to ground state, if a $\sim 10^{-4}$ error rate at 298 K or a $\sim 10^{-14}$ error rate at 77 K is acceptable then the speed of tool operation is unconstrained by the required transition time.

4.4 Conclusions

The abstraction of hydrogens from prototypical hydrocarbon molecules has been studied using high level *ab initio* techniques. The calculated activation barriers and enthalpies of reaction are found to be in good agreement with experiment. In general, MP2 overestimates barriers and is particularly sensitive to spin contamination of the reference wavefunction. Density functional methods, namely B3LYP and BHLYP, significantly underestimate barriers due to self-interaction errors. The more reliable CCSD(T) method predicts barrier heights and enthalpies of reaction which are generally in excellent agreement with experiment. The hydrogen abstraction activation energy from sp^2 and sp^3 carbons by ethynyl

radical is less than 3 kcal mol^{-1}. For the reaction of ethynyl radical with isobutane, the abstraction reaction is barrierless. This makes ethynyl-type radicals appealing as possible tooltips for use in the mechanosynthesis of diamond, particularly at low temperatures where they would have a high degree of positional selectivity and control.

The material of this chapter was published as a paper in the *Journal of Physical Chemistry A* [225].

CHAPTER V

THEORETICAL STUDY OF HYDROGENATION OF RADICAL SITES USING SILICON, GERMANIUM, TIN AND LEAD BRIDGEHEAD-SUBSTITUTED METHANE AND ISOBUTANE

A series of reactions of the type Y· + XH_4→YH + XH_3· and Y′· + $HX(CH_3)_3$ → Y′H +· $X(CH_3)_3$ where Y=H, CH_3, Y′=CH_3, $C(CH_3)_3$ and X=Si, Ge, Sn, Pb are studied using state-of-the-art *ab initio* electronic structure methods. Second-order Møller-Plesset perturbation theory (MP2) and the coupled-cluster singles, doubles and perturbative triples [CCSD(T)] as well as density functional theory (DFT) methods with correlation consistent basis sets (cc-pVNZ, where N = D,T,Q) and their pseudopotential analogs (cc-pVNZ-pp, where N = D,T,Q) in order to determine the transition-state geometries, activation barriers, and thermodynamic properties of these reactions. Trends are observed to evaluate the dependence of barriers to hydrogen donation to a radical site on the nature of the Group IVA bridgehead (Si, Ge, Sn and Pb). The use of a tooltip hydrogen attached to a Group IVA element as a possible hydrogen donation tool in the mechanosynthesis of diamondoids appears feasible.

5.1 Introduction

Abstracting surface hydrogens to create radical sites and rehydrogenation of radical sites can help control the reactivity of surfaces. One scheme which attempts to take advantage of abstraction/rehydrogenation to control reactivity is the mechanosynthesis of diamondoids[111, 112, 113, 114, 115, 116, 117, 118, 119, 120]. Mechanosynthesis is a paradigm which proposes to attach a molecular tooltip to a scanning probe microscope (SPM) to perform elementary synthetic operations such as carbon deposition or hydrogen abstraction/donation at a specific location on the substrate. The first elementary step, namely hydrogen abstraction, is critical in mechanosynthesis as well as chemical vapor deposition (CVD) of diamond. In the CVD synthesis of diamond, a precursor hydrocarbon gas like methane enters a

plasma/thermal/electric activation chamber in excess hydrogen gas. The activation process leads to the formation of atomic hydrogen, which abstracts hydrogen from the gas-phase hydrocarbons to yield very reactive carbon-containing radicals. These radicals deposit on the substrate and form carbon-carbon bonds leading to diamond growth. Atomic hydrogens also abstract hydrogen from the diamond surface, thereby creating nucleation sites for further diamond growth. They promote the preferential growth of diamond over graphite by etching graphite at a higher rate than diamond. Regarding the mechanosynthesis of diamondoids, hydrogen abstraction has been thoroughly studied in several works[122, 111, 123, 124, 226]. In a recent high-level *ab initio* theoretical study, we found that hydrogen abstraction from saturated hydrocarbons using ethynyl radical is highly exothermic and has a very small barrier[225]. In the case of ethynyl radical abstracting a hydgogen from isobutane, which has been suggested as a good model for diamond C(111) surface[143], the reaction is virtually barrierless, indicating that an SPM tip with an ethynyl radical moiety could serve as a viable hydrogen abstraction tool. Such an approach has already been demonstrated theoretically and experimentally with non-ethynyl tips for the abstraction of hydrogens from a Si(100) surface and the selective manipulation of silicon atoms[121].

Naturally, the next elementary step would be hydrogen donation to radical sites, and a few promising works have appeared in recent years. Yamamoto *et al.*[227] demonstrated the deposition of hydrogen atoms from a scanning tunneling microscope (STM) with a tungsten tip to a monohydride Si(100)-2x1:H surface through the application of +3.5V voltage bias to diffuse the hydrogens to the tungsten tip and followed by -8.5V 300 ms pulses to induce electronic excitations that break the tungsten-hydrogen bond. Thirstrup *et al.*[228] used a clean and hydrogen covered STM tips to perform atomic scale desorption and deposition of hydrogens from Si(001)-(2 x 1)-H and Si(001)-(3 x 1)-H surfaces for both positive and negative sample bias voltages with a resolution of one to two atomic rows. McIntyre *et al.*[229], in an effort to demonstrate nanocatalytic capabilities of a platinium-rhodium STM tip operating in a reactor cell with excess H_2, managed to rehydrogenate partially dehydgrogenated carbonaceous fragments on Pt(111) surface. Yet in another study of catalytic hydrogenation, Müller *et al.*[230] use a platinum-coated atomic force microscope (AFM) tip

to hydrogenate terminal azide groups on a self-assembled monolayer. They suggest that variation of the catalytic tip and surface could enable the fabrication of structures that can not be made by conventional techniques. In contrast to these experimental studies, there has been little theoretical work done proposing candidate tools for the rehydrogenation of reactive surfaces as it pertains to mechanosynthesis[113, 115]. The simplest rehydrogenation reaction would involve the transfer of a weakly bound hydrogen to a hydrocarbon radical site. Substituting the bridgeheads of methane, isobutane, adamantane, ... etc, with other Group IVA (Si, Ge, Sn, Pb, ...) elements is one proposal for a hydrogen donor to a carbon radical site. A few theoretical and experimental works have explored a set of relavant reactions. Song *et al.*[231] used breathing orbital valence bond (BOVB)[232] and a variety of other models built upon the valence bond (VB) theory to get barriers to nonsymmetric (nonidentity) reactions of type X + X′H → XH + X′ where X≠X′=H, CH_3, SiH_3, GeH_3, SnH_3, and PbH_3. Their VB predicted barriers and reaction energies deviate by as much as 7 kcal mol^{-1} from those computed using MP2. Drozdova *et al.*[233] studied the hydrogen abstraction of Ge and Sn containing species by radicals. Chatgilialoglu *et al.*[234] investigated the reaction of germanium hydrides to determine their hydrogen donation abilities. Arthur *et al.*[235] measured the rate constant for the reaction H + $(CH_3)_3GeH$ in the temperature range of 298-510 K. Zavitsas *et al.*[236] devised a scheme to predict activation energies of hydrogen abstraction reactions by radicals on the basis of bond dissociation energy, bond length and infrared stretching frequency of the reactants and products of the abstraction reaction. They then apply their model to 47 reactions, including some relevant to this work, and get fairly good agreement with experiment. Shimokawa *et al.*[237] studied the temperature dependence of thermal desorption, abstraction and collision-induced desorption of H_2 and D_2 off a Ge(100) and Si(100) surfaces. Despite these and other studies on the adsorption and desorption of hydrogen from Group IVA surfaces[238, 239, 240], there remains a lack of high-level *ab initio* or experimental data on the hydrogen exchange reactions of methane and isobutane with their Group IVA bridgehead substituted counterparts.

High-level quantum chemical methods are capable of providing very accurate estimates of reaction thermodynamics. Indeed, the so-called Gaussian-1 (G1)[125], Gaussian-2 (G2)[126,

127] and Gaussian-3 (G3)[128, 129, 130] composite methods and their variants are capable of providing reaction enthalpies typically within 1-2 kcal mol^{-1} of experiment. Although these theoretical approaches are rather expensive computationally and applicable only to small molecular systems, they demonstrate that truly high-quality energetics are possible using modern *ab initio* methods. In a continued effort to explore the feasibility of mechanosynthesis of diamondoids, an understanding of the thermochemistry and kinetics involved in the elementary processes becomes imperative, and modern theoretical methods are very useful in this endeavor.

5.2 Theoretical Methodology

The hydrogen transfer reactions considered in this study are given in (1) – (4) along with the point-group symmetry considered for the reaction (and the corresponding Abelian computational subgroup); X=Si, Ge, Sn, Pb.

$$\mathrm{H}\cdot + \mathrm{XH_4} \rightarrow \mathrm{H_2} + \cdot\mathrm{XH_3} \qquad C_{3v}/C_s \tag{89}$$

$$\cdot\mathrm{CH_3} + \mathrm{XH_4} \rightarrow \mathrm{CH_4} + \cdot\mathrm{XH_3} \qquad C_{3v}/C_s \tag{90}$$

$$\cdot\mathrm{CH_3} + \mathrm{HX(CH_3)_3} \rightarrow \mathrm{CH_4} + \cdot\mathrm{X(CH_3)_3} \qquad C_s/C_s \tag{91}$$

$$\cdot\mathrm{C(CH_3)_3} + \mathrm{HX(CH_3)_3} \rightarrow \mathrm{HC(CH_3)_3} + \cdot\mathrm{X(CH_3)_3} \qquad C_s/C_s \tag{92}$$

Dunning's correlation consistent basis sets (cc-pVNZ, N=D,T,Q)[13, 16], which provide a systematic convergence of energies and properties toward the complete basis set (CBS) limit were used where available. For reactions involving heavier atoms like germanium, tin and lead, we use Peterson's[241, 242] small-core pseudopotentials (cc-pVNZ-pp, N=D,T,Q) of comparable quality due to the size of the system as well as the need to account for relativistic effects. For the sake of brevity, we will occasionally refer to the correlation consistent basis sets simply as DZ and TZ, their pseudopotential analogs as NZ-pp. To account for relativistic effects for explicit all electron basis sets, we use the first-order Douglas-Kroll-Hess (losadk) formalism[46] as implemented in MOLPRO 2006.1[243]. The use of these

Douglas-Kroll-Hess one-electron integrals with a correlation consistent basis set is designated by cc-pVNZ-dk and often abbreviated as NZ-dk. As demonstrated in Table 21, these

Table 21: Quality of small- and large-core pseudopotentials: the tase of H· + $GeH_4 \rightarrow H_2$ + · GeH_3

	Size(e^-s in core)	B3LYP	BHLYP	MP2	CCSD(T)
		$\Delta E^{\ddagger}$			
cc-pVDZ	-	0.5	2.8	7.5	5.2
cc-pVDZ-dk	-	0.5	2.7	7.4	5.1
cc-pVDZ-pp	10	0.4	2.6	7.3	5.0
CRENBL	18	0.7	3.2	8.4	5.9
LANL2DZ	28	0.8	3.1	7.9	5.0
		ΔE			
cc-pVDZ	-	-19.6	-17.8	-15.7	-18.1
cc-pVDZ-dk	-	-19.9	-18.0	-15.8	-18.2
cc-pVDZ-pp	10	-20.5	-18.6	-16.4	-18.8
CRENBL	18	-17.5	-15.2	-12.1	-14.2
LANL2DZ	28	-19.1	-17.7	-14.6	-16.5

small-core pseudopotentials give results that are very comparable to those from explicit all electron basis sets of the same cardinal number for Reaction (30) with X=Ge, an atom for which relativistic effects are small. For an atom with an outermost shell of quantum number n, the cc-pVNZ-pp pseudopotentials explicitly treat the nsp and $(n-1)spd$ shells, leaving a core of 10, 28 and 60 electrons for germanium, tin and lead, respectively, compared to LANL2DZ and SBKJC VDZ which have a larger core of 28, 46, 78 and CRENBL with 18, 36, 68 for the three atoms, respectively[17]. Reaction barriers and energies can be rather sensitive to the choice of the pseudopotential, as shown in Table 21 and discussed in the next Section. Reaction barriers and energies predicted using all electron basis (DZ), and all electron basis with first-order Douglas-Kroll relativistic correction (DZ-dk) and those using correlation consistent pseudopotentials (DZ-pp) agree remarkably well while predictions using the large-core CRENBL and LANL2DZ deviate significantly, particularly for the case of CRENBL ECP.

For correlation consistent polarized valence basis sets designed to capture valence electron correlation, we do employ the frozen-core approximation in all MP2 and CCSD(T) computations. When using the cc-pVNZ-pp pseudopotentials in correlated calculations

such as MP2 and CCSD(T), we still freeze the $3s^2 3p^6 3d^{10}$, $4s^2 4p^6 4d^{10}$ and $5s^2 5p^6 5d^{10}$ "core" orbitals for Ge, Sn and Pb, respectively. Even when using explicit basis sets like the cc-pVNZ class, the same core-freezing scheme is typically used by default. For instance, all but the $4s^2 4p^2$ electrons of Ge are typically frozen in correlated calculations using the cc-pVNZ basis to reduce computational cost even though some studies suggest that correlating some $3/4/5d$ orbitals might be important[244]. Our preliminary analysis shows that such a scheme does not introduce significant error while making it possible to study large systems using highly correlated methods.

When computing classical barriers and energies of reaction with pseudopotentials, energies for H, H_2, CH_3, CH_4, $X(CH_3)_3$ and $HX(CH_3)_3$ are computed using the standard cc-pVNZ basis. Electron correlation is accounted for using second-order Møller-Plesset perturbation theory (MP2) and coupled-cluster theory with single, double, and perturbative triple substitutions [CCSD(T)][146]. We have also employed the B3LYP[147] and BHLYP[148] (also called BH&HLYP) functionals as implemented in MOLPRO 2006.1[243]. Because DFT methods underestimate reaction barriers, especially for hydrogen transfer reactions (see Ref. [225] and references within), it is interesting to examine their performance for the present reactions. B3LYP and other functionals lacking in exact Hartree-Fock (HF) exchange have been particularly susceptible to self-interaction errors which lead to the underestimation of barriers. Functionals such as BHLYP[148], which includes 50% Hartree-Fock exchange (compared to 20% in B3LYP) and 50% Becke88 exchange[151] in conjunction with the LYP correlation functional[152] perform better. (Of the many other exchange-correlation functionals designed to predict improved hydrogen abstraction barriers, the MPW1K[153] functional has also had some success[140].)

All DFT, MP2 and CCSD(T) computations employed the MOLPRO 2006.2 program[243]. For open-shell systems, we use RMP2[158] and the partially spin restricted CCSD(T), designated as RHF-RCCSD(T) or simply RCCSD(T)[159, 160]. Although we use restricted orbitals, the $< \hat{S}^2 >$ values even for unrestricted orbitals indicate that spin contamination is very minimal in the systems. Experimental enthalpies of formation ΔH_f^o(298 K) for our

reactants and products are readily available[165], and they entail relatively small uncertainties. These values have been used to obtain heats of reaction, $\Delta H(298\ \mathrm{K})$, for the reactions considered. In order to compare more directly with the experimental thermochemical data, we have converted our *ab initio* bare energy differences, ΔE, into 0 K enthalpy differences, $\Delta H(0\ \mathrm{K})$, by adding the zero-point vibrational energy correction (ΔZPVE), estimated simply as one-half of the sum of the (unscaled) vibrational frequencies. We also obtain 298 K enthalpy differences, $\Delta H(298\ \mathrm{K})$, by adding finite temperature corrections using the usual vibrational, rotational, and translational partition functions in conjunction with the harmonic oscillator, rigid rotator, and particle-in-a-box models.

The phenomenological activation barriers, E_a, are determined from experiment by an indirect process in which the reaction rate, k, is obtained at a series of temperatures, T. Fitting the temperature-dependent rate to a simple Arrhenius form, $k(T)$=$Ae^{-E_a/RT}$, the physical activation barrier can be determined. The problem with this approach is that most rate-vs-temperature relations do not fit the Arrhenius form for all temperature regimes due to effects like hydrogen tunneling and the strong temperature dependence of the vibrational partition function when there are low-frequency bending modes. We compared our theoretical barriers with experimental values derived from rate-vs-temperature data in temperature ranges where a simple Arrhenius fit seems suitable. Where applicable, these temperature ranges are indicated. It must be stressed that these experimentally deduced activation barriers depend on the temperature range used for the Arrhenius fit, and that this complicates a direct comparison with reaction barriers computed quantum mechanically.

To compare our "classical" activation barriers, $\Delta E^{\ddagger}$, with these experimentally deduced activation energies, E_a, we first add zero-point vibrational corrections and finite-temperature corrections (as discussed above) to obtain $\Delta H^{\ddagger}(T)$. Next, it follows from transition state theory [172] that for a reaction which undergoes a change of $\Delta n^{\ddagger}$ in the number of molecules while going from reactants to a transition state, the experimental $E_a(T)$ is related to $\Delta H^{\ddagger}(\mathrm{T})$ by

$$E_a(T) = \Delta H^{\ddagger}(T) + (1 - \Delta n^{\ddagger})RT. \tag{93}$$

$\Delta n^{\ddagger}$ for these bi-molecular hydrogen abstraction reactions is -1 since the two reactants form one complex in the transition state.

One possible cause for a deviation from Arrhenius behavior is quantum mechanical tunneling of hydrogen atoms through classical barriers. The simplest approach to assess the role of quantum tunneling is the Wigner correction to the reaction rate[173, 174]. Given the magnitude ν_t of the imaginary frequency along the reaction coordinate at the transition state, the rate is enhanced by a factor of

$$K_W(T) = 1 + \frac{1}{24}\left(\frac{h\nu_t}{k_bT}\right)^2. \tag{94}$$

Note that this correction predicts tunneling to be faster through thin barriers (with large ν_t) than through wide barriers (small ν_t), as one would expect. Because we are comparing activation energies rather than rates, we may incorporate this correction into our theoretical results as an effective barrier height lowering by evaluating

$$\Delta E_a = -k_b \frac{dlnK_W}{d(1/T)} = -2k_bT\frac{y(T)}{1+y(T)}, \tag{95}$$

where $y(T) = \frac{1}{24}\left(h\nu_t/k_bT\right)^2$. As discussed below, this correction amounts to a few tenths of one kcal mol^{-1} for the systems studied. Wigner-corrected activation energies will be denoted E_a-W.

5.3 Results and Discussion

5.3.1 Transition State Geometries

As predicted by Hammond's postulate[175], reactions with a small barrier and high exothermicity have a transition state that closely resembles the reactants. Our data agrees with the predictions of Hammond's postulate. For the four reactions studied for each type of bridgehead, the transition state shows more reactant-like character as the bridgehead changes from Si to Ge to Sn to Pb. Reactions involving the lead bridgehead typically have low barriers ($\Delta E^{\ddagger} < 4$ kcal mol^{-1} at the RMP2/DZ-pp level) and high exothermicities ($\Delta E \sim$ -45 – -35 kcal mol^{-1} at the RMP2/DZ-pp level) and the Pb-H, H-C and H-H bond lengths along the abstraction coordinate are R[Pb-H]$\sim$ 1.8 Å, R[C-H]$\sim$Y and R[H-H]$\sim$1.4 Å, respectively. This is in contrast to reactions involving the silicon bridgeheads where $\Delta E^{\ddagger} \sim$ 8 – 11 kcal

mol^{-1}, ΔE $\sim$ -20 to -10 kcal mol^{-1}, R[Si-H]$\sim$1.6 Å, R[C-H]$\sim$Y and R[H-H]$\sim$1.1 Åat the RMP2/DZ-pp level.

5.3.2 Basis Set Dependence

The quality of our predicted barriers and energies of reactions largely depends on the quality of the basis sets employed and the level of electron correlation included. In the case of the heavy Group IVA bridgeheads, it is important to properly account for relativistic effects as well. A very efficient compromise that enables the use of reliable basis sets and correlation methods while accounting for relativistic effects is achieved by utilizing pseudopotentials. Small-core pseudopotentials replace only a few core orbitals by a pseudopotential, while large-core pseudopotentials replace more core orbitals and leave few orbitals to be described explicitly by a self-consistent field procedure. There is an apparent difference in the quality of predictions made using small-core and large-core pseudopotentials as demonstrated in Table 21 for the reaction H$\cdot$ + GeH_4 $\rightarrow$ H_2 + $\cdot GeH_3$. The comparison was most convenient for a reaction involving a Ge bridgehead because there are explicit basis sets as well as pseudopotentials for germanium.

In Table 21, the most accurate representation is the all electron DZ basis set with a first order Douglas-Kroll-Hess relativistic correction, designated as DZ-dk. Comparing $\Delta E^{\ddagger}$ and ΔE predicted by other basis sets and pseudopotentials with DZ-dk, it is clear that CRENBL and LANL2DZ ECPs deviate rather significantly. LANL2DZ and CRENBL are common pseudopotentials with a large core of 28 and 18 electrons, respectively. While barriers and energies of reaction predicted by the small-core DZ-pp match those of DZ-dk almost exactly, the CRENBL and LANL2DZ analogs introduce an error as much as $\sim$ 1 kcal mol^{-1} on barriers and $\sim$ 4 kcal mol^{-1} on energies of reaction even for a seemingly easy reaction. Compared to the all-electron, relativistic DZ-dk results, it is particularly striking that the small-core CRENBL ECP does not perform as well as the large-core LANL2DZ ECP. One must also note that the variation among predicted properties is more significant for MP2 and CCSD(T) than for DFT methods.

Table 21 clearly shows that the ccpVNZ-pp pseudopotentials are the most reliable pseudopotentials to use. Within the ccpVNZ and ccpVNZ-pp pseudopotentials, it would be worthwhile to investigate the basis set dependence of predicted barriers and energies of reaction. We can perform that investigation for Reactions (30) and (31) for which calculations using TZ and QZ quality basis and pseudopotentials are feasible. Tables 22 – 23 show that DZ basis sets and the DZ-pp pseudopotentials are not close to the complete basis set limit as indicated by the significant difference between DZ and TZ or QZ results. The convergence of energies of activation and reaction with respect to basis set or pseudopotentials, however, shows very different behavior for DFT compared to ab initio methods like MP2 and CCSD(T). While energies of activation predicted by ab initio methods typically decrease by $\sim$1 kcal mol^{-1} going from DZ[-pp] to TZ[-pp], and another $\sim$0.5 kcal mol^{-1} going from TZ[-pp] to QZ[-pp], B3LYP and BHLYP show either no (as in Reaction (30)) or a small increase (as in Reaction (31)). The pattern in the energies of reaction predicted by DFT and ab initio methods is much less dramatic – going from DZ to TZ quality basis or pseudopotentials decreases ΔE by 1 – 4 kcal mol^{-1}. It is safe to claim that the QZ-[pp] energies of activation and reaction are reasonably converged with respect to basis set or pseudopotential size. Overall, for all the reactions including 91 and 92 for which calculations with TZ and QZ basis and pseudopotentials are not available, one must keep in mind a typical basis set correction of $\sim$ -1.5 kcal mol^{-1} on barriers and -4 to -1 kcal mol^{-1} on energies of reaction just from increasing the basis/pseudopotential from DZ to QZ quality.

Table 22: Basis set and method dependence of energies of activation ($\Delta E^{\ddagger}$) and aeaction (ΔE) for $H\cdot + XH_4 \rightarrow H_2 + \cdot XH_3$, where X = Si, Ge, Sn or Pb in kcal mol^{-1} [a]

	$\Delta E^{\ddagger}$						ΔE					
	DZ	DZ-pp	TZ	TZ-pp	QZ	QZ-pp	DZ	DZ-pp	TZ	TZ-pp	QZ	QZ-pp
						X = Si						
B3LYP	1.6	-	1.9	-	2.0	-	-13.9	-	-15.2	-	-14.9	-
BHLYP	4.7	-	5.1	-	5.2	-	-12.4	-	-13.0	-	-12.7	-
MP2	9.6	-	8.6	-	8.4	-	-10.0	-	-11.1	-	-10.7	-
CCSD(T)	6.9	-	5.8	-	5.5	-	-12.4	-	-13.5	-	-13.1	-
						X = Ge						
B3LYP	0.5	0.4	0.6	0.5	N/A	0.5	-19.6	-20.5	-21.5	-22.4	N/A	-22.3
BHLYP	2.8	2.6	2.9	2.7	N/A	2.7	-17.7	-18.6	-19.6	-20.3	N/A	-20.2
MP2	7.5	7.3	6.2	6.2	N/A	5.9	-15.7	-16.4	-18.0	-18.3	N/A	-18.4
CCSD(T)	5.1	5.0	3.8	3.7	N/A	3.3	-18.1	-18.8	-20.2	-20.5	N/A	-20.5
						X = Sn						
B3LYP	-	0.0	-	0.1	-	0.1	-	-29.5	-	-31.8	-	-31.5
BHLYP	-	1.2	-	1.3	-	1.3	-	-27.6	-	-29.7	-	-29.5
MP2	-	5.5	-	4.4	-	4.1	-	-25.7	-	-28.0	-	-27.9
CCSD(T)	-	3.6	-	2.3	-	2.0	-	-28.0	-	-29.9	-	-29.8
						X = Pb						
B3LYP	-	0.0	-	0.0	-	0.0	-	-39.0	-	-41.5	-	-41.1
BHLYP	-	0.4	-	0.4	-	0.4	-	-36.9	-	-39.2	-	-38.8
MP2	-	3.9	-	2.9	-	2.2	-	-34.9	-	-37.4	-	-37.2
CCSD(T)	-	2.4	-	1.3	-		-	-37.3	-	-39.5	-	-39.2

[a] "-" indicates the absence of a particular basis set or pseudopotential for the Group IVA element.

Table 23: Basis set and method dependence of energies of activation ($\Delta E^{\ddagger}$) and reaction (ΔE) for $\cdot CH_3 + XH_4 \rightarrow CH_4 + \cdot XH_3$, where X = Si, Ge, Sn or Pb in kcal mol^{-1} [a]

	$\Delta E^{\ddagger}$						ΔE					
	DZ	DZ-pp	TZ	TZ-pp	QZ	QZ-pp	DZ	DZ-pp	TZ	TZ-pp	QZ	QZ-pp
						X = Si						
B3LYP	5.8	-	7.0	-	7.2	-	-14.9	-	-17.1	-	-16.6	-
BHLYP	10.2	-	11.4	-	11.7	-	-16.4	-	-15.2	-	-14.7	-
MP2	10.4	-	9.8	-	9.7	-	-18.5	-	-17.9	-	-17.3	-
CCSD(T)	10.2	-	9.4	-		-	-16.8	-	-16.5	-	-16.1	-
						X = Ge						
B3LYP	3.5	3.1	4.3	4.0	N/A	4.1	-20.6	-21.5	-23.4	-24.2	N/A	-23.9
HLYP	7.5	7.2	8.3	8.0	N/A	8.1	-21.8	-22.6	-21.8	-22.4	N/A	-22.2
MP2	8.2	8.0	7.2	7.6	N/A	6.7	-24.2	-24.9	-24.7	-25.1	N/A	-24.9
CCSD(T)	8.0	7.7	6.8	6.5	N/A	6.2	-22.5	-23.2	-23.1	-23.5	N/A	-23.5
						X = Sn						
B3LYP	-	1.7	-	2.2	-	2.4	-	-30.4	-	-33.7	-	-33.2
BHLYP	-	5.0	-	5.4	-	5.6	-	-31.6	-	-31.9	-	-31.4
MP2	-	6.2	-	5.0	-	4.8	-	-34.3	-	-34.7	-	-34.4
CCSD(T)	-	5.8	-	4.4	-	4.2	-	-32.4	-	-32.9	-	-32.7
						X = Pb						
B3LYP	-	0.2	-	0.5	-	0.7	-	-40.0	-	-43.4	-	-42.7
BHLYP	-	2.6	-	2.9	-	3.1	-	-41.0	-	-41.4	-	-40.8
MP2	-	3.9	-	2.8	-	2.6	-	-43.4	-	-44.2	-	-43.8
CCSD(T)	-	3.5	-	2.2	-		-	-41.7	-	-42.4	-	-42.2

[a] "-" indicates the absence of a particular basis set or pseudopotential for the Group IVA element.

Table 24: Energies of activation ($\Delta E^{\ddagger}$) and reaction (ΔE) for silicon based reactions in kcal mol^{-1} [a]

	B3LYP			BHLYP			MP2			CCSD(T)			
	DZ	TZ	QZ	DZ	TZ	QZ	DZ	TZ	QZ	DZ	TZ	QZ	Expt.
$\cdot H + SiH_4 \rightarrow H_2 + \cdot SiH_3$													
$\Delta E^{\ddagger}$	1.6	1.9	2.0	4.7	5.1	5.2	9.6	8.6	8.4	6.9	5.8	5.5	
$\Delta H^{\ddagger}(0)$	1.2	1.5	1.6	4.0	4.4	4.5	8.8	7.8	7.6	7.0	5.9	5.6	
$\Delta H^{\ddagger}(298)$	0.9	1.2	1.3	3.6	4.0	4.1	8.5	7.5	7.3	6.7	5.6	5.3	
$E_a(298)$	2.1	2.4	2.5	4.8	5.2	5.3	9.7	8.7	8.5	7.8	6.8	6.5	
$E_a(298)$-W	1.8	2.1	2.2	4.1	4.5	4.6	8.7	7.7	7.5	7.1	6.1	5.8	2.5-3.8[b]
ΔE	-13.9	-15.2	-14.9	-12.4	-13.1	-12.7	-10.0	-11.1	-10.7	-12.4	-13.5	-13.1	
$\Delta H(0)$	-13.9	-15.2	-14.9	-12.4	-13.1	-12.7	-9.9	-11.0	-10.6	-11.6	-12.7	-12.3	
$\Delta H(298)$	-13.3	-14.6	-14.3	-11.8	-12.5	-12.1	-9.3	-10.4	-10.0	-11.0	-12.1	-11.7	
$\cdot CH_3 + SiH_4 \rightarrow CH_4 + \cdot SiH_3$													
$\Delta E^{\ddagger}$	5.8	7.0	7.2	10.2	11.4	11.7	10.4	9.8	9.7	10.2	9.4		
$\Delta H^{\ddagger}(0)$	6.1	7.3	7.5	10.7	11.9	12.2	10.6	10.0	9.9	11.4	10.6		
$\Delta H^{\ddagger}(298)$	4.9	6.1	6.3	9.3	10.5	10.8	9.6	9.0	8.9	9.4	8.6		
$E_a(298)$	6.1	7.3	7.5	10.5	11.7	12.0	10.8	10.2	10.1	10.6	9.8		
$E_a(298)$-W	5.6	6.8	7.0	9.7	10.9	11.2	10.0	9.4	9.3	9.8	9.0		6.2-7.5 [c]
ΔE	-14.9	-17.1	-16.6	-16.4	-15.2	-14.7	-18.5	-17.9	-17.3	-16.8	-16.5	-16.0	
$\Delta H(0)$	-11.7	-13.9	-13.4	-13.0	-11.8	-11.3	-15.2	-14.6	-14.0	-12.7	-12.4	-11.9	
$\Delta H(298)$	-11.9	-14.1	-13.6	-13.2	-12.0	-11.5	-15.4	-14.8	-14.2	-12.9	-12.6	-12.1	
$\cdot CH_3 + HSi(CH_3)_3 \rightarrow CH_4 + \cdot Si(CH_3)_3$													
$\Delta E^{\ddagger}$	7.1			12.0			10.9						
$\Delta H^{\ddagger}(0)$	7.1			12.2			12.0						
$\Delta H^{\ddagger}(298)$	6.7			11.8			11.6						
$E_a(298)$	7.9			13.0			12.8						
$E_a(298)$-W	7.3			12.1			11.9						7.0-8.3 [d]
ΔE	-13.3			-13.8			-15.9			-14.3			
$\Delta H(0)$	-9.7			-9.9			-12.2			-10.5			
$\Delta H(298)$	-9.9			-10.1			-12.4			-10.7			
$\cdot C(CH_3)_3 + HSi(CH_3)_3 \rightarrow HC(CH_3)_3 + \cdot Si(CH_3)_3$													
$\Delta E^{\ddagger}$	11.2			15.2			8.0						
$\Delta H^{\ddagger}(0)$	10.4			14.5			7.3[e]						
$\Delta H^{\ddagger}(298)$	10.6			14.6			7.4[e]						
$E_a(298)$	11.8			15.8			8.6[e]						
$E_a(298)$-W	11.0			14.9			7.7[e]						
ΔE	-4.6			-4.0			-9.1			-7.0			
$\Delta H(0)$	-1.1			-0.4			-5.8			-3.6[f]			
$\Delta H(298)$	-1.5			-0.8			-6.2			-4.1[f]			

[a] All ZPVE, thermal and Wigner tunneling corrections done using cc-pVDZ basis unless indicated otherwise. [b] Ref. [245, 246, 247]. [c] Ref. [248, 249, 250, 251, 252]. [d] Ref. [248, 253, 252, 254]. [e] Thermal, ZPVE and Wigner corrections computed using BHLYP frequencies. [f] Thermal and ZPVE corrections computed using MP2 frequencies.

Table 25: Energies of activation ($\Delta E^{\ddagger}$) and reaction (ΔE) for germanium based reactions in kcal mol^{-1} [a]

	B3LYP			BHLYP			MP2			CCSD(T)			
	DZ-pp	TZ-pp	QZ-pp	DZ-pp	TZ-pp	QZ-pp	DZ-pp	TZ-pp	QZ-pp	DZ-pp	TZ-pp	QZ-pp	Expt.
$\cdot H + GeH_4 \rightarrow H_2 + \cdot GeH_3$													
$\Delta E^{\ddagger}$	0.4	0.5	0.5	2.6	2.7	2.7	7.3	6.2	5.9	5.0	3.7	3.3	
$\Delta H^{\ddagger}(0)$	0.5	0.6	0.5	2.2	2.3	2.3	6.8	5.7	5.4	4.4	3.1	2.7	
$\Delta H^{\ddagger}(298)$	0.3	0.4	0.4	1.9	2.0	2.0	6.4	5.3	5.0	4.2	2.9	2.5	
$E_a(298)$	1.5	1.6	1.6	3.1	3.2	3.2	7.6	6.5	6.2	5.3	4.1	3.7	
$E_a(298)$-W	1.4	1.5	1.5	2.6	2.7	2.7	6.8	5.7	5.4	4.7	3.5	3.1	1.8-2.3[b]
ΔE	-20.5	-22.4	-22.3	-18.6	-20.3	-20.2	-16.4	-18.3	-18.4	-18.8	-20.5	-20.5	
$\Delta H(0)$	-20.3	-22.2	-22.1	-18.3	-20.0	-19.9	-16.0	-17.9	-18.0	-18.6	-20.3	-20.3	
$\Delta H(298)$	-19.7	-21.6	-21.5	-17.8	-19.5	-19.4	-15.5	-17.4	-17.5	-18.0	-19.7	-19.7	
$\cdot CH_3 + GeH_4 \rightarrow CH_4 + \cdot GeH_3$													
$\Delta E^{\ddagger}$	3.1	4.0	4.1	7.2	8.0	8.1	8.0	7.6	6.7	7.7	6.5	6.2	
$\Delta H^{\ddagger}(0)$	3.8	4.7	4.8	7.8	7.4	7.5	8.3	7.9	7.0	8.0	6.9	6.6	
$\Delta H^{\ddagger}(298)$	3.0	3.9	4.0	7.0	6.6	6.7	7.5	7.1	6.2	7.2	6.1	5.8	
$E_a(298)$	4.2	5.1	5.2	8.1	7.7	7.8	8.7	8.3	7.4	8.4	7.3	7.0	
$E_a(298)$-W	4.0	4.9	5.0	7.5	7.1	7.2	8.0	7.6	6.7	7.7	6.6	6.3	
ΔE	-21.5	-24.4	-23.9	-22.6	-22.5	-22.2	-24.9	-25.1	-24.9	-23.2	-23.5	-23.5	
$\Delta H(0)$	-18.1	-21.0	-20.5	-19.0	-18.9	-18.6	-21.4	-21.6	-21.4	-19.7	-20.0	-20.0	
$\Delta H(298)$	-18.3	-21.2	-20.7	-19.2	-19.1	-18.8	-21.6	-21.8	-21.6	-19.9	-20.2	-20.2	
$\cdot CH_3 + HGe(CH_3)_3 \rightarrow CH_4 + \cdot Ge(CH_3)_3$													
$\Delta E^{\ddagger}$	4.0			8.6			8.3						
$\Delta H^{\ddagger}(0)$	4.3			8.8			8.4						
$\Delta H^{\ddagger}(298)$	3.9			8.3			7.9						
$E_a(298)$	5.1			9.5			9.1						
$E_a(298)$-W	4.8			8.8			8.4						
ΔE	-21.3			-21.5			-23.3		21.6				
$\Delta H(0)$	-17.5			-17.6									
$\Delta H(298)$	-18.0			-18.1									
$\cdot C(CH_3)_3 + HGe(CH_3)_3 \rightarrow HC(CH_3)_3 + \cdot Ge(CH_3)_3$													
$\Delta E^{\ddagger}$	7.0			10.8			4.9						
ΔE	-12.7			-11.7			-16.5			-14.3			
$\Delta H(0)$	-8.9			-7.9			-13.0						
$\Delta H(298)$	-9.3			-8.4			-13.4						

[a] All ZPVE, thermal and Wigner tunneling corrections done using cc-pVDZ basis unless indicated otherwise.

[b] Ref. [255, 256, 257].

Table 26: Energies of activation ($\Delta E^{\ddagger}$) and reaction (ΔE) for tin based reactions in kcal mol^{-1}

	B3LYP			BHLYP			MP2			CCSD(T)			
	DZ-pp	TZ-pp	QZ-pp	DZ-pp	TZ-pp	QZ-pp	DZ-pp	TZ-pp	QZ-pp	DZ-pp	TZ-pp	QZ-pp	Expt.
						$\cdot H + SnH_4 \rightarrow H_2 + \cdot SnH_3$							
$\Delta E^{\ddagger}$	0.0	0.1	0.1	1.2	1.3	1.3	5.5	4.4	4.1	3.6	2.3	2.0	
$\Delta H^{\ddagger}(0)$	0.2	0.3	0.3	1.2	1.3	1.3	5.3	4.2	3.9	3.4	2.1	1.8	
$\Delta H^{\ddagger}(298)$	0.2	0.3	0.3	1.0	1.1	1.1	5.0	3.9	3.6	3.1	1.8	1.5	
$E_a(298)$	1.4	1.5	1.5	2.2	2.3	2.3	6.2	5.1	4.8	4.3	3.0	2.7	
$E_a(298)$-W	1.4	1.5	1.5	1.9	2.0	2.0	5.4	4.3	4.0	3.8	2.5	2.2	
ΔE	-29.5	-31.8	-31.5	-27.6	-29.7	-29.5	-25.7	-18.0	-27.9	-28.0	-29.9	-29.8	
$\Delta H(0)$	-28.5	-30.8	-30.5	-26.5	-28.6	-28.4	-24.6	-16.9	-26.8	-26.9	-28.8	-29.7	
$\Delta H(298)$	-28.0	-30.3	-30.0	-26.0	-28.1	-27.9	-24.1	-16.4	-26.3	-26.4	-28.3	-28.2	
						$\cdot CH_3 + SnH_4 \rightarrow CH_4 + \cdot SnH_3$							
$\Delta E^{\ddagger}$	1.7	2.2	2.4	5.0	5.5	5.6	6.3	5.1	4.8	5.9	4.4	4.2	
$\Delta H^{\ddagger}(0)$	2.7	3.2	3.4	5.8	6.3	6.4	6.7	5.5	5.2	6.4	4.9	4.7	
$\Delta H^{\ddagger}(298)$	2.0	2.5	2.7	5.0	5.5	5.6	6.0	4.8	4.5	5.7	4.2	4.0	
$E_a(298)$	3.2	3.7	3.9	6.2	6.7	6.8	7.2	6.0	5.7	6.8	5.3	5.1	
$E_a(298)$-W	3.1	3.6	3.8	5.8	6.3	6.4	6.7	5.5	5.2	6.4	4.9	4.7	
ΔE	-30.4	-33.7	-33.2	-31.6	-31.9	-31.4	-34.3	-34.7	-34.4	-32.4	-32.9	-32.7	
$\Delta H(0)$	-26.3	-29.6	-29.1	-27.2	-27.5	-27.0	-30.0	-30.4	-30.1	-28.0	-28.5	-28.3	
$\Delta H(298)$	-26.5	-29.8	-29.3	-27.5	-27.8	-27.3	-30.2	-30.6	-30.3	-28.3	-28.8	-28.6	
						$\cdot CH_3 + HSn(CH_3)_3 \rightarrow CH_4 + \cdot Sn(CH_3)_3$							
$\Delta E^{\ddagger}$	2.4			6.0			6.5						
$\Delta H^{\ddagger}(0)$	3.1			6.4			6.4						
$\Delta H^{\ddagger}(298)$	2.7			6.0			5.7						
$E_a(298)$	3.8			7.2			6.9						
$E_a(298)$-W	3.8			6.7			6.3						3.2[a]
ΔE	-30.9			-31.1			-33.5			-31.5			
$\Delta H(0)$	-26.4			-26.3			-28.7						
$\Delta H(298)$	-26.7			-26.6			-29.1						
						$\cdot C(CH_3)_3 + HSn(CH_3)_3 \rightarrow HC(CH_3)_3 + \cdot Sn(CH_3)_3$							
$\Delta E^{\ddagger}$	3.9			7.1			2.7						
ΔE	-22.3			-21.4			-26.7			-24.2			
$\Delta H(0)$	-17.8			-16.8			-22.4						
$\Delta H(298)$	-18.3			-17.4			-22.9						

[a] Ref. [236].

Table 27: Energies of activation ($\Delta E^{\ddagger}$) and reaction (ΔE) for lead based reactions in kcal mol^{-1}

	B3LYP			BHLYP			MP2			CCSD(T)			
	DZ-pp	TZ-pp	QZ-pp	DZ-pp	TZ-pp	QZ-pp	DZ-pp	TZ-pp	QZ-pp	DZ-pp	TZ-pp	QZ-pp	Expt.
						$\cdot H + PbH_4 \rightarrow H_2 + \cdot PbH_3$							
$\Delta E^{\ddagger}$	0.0	0.0	0.0	0.4	0.4	0.4	3.9	2.9	2.2	2.4	1.3		
$\Delta H^{\ddagger}(0)$	0.0	0.0	0.0	0.5	0.5	0.5	3.8	2.8	2.1	2.3	1.2		
$\Delta H^{\ddagger}(298)$	0.3	0.3	0.3	0.4	0.4	0.4	3.5	2.5	1.8	2.2	1.1		
$E_a(298)$	1.5	1.5	1.5	1.6	1.6	1.6	4.7	3.7	3.0	3.3	2.2		
$E_a(298)$-W	1.5	1.5	1.5	1.5	1.5	1.5	4.2	3.2	2.5	3.0	1.9		
ΔE	-39.0	-41.5	-41.1	-36.9	-39.2	-38.8	-34.9	-37.4	-37.2	-37.3	-39.5	-39.2	
$\Delta H(0)$	-38.0	-40.5	-40.1	-35.8	-38.1	-37.7	-33.6	-36.1	-35.9	-36.1	-38.3	-38.0	
$\Delta H(298)$	-37.5	-40.0	-39.6	-35.4	-37.7	-37.3	-33.2	-35.7	-35.5	-35.7	-37.9	-37.6	
						$\cdot CH_3 + PbH_4 \rightarrow CH_4 + \cdot PbH_3$							
$\Delta E^{\ddagger}$	0.2	0.5	0.7	2.6	2.9	3.1	3.9	2.8	2.6	3.5	2.2	2.0	
$\Delta H^{\ddagger}(0)$	1.3	1.6	1.8	3.7	4.0	4.2	4.6	3.5	3.3	4.2	2.9	2.7	
$\Delta H^{\ddagger}(298)$	0.7	1.0	1.2	2.9	3.2	3.4	3.9	2.8	2.6	3.6	2.3	2.1	
$E_a(298)$	1.9	2.2	2.4	4.1	4.4	4.6	5.1	4.0	3.8	4.7	3.4	3.2	
$E_a(298)$-W	1.9	2.2	2.4	4.0	4.3	4.5	4.9	3.8	3.6	4.6	3.3	3.1	
ΔE	-40.0	-43.4	-42.7	-41.0	-41.4	-40.8	-43.4	-44.2	-43.8	-41.7	-42.4	-42.2	
$\Delta H(0)$	-35.8	-39.2	-38.5	-36.5	-36.9	-36.3	-39.0	-39.8	-39.4	-37.2	-37.9	-37.7	
$\Delta H(298)$	-36.1	-39.5	-38.8	-36.8	-37.2	-36.6	-39.3	-40.1	-39.7	-37.5	-38.2	-38.0	
						$\cdot CH_3 + HPb(CH_3)_3 \rightarrow CH_4 + \cdot Pb(CH_3)_3$							
$\Delta E^{\ddagger}$	0.7			3.3			4.0						
$\Delta H^{\ddagger}(0)$													
$\Delta H^{\ddagger}(298)$													
$E_a(298)$													
$E_a(298)$-W													
ΔE	-42.6			-42.4			-44.8			-43.0			
$\Delta H(0)$													
$\Delta H(298)$													
						$\cdot C(CH_3)_3 + HPb(CH_3)_3 \rightarrow HC(CH_3)_3 + \cdot Pb(CH_3)_3$							
$\Delta E^{\ddagger}$	1.2			3.7									
$\Delta H^{\ddagger}(0)$													
$\Delta H^{\ddagger}(298)$													
$E_a(298)$													
$E_a(298)$-W													
ΔE	-33.9			-32.6			-38.1			-35.7			
$\Delta H(0)$													
$\Delta H(298)$													

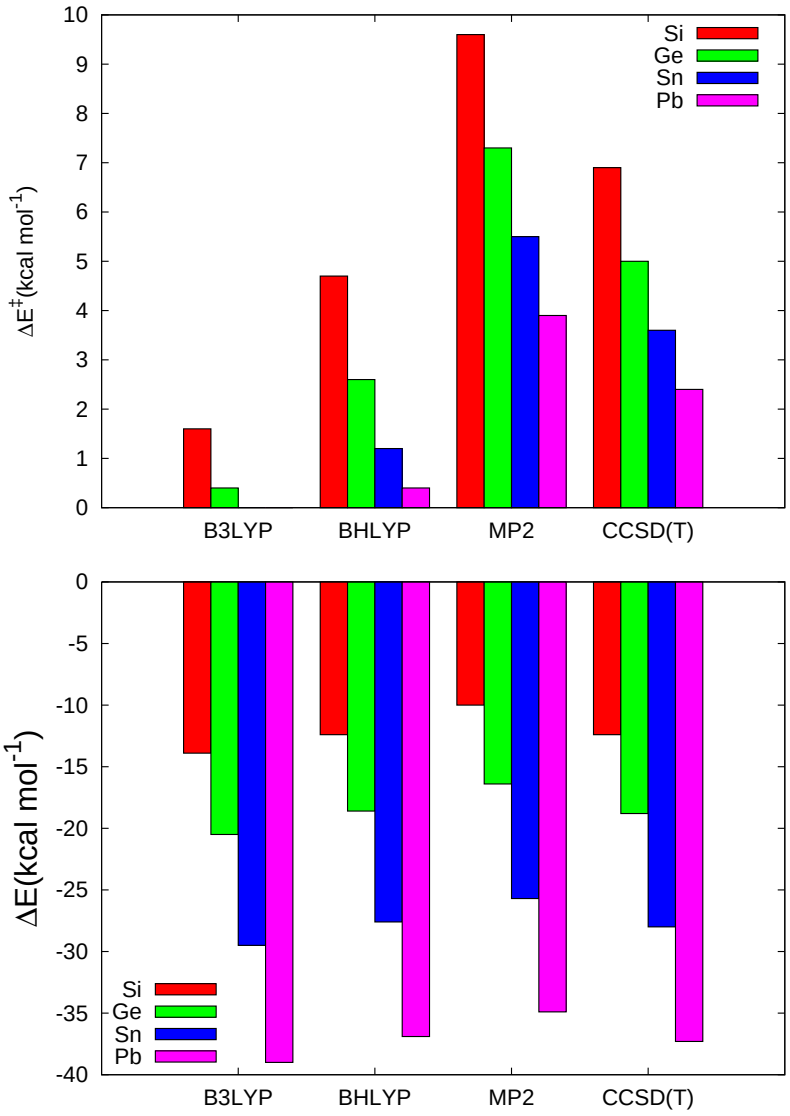

Figure 26: Classical barriers (top) and energies of reactions (bottom) for H· + XH_4 → H_2 + · XH_3

5.3.3 Levels of Theory

Most density functionals underestimate hydrogen abstraction barriers due to self-interaction error. This phenomenon is particularly stark in the case of pure functionals such as BLYP and hybrid functionals lacking in HF exchange such as B3LYP. BHLYP, which contains 50% HF exchange largely corrects this problem and predicts hydrogen abstraction barriers reasonably accurately. For Reactions (30) and (31), B3LYP predicts very low activation barriers while BHLYP gives barriers that are comparable to MP2. For Reactions (32) and

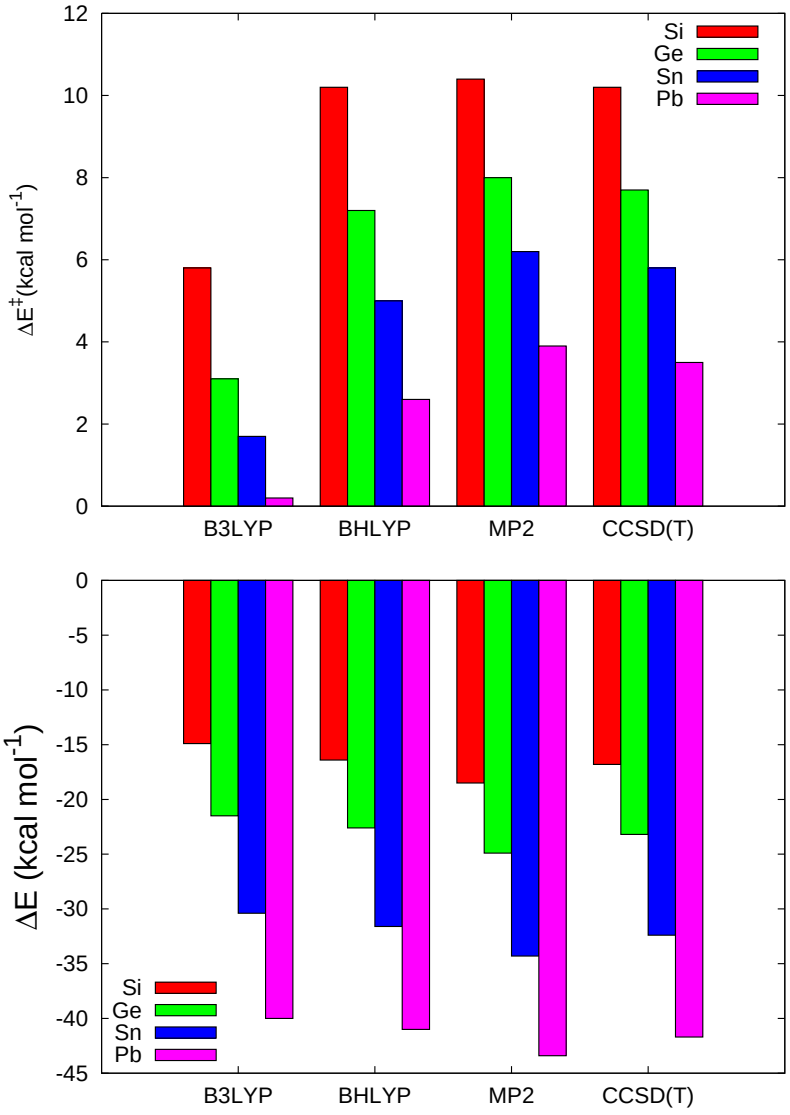

Figure 27: Classical barriers (top) and energies of reactions (bottom) for $\cdot CH_3 + XH_4 \rightarrow CH_4 + \cdot XH_3$

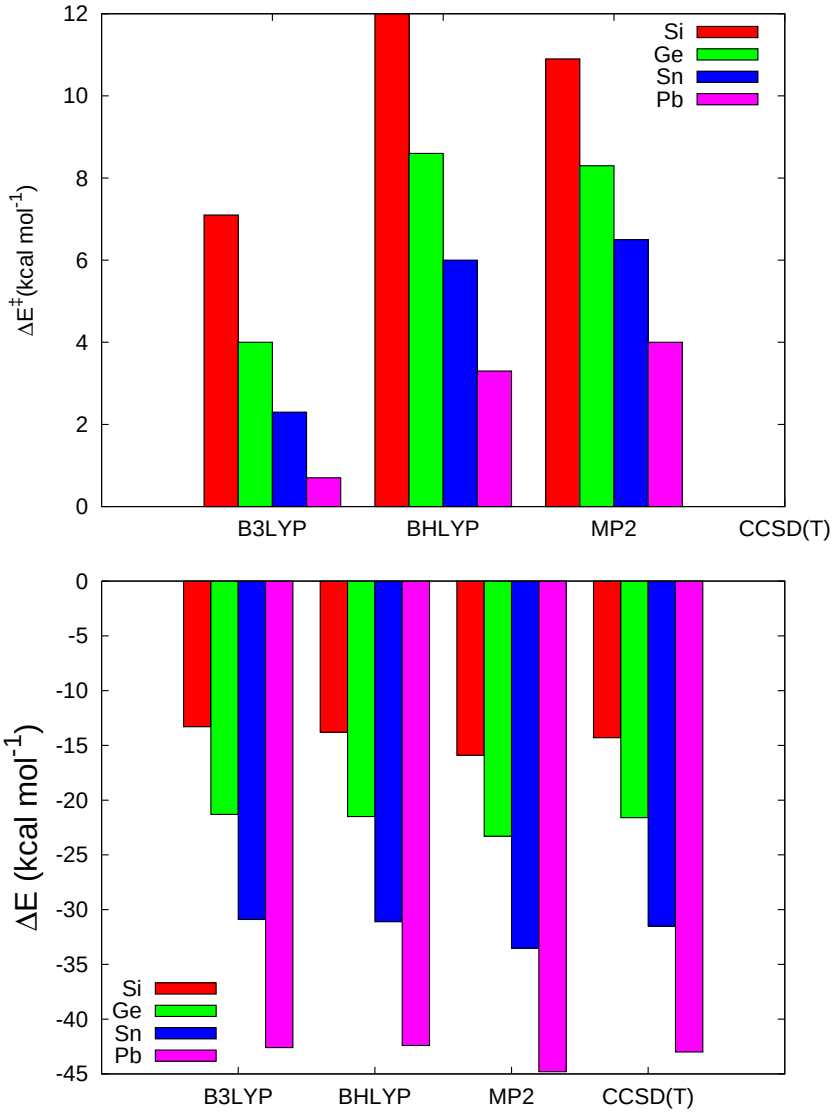

Figure 28: Classical barriers (top) and energies of reactions (bottom) for $\cdot CH_3 + HX(CH_3)_3 \rightarrow CH_4 + \cdot X(CH_3)_3$

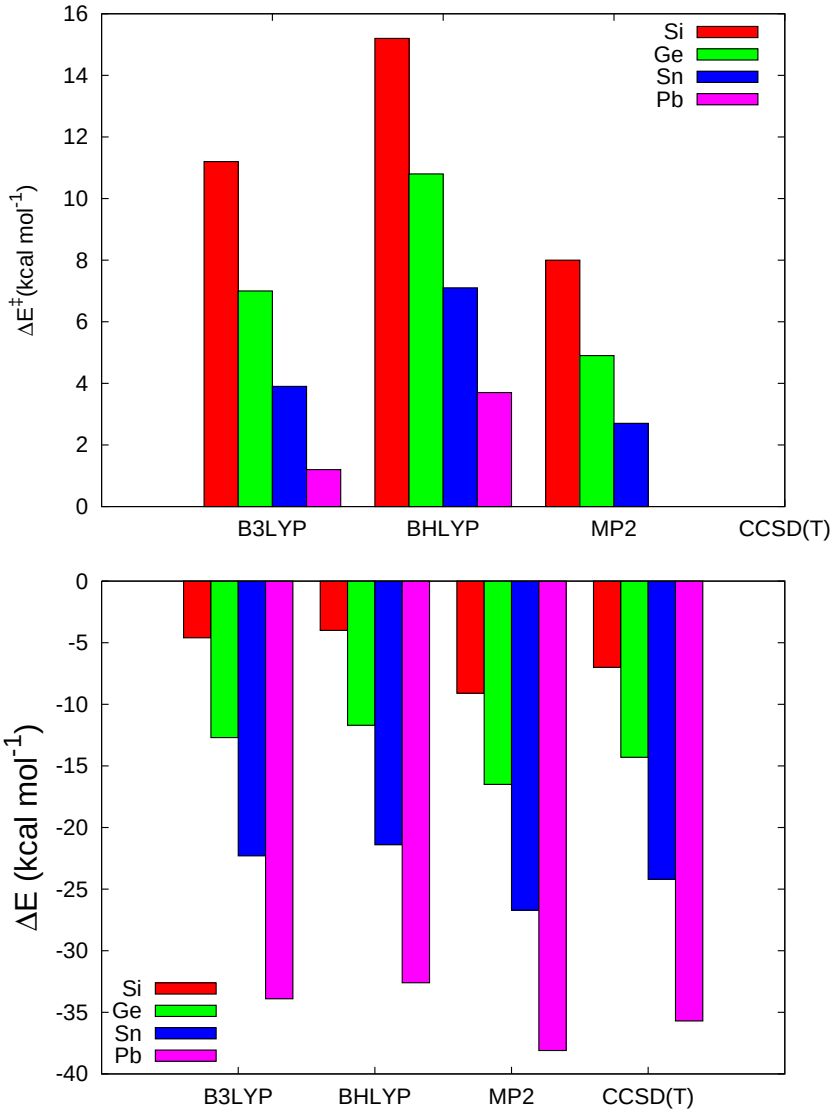

Figure 29: Classical barriers (top) and energies of reactions (bottom) for $\cdot C(CH_3)_3 + HX(CH_3)_3 \rightarrow HC(CH_3)_3 + \cdot X(CH_3)_3$

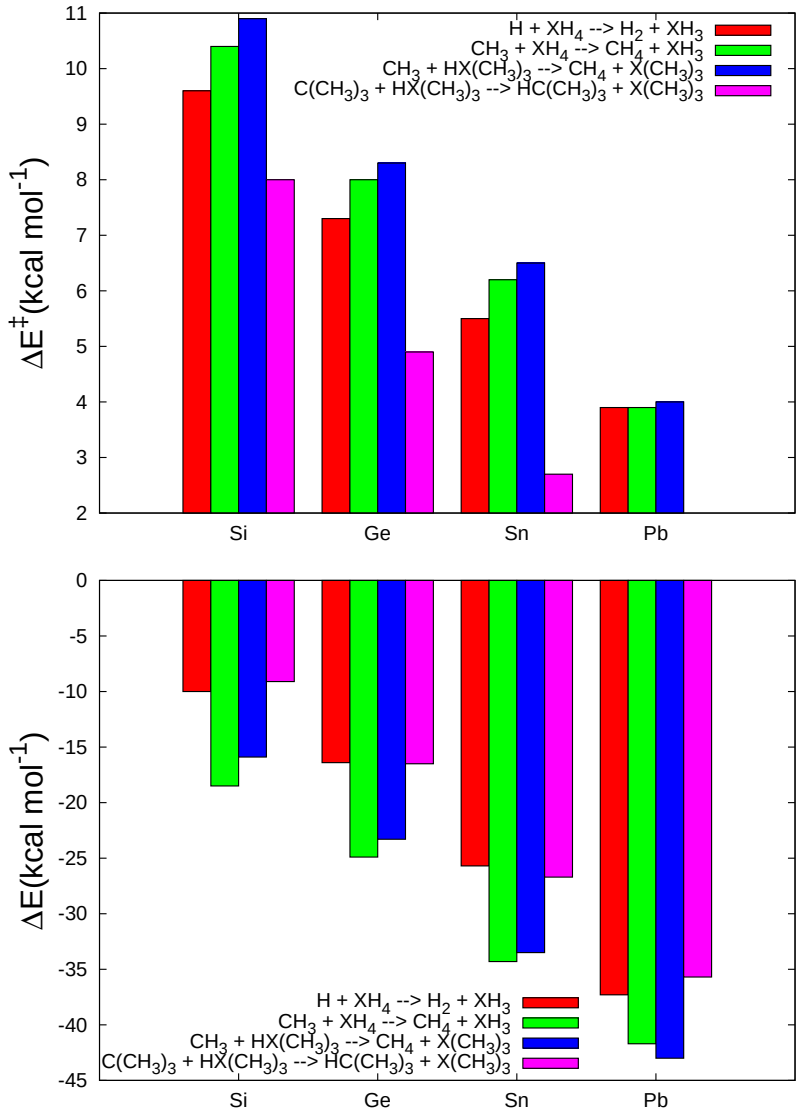

Figure 30: RMP2/DZ classical barriers (top) and energies of reactions (bottom) for Reactions (30) - (33)

(33), however, BHLYP barriers are sometimes larger than those predicted by B3LYP as well as MP2 and CCSD(T), particularly for the case of reactions involving a tin or lead bridgehead.

For a set of hydrogen transfer reactions, Hoz *et al.* demonstrated that B3LYP barriers are usually lower than those from experiment and that the disparity between the two gets larger as the hydrogen donor and/or acceptor becomes more electronegative[184]. While the lack of experimental barriers limits our ability to verify the observations of Hoz *et al.*, For our systems, the electronegativity of the bridgehead atoms increases in the order Pb(1.80) < Si(1.91) < Sn(1.96) < Ge(2.01) < H(2.2) < C(2.55)[165]. Since the electronegativities of our donor bridgeheads (Si, Ge, Sn and Pb) are fairly similar, we would expect B3LYP to perform comparably for them all. Our results do show that the performance of B3LYP compared to CCSD(T) is fairly independent of the donor bridgehead. We do, however, see that both B3LYP and BHLYP are comparable to MP2 and CCSD(T) for Reaction (32) and (33) than they do for Reactions (30) and (31). While a simple electronegavity argument may not explain that pattern, a close look at the bond dissociation energy ($D_{298}{}^{0}$) can. For the H–H, H–CH_3 and H-t-C_4H_9 bond dissociation energies, $D_{298}{}^{0}$, 104.2, 104.9 and 96.5 kcal mol^{-1}, respectively. The weaker C-H bond in isobutane suggests that the bridgehead carbon is somewhat "less electronegative". Assuming the X-H bond dissociation energy for other H-XH_3 is larger than that for H-t-XC_3H_9, B3LYP would perform better for reactions involving the substituted isobutanes, such as Reactions (32) and (33), than it would for substituted methane reactants.

As noted in our previous paper[225], MP2 has a tendency to overestimate barriers relative to CCSD(T) and the same pattern is observed here. This overestimation is most pronounced for Reaction (30). MP2 energies of reaction are typically 2 kcal mol^{-1} higher than those of CCSD(T) for Reaction (30) and 2 kcal mol^{-1} lower for Reactions (31)-(33). These deviations of MP2 from CCSD(T) highlight the importance of correlation treatment to get the right barriers and energies of reaction.

5.3.4 Activation Barriers

Surprisingly, B3LYP barriers match experimental values better than any of the other methods for the reactions for which comparison with experiment was possible. One could discount the reasonable agreement between B3LYP barriers and experiment as purely fortuitous but B3LYP performs reasonably well for all four reactions for which we have experimental barriers. How can we account for this difference between CCSD(T) and experimental values? A few possibilities include:

- The inclusion of diffuse functions is very important, especially in MP2 and CCSD(T) calculations. When using a double-ζ quality basis set in MP2 and CCSD(T) calcualtions, the difference between including and excluding diffuse functions could be as much as 2 kcal mol^{-1} on activation barriers. For the more complete triple- and quaduple-ζ basis sets, that difference goes down to well below the 1 kcal mol^{-1} mark.

- Our core-freezing scheme for cc-pVNZ basis sets as well as cc-pVNZ-pp pseudopotentials did not correlate the highest lying d-electrons. While the freezing of these d-electrons is justified[241], correlating them might be necessary to achieve high accuracy.

- While CCSD(T) is considered to be the "gold standard of quantum chemistry",it does occasionally suffer especially in describing systems systems that have any orbital or configurational near-degeneracies. Such cases can arise in the transition state regime as one bond is breaking and another forming and a single determinant reference wavefunction is inadequate. In coupled cluster theory, the inclusion of the single excitations allows the HF MOs to relax in order to describe any multireference character in the system Thus, the size of these T_1 amplitudes could be very helpful in gauging the quality of the reference HF determinant – a large T_1 amplitude would suggest a poor reference while a smaller T_1 would indicate otherwise. Based on that concept, T_1[215, 216] and D_1[258, 259] diagnostics have been developed for MP2 and CCSD wavefunctions. For T_1 diagnostic values below 0.02, CCSD performs well while higher values call for a multireference treatment. CCSD also does well for a D_1 diagnostic of

less than 0.02 but suffers significantly for values exceeding 0.05. Due to the similarity in the CCSD and CCSD(T) T_1 amplitudes, these diagnostics are also indicative of the quality of the single determinant reference wavefunction for CCSD(T) wavefunctions. While there are only two instances of a T_1 diagnostic eclipsing the 0.02 threshold, numerous systems come close. A large number of the D_1 diagnostic values are in the intermediate regime ($0.02<D_1<0.05$) where CCSD performs fairly but not exceptionally well. A preliminary look at these diagnostics indicates that some multireference character might be important for some of these systems. The relatively large T_1 and D_1 diagnostic values might imply a poor description by CCSD and CCSD(T) and hence an erroneous barrier.

- The experimental data was gathered at a different temperature regime than 298 K. Considering activation barriers are inherently sensitive to temperature, it is possible that the choice of temperature regime could account for some of the discrepancy between our values and that of experiment. However, the experimental barriers we report are generated by fitting kinetics data from different experiments over various temperature ranges and they represent the best fit. Fitting limited data in the proximity of 298 K yielded barriers that are not very different from those inferred by fitting kinetics data over a much larger temperature range.

Figures 26, 27, and 28 show that barriers computed using DFT differ from MP2 and CCSD(T) ones most significantly for Reaction (30), where B3LYP and BHLYP classical barriers are as much as 8 and 4 kcal mol^{-1} lower than MP2 barriers, respectively. B3LYP has difficulty predicting barriers for reactions involving atomic hydrogen, as indicated for the simple reaction $H_2 + H \rightarrow H + H_2$ where UB3LYP/DZ and RB3LYP/DZ classical barriers deviated from experiment by 6.7 and 4.9 kcal mol^{-1}[225]. The comparison of classical barriers among the different methods gets progressively better for Reactions (31)-(33), as shown in Figures 27 to 29.

5.3.5 Hydrogen Donation Tool

For mechanosynthesis of diamond to be realized, it is imperative that the abstraction and deposition tools have favorable thermodynamics, facile kinetics, and good positional control[111, 112, 113, 114, 115, 116]. The most natural tool for these purposes would be something like a scanning probe microscopy (SPM) tip[112], which has already been used for sub-nanometer manipulation of atoms[120]. We can model the SPM tip with a Si/Ge/Sn/Pb bridgehead substituted isobutane. The donation of a hydrogen from this tool has low barriers and high exothermicities.

Figure 30 shows general trends in the thermochemistry of the different models we have looked at. The classical barriers for our four model reactions decrease monotonically as the Group IVA bridgehead changes in the order Si $\rightarrow$ Ge $\rightarrow$ Sn $\rightarrow$ Pb. For each Group IVA bridgehead, as the size of our model reactions increased from Reaction (30) to (32), we notice a moderate increase in classical barriers. However, there is a significant drop in classical barrier heights going from Reaction (32) to Reaction (33), our largest model. The energies of reaction become progressively more exothermic as the Group IVA bridgehead gets heavier. Within each individual bridgehead, the energies of reaction are small for Reactions (30) and (33) and and larger for Reactions (31) and (32).

The type of hydrogen donation tool proposed in our study is one where an SPM tip is mounted with one of the four bridgeheads, namely Si, Ge, Sn and Pb to which a hydrogen is loosely bound. Of the four models of hydrogen transfer reactions studied for each type of bridgeheads, the reactions of type $\cdot C(CH_3)_3 + HX(CH_3)_3 \rightarrow HC(CH_3)_3 + \cdot X(CH_3)_3$, X=Si, Ge, Sn, and Pb best represent a realistic model. Upon the approach of a radical site, the hydrogen bound to the bridgehead would be abstracted by the radical site. Ideally, one would want this abstraction process to be kinetically fast and positionally selective. Of the four bridgeheads we have looked at, the lead containing tool has the smallest barrier to hydrogen donation ($\Delta E^{\ddagger}$ = 3.7 kcal mol^{-1} at the BHLYP/DZ-pp level. is also the most exothermic with a $\Delta H(298)$ of -32.6 kcal mol^{-1} at the BHLYP/DZ-pp level. Nevertheless, all tooltips perform the required hydrogen donation function adequately; choice of tooltip for a given application will involve design tradeoffs among other factors.

Figure 31 shows the C-X-H (X=Si, Ge, Sn, Pb) bending potential of $HX(CH_3)_3$ computed at the MP2/DZ[-pp] level of theory. Since many modes contribute to the C-X-H bending, it was not possible to map the vibrational energy levels and determine the positional selectivity of a hydrogen donation tool modeled simply as $HX(CH_3)_3$. One can however take the potential energy curve and compute the classical turning points (ignoring zero-point vibrational energy). At a given temperature, we can approximate the positional selectivity or positional uncertainty of the hydrogen donor due to thermal motion. Table 28 lists the classical turning points and associated positional uncertainties for tools with various bridgeheads. The bending curve is generated by fixing the $HX(CH_3)_3$ at its RMP2/DZ-[pp] optimized geometry and varying only the C-X-H ending coordinate. Positional uncertainty is ≤ 0.22 Åat 298 K for all tooltips, or one-tenth the ~ 2.5 Åmean spacing between two closest hydrogens on H-terminated C(111) diamond surface[122], potentially allowing excellent positional control during hydrogen donation.

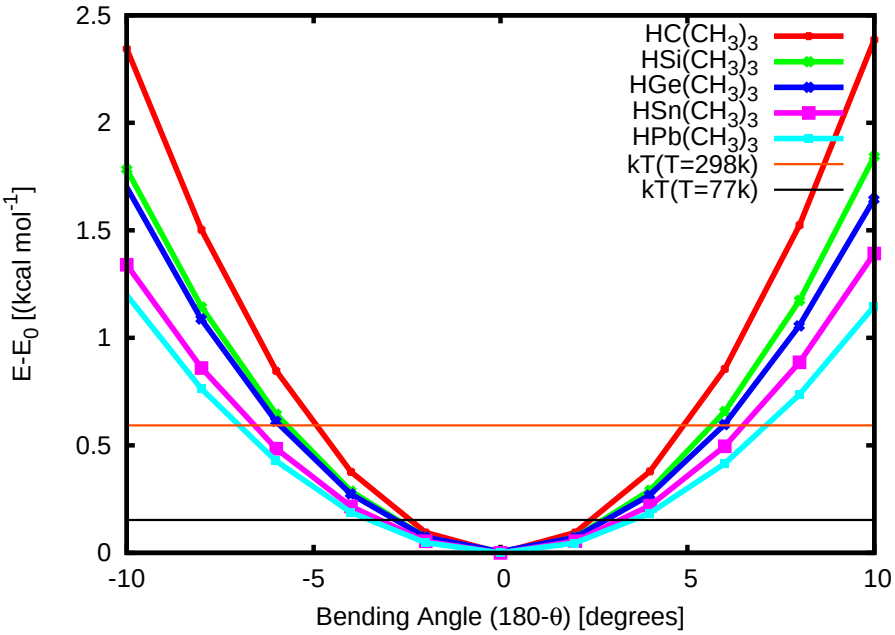

Figure 31: MP2/DZ[-pp] bending potential for $HX(CH_3)_3$ where X=C, Si, Ge, Sn and Pb

A legitimate concern for the feasibility of hydrogen donation via a lead-based tool is whether the hydrogen is bound tightly enough to be maneuvered around and donated to a radical site. The X-H (X=Si, Ge, Sn, Pb) bond strength can be gauged from bond

Table 28: Positional uncertainty of $HX(CH_3)_3$-type tools (where X=Si,Ge,Sn,Pb) due to thermal motion computed from classical turning points. All computations done at MP2/DZ[-pp][a] level.

	R[X-H] (Å)	Angular Uncertainty (Deg.)		Positional Uncertainty (Å)	
		77 K	298 K	77 K	298 K
C	1.11	2.4	4.9	0.05	0.09
Si	1.50	2.8	5.7	0.07	0.15
Ge	1.55	2.8	5.9	0.08	0.16
Sn	1.73	3.2	6.6	0.10	0.20
Pb	1.78	3.5	7.0	0.11	0.22

[a] cc-pVDZ basis set for Si and cc-pVDZ-pp pseudopotential for Ge, Sn and Pb.

enthalpy of the analogous diatomic hydrides. The X-H bond enthalpies increase in the order Pb-H(37.5) < Sn-H(63.1) < Si-H(71.5) < Ge-H(76.9) < C-H(80.9 kcal mol^{-1})[165]. The Arrhenius equation for the one-step thermal desorption rate $k_1 = \nu\ e^{-E_d/k_BT}$ may be used to crudely approximate the canonical residence time for an H atom chemisorbed to a tooltip heated to temperature T[260]. Taking T = 300 K, k_B = 1.381 x 10^{-23} J/K (Boltzmann's constant), E_d = 1.6 eV for the weakest Pb-H bonded tooltip, and the pre-exponential constant $\nu \sim k_BT/h \sim 6$ x 10^{12} s^{-1} (h = 6.63 x 10^{-34} J-s) typically used for thermally migrating chemisorbed hydrogen adatoms on diamond surface[260, 261, 262] (the precise value of which does not sensitively influence the conclusion), the lifetime of the H atom against spontaneous dissociation from the Pb-based tooltip is ${k_1}^{-1} \sim 10^{14}$ s, allowing sufficient time to maneuver the hydrogen until it reaches the radical site.

5.4 Conclusions

Hydrogen transfer from Si, Ge, Sn and Pb bridgehead substituted methane and isobutane to methyl and t-butyl radical sites is investigated theoretically using high-level electronic structure theory methods. The importance of using a small-core pseudopotentials in getting accurate barriers and reaction energies is demonstrated. The use of a tooltip hydrogen attached to a bridgehead Group IVA element as a possible hydrogen donation tool in the mechanosynthesis of diamondoids appears feasible, with reaction energy barriers decreasing and reaction exoergicities increasing for the Si → Ge → Sn → Pb methane and isobutane bridgehead substituent series.

CHAPTER VI

HYBRID CORRELATION MODELS BASED ON ACTIVE-SPACE PARTITIONING: SEEKING ACCURATE O(N^5) AB INITIO METHODS FOR BOND BREAKING

Møller-Plesset second-order MP2 perturbation theory remains the least expensive standard ab initio method that includes electron correlation, scaling as $\mathcal{O}(N^5)$ with the number of molecular orbitals N. Unfortunately, when restricted Hartree-Fock orbitals are employed, the potential energy curves calculated with this method are of little use at large interatomic separations because of the divergent behavior of MP2 in these regions. In a previous study,[263] Bochevarov *et al.* combined the MP2 method with the singles and doubles coupled cluster CCSD method to produce a hybrid method that retains the computational scaling of MP2 and improves PR dramatically the shape of the MP2 curves. In this work we expand the hybrid methodology to several other schemes. We investigate a new, improved MP2-CCSD method as well as a few other O N5 methods related to the Epstein-Nesbet pair correlation theory. Nonparallelity errors across the dissociation curve as well as several spectroscopic constants are computed for BH, HF, H_2O, CH^+, CH_4, and Li_2 molecules with the 6-31G* basis set and compared with the corresponding full conguration interaction results. We show that among the $\mathcal{O}(N^5)$ methods considered, our new hybrid MP2-CCSD method is the most accurate and signicantly outperforms MP2 not only at large interatomic separations, but also near equilibrium geometries.[1]

6.1 Introduction

The accurate description of potential energy surfaces (PES's) has been and still remains one of the primary objectives of quantum chemistry [161]. Unfortunately, the standard hierarchy of single-reference electron correlation methods does not work reliably for bond-breaking reactions, particularly for reactions which make or break multiple bonds. The standard

[1] Adapted from A. Bochevarov, B. Temelso, and C.D. Sherrill, J. Chem. Phys. 125 (2006) 054109.

flavors of density functional theory (DFT) are usually unsuitable for the computation of PES's due to their poor qualitative and quantitative performance, especially at stretched geometries [155, 264]. Although a variety of multireference methods can provide accurate results in virtually any bond-breaking reaction, in practice they tend to be difficult to derive, implement, and use, and moreover they can be very expensive computationally. Thus it remains desirable to investigate more "black box" bond-breaking methods with favorable computational scaling. Recent work along these lines includes new methods by Head-Gordon and co-workers based on ideas from the generalized valence bond perfect-pairing approach [265, 266, 267], the spin-flip approach of Krylov [268, 269, 270, 271, 272], and the method of moments and completely-renormalized coupled-cluster methods of Piecuch [273, 274, 275, 276]. In this work, we explore hybrids of coupled-cluster and perturbation theories for reactions breaking single bonds.

Among the standard quantum chemical methods based on the restricted Hartree-Fock (RHF) reference, the cheapest qualitatively correct method for breaking single bonds in the ground state is the coupled cluster theory with the inclusion of single and double excitations (CCSD) [277, 278]. Its formal scaling with the total number of occupied (o) and virtual (v) molecular orbitals and the number of iterations N_{it} required to converge the nonlinear CCSD equations is $N_{\mathrm{it}}o^2v^4$. When we refer to the quality of the method in relation to bond breaking we mean the correctness of the shape of the potential energy curve produced by this method rather than the absolute error in energy. The CCSD energy curves for reactions breaking single bonds usually overestimate the dissociation energy but they are smooth and devoid of artifacts such as divergence at large interatomic distances. The latter defect is only too common among the methods which utilize the perturbation theory: for example, both the second-order Møller-Plesset (MP2) theory and the CCSD(T) method [146] (often referred to as the "golden standard" of quantum chemistry) fail catastrophically at non-equilibrium geometries [155, 279]. The failure of MP2 is especially regrettable since this method has a very low computational scaling, $\mathcal{O}(N^5)$, where N is the total number of orbitals, $N = o + v$. Another method that has a low formal scaling, $N_{\mathrm{it}}N^5$, is the CC2 method of Christiansen *et al.* [280] Unfortunately, its behavior at large interatomic distances

remains largely unexplored (see, however, studies of CC2 energy curves around equilibrium geometries in Refs. [281, 282]). We touch on this topic in the current study.

Alternatively, when standard single-reference methods are used in conjunction with unrestricted Hartree-Fock (UHF) orbitals, the divergence at large interatomic distances is remedied. However, the UHF-based correlated wave functions often suffer from the serious spin contamination [211, 283]. Besides, the potential energy curves obtained by these methods can display an erroneous behavior in the intermediate bond-breaking region. In the case of UMP2 this erroneous behavior sometimes becomes so pronounced that it may be regarded as a grave defect of the method [155]. Thus, it appears that one has to tolerate the computational scaling of $N_{\rm it}N^6$ or higher in order to study the bond-breaking processes with at least qualitative correctness. Recently [284], we proposed a very simple computational scheme which scales as N^5 but approaches the CCSD method in accuracy. This method, which we originally denoted as MP2-CCSD [in this paper we refer to it as MP2-CCSD(I)], is a hybrid between the MP2 and the CCSD theories and benefits from the scaling of the former and the accuracy of the latter. It relies on the orbital partitioning into active and restricted spaces, which might seem unfortunate in that the user must choose which orbitals to make active. However, we verified that even in the case of the minimal active spaces (which can often be determined *a priori*) our method performs in a very satisfactory manner and is a vast improvement over MP2. With the modest increase of the size of the active space (which does not deteriorate the favorable N^5 scaling) the potential energy curves generated by MP2-CCSD(I) become essentially parallel to those generated by CCSD. In this work we describe and test a new $\mathcal{O}(N^5)$ hybrid method MP2-CCSD(II) which is similar to MP2-CCSD(I) in structure but is significantly more accurate so that it rivals CCSD in accuracy even when the minimal active spaces are used. In section II we present the methodology behind the MP2-CCSD(I) method and in section III we give the description of the MP2-CCSD(II) method. Illustrative results are presented in section IV.

6.2 Hybrid Methodology

For RHF or UHF orbitals, the correlation energy of MP2 theory is written as the sum over all possible double excitations. It is always possible to formally divide the orbital space into four disjoint subsets: occupied active, occupied restricted, virtual active and virtual restricted orbitals [see Figure 32(a)]. Note that, so far, the denominations 'restricted' (R) and 'active' (A) do not indicate any constraint on the orbital excitations – these names are simply used for the notational convenience.

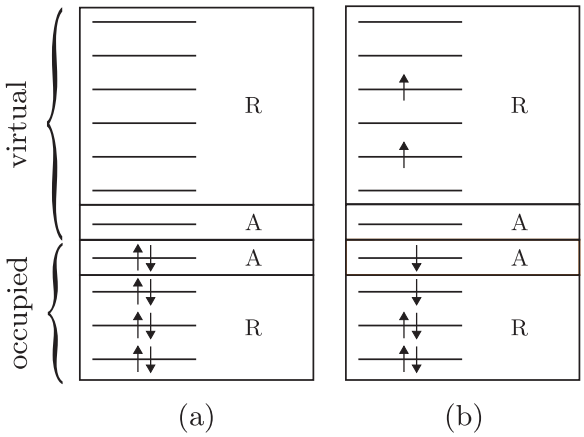

Figure 32: (a) The separation of the orbital space into four subspaces. (b) An example of our notation: ARRR-type excitation.

Any double excitation from the closed-shell reference shown symbolically in Figure 32(a) may be then labelled by the four-letter code $WXYZ$ where the first two letters (W and X) stand for the subspaces (A or R) from which the excitation was made and the last two letters (Y and Z) indicate the subspaces to which the electrons were excited. Obviously, $WXYZ$ is equivalent to $XWYZ$ etc. As an example, Figure 32(b) shows a ARRR-type excitation. In a similar manner, any single excitation may be labelled by the two-letter code WX where W shows from which subspace the electron was excited and X to which space it was excited.

Using this notation, we may rewrite the energy expression for the MP2 correlation energy

as the sum of nine contributions:

$$E_{\rm corr}^{\rm MP2} = E_{AAAA}^{\rm MP2} + E_{AAAR}^{\rm MP2} + E_{AARR}^{\rm MP2} + E_{ARAA}^{\rm MP2} + E_{ARAR}^{\rm MP2} + E_{ARRR}^{\rm MP2} + E_{RRAA}^{\rm MP2} + E_{RRAR}^{\rm MP2} + E_{RRRR}^{\rm MP2}. \tag{96}$$

We note that the CCSD spin-orbital energy expression,

$$E_{\rm corr}^{\rm CCSD} = \frac{1}{4}\sum_{ijab}\langle ij||ab\rangle \left(t_{ij}^{ab} + 2t_i^a t_j^b\right), \tag{97}$$

reduces to the MP2 spin-orbital expression in the event that single excitations are neglected ($t_i^a = 0$) and the doubles amplitudes are fixed in their first-order form, $t_{ij}^{ab(1)} = \langle ij||ab\rangle/(\epsilon_i + \epsilon_j - \epsilon_a - \epsilon_b)$. Indeed, the MP2 energy is given as the first iteration of the CCSD procedure for RHF or UHF orbitals when the MP2 guesses are used for the amplitudes. This close connection between MP2 and CCSD is exploited in the current study.

In our previous work [263] we demonstrated for several small molecules that the $AAAA$ term, comprising no more than a handful of excitations for small active spaces, is primarily responsible for the divergence of the MP2 energy at large interatomic separations. The mechanistic substitution of the $E_{AAAA}^{\rm MP2}$ term with the $E_{AAAA}^{\rm CCSD}$ term (obtained from the CCSD calculation either in the full or active orbital space) in (96), which we called MP2+CCSD, does not lead to a very satisfactory potential energy curve, although even this simple operation redresses the sharp divergence of the MP2 energy curve. The MP2+CCSD energy curves show a small but nevertheless noticeable 'turning over' at large interatomic distances which is clearly not a physical behavior. The recipe for the proper replacement of $E_{AAAA}^{\rm MP2}$ is to do so *self-consistently*, that is adjust the $AAAA$-contribution in the presence of other contributions. This idea lies in the foundation of hybrid methods previously developed by Nooijen [285] for the investigation of excited states. The method that employs this methodology includes the following simple steps:

(i) Set up a CCSD calculation using the MP2 t_i^a and t_{ij}^{ab} amplitudes as a guess: $t_i^a = 0$ and $t_{ij}^{ab} = \langle ij||ab\rangle/(\varepsilon_i + \varepsilon_j - \varepsilon_a - \varepsilon_b)$.

(ii) Procede with solving the CCSD equations but update only the those single and double t-amplitudes that involve excitations within the active space only.

(iii) Terminate the iterations when the active space amplitudes and energy no longer change.

This approach which we called MP2-CCSD in our previous paper [263] will be referred to as MP2-CCSD(I) in the present paper. The convergence of this procedure is usually no worse than the convergence of the conventional CCSD equations. If the typical dimension of the active space is on the order of just a few orbitals (σ and σ^* for the minimal active space), then step (ii) has the computational expense around $\mathcal{O}(N^4)$. The next section introduces an improved MP2-CCSD(II) method and gives details as to the scaling of the intermediates which are computed on each iteration step. In summary, the cost of the MP2-CCSD(I) method is dominated by the atomic orbital (AO) to molecular orbital (MO) transformation and is $\mathcal{O}(N^5)$. The potential energy curves generated by the MP2-CCSD(I) method normally level off at stretched geometries and show qualitative and quantitative advantages over the MP2+CCSD curves and dramatic improvements over simple MP2.

It is easy to notice, however, that updating certain other types of amplitudes together with the AA and $AAAA$ amplitudes increases the cost of the resulting hybrid method only marginally and still keeps it much lower than the cost of the regular CCSD method. If we update the AR, RA, and RR single-excitation amplitudes, the cost of this operation will scale as o^2v^3. Further, if we also update the $ARAA$ and $AAAR$ double-excitation amplitudes, the worst scaling that will result from this operation will be o^2v^3V, or simply o^2v^3 if V is on the order of 1. The method in which we update the AR, RA, RR, $AAAA$, $ARAA$ and $AAAR$ amplitudes self-consistently in the presense of the rest of the amplitudes computed by the MP2 method we call the MP2-CCSD(II) method, scaling as $\mathcal{O}(N_{\mathrm{it}}o^2v^3)$. With respect to the increase of the size of the system (if N_{it} is assumed constant), the scaling of MP2-CCSD(II) is still not worse than that of the MP2 method.

In constructing the MP2-CCSD(I) and MP2-CCSD(II) methods we relied on the MP2 theory as a source of inexpensive t-amplitudes. One might ask whether there exists some other choice of the low-cost method. The Epstein-Nesbet (EP) pair-correlation theory or related constructs, whose computational cost is dominated by the AO-MO transformation, is worthy of investigation in this respect. We utilized the following formula for the computation

of the double excitation amplitudes:

$$t_{ij}^{ab} = \frac{\langle ij||ab\rangle}{e_{ij} - \langle \Psi_{ij}^{ab}|H - E_0|\Psi_{ij}^{ab}\rangle}, \tag{98}$$

where E_0 is the Hartree-Fock energy and e_{ij} are pair energies

$$e_{ij} = \sum_{a<b} \langle ij||ab\rangle t_{ij}^{ab} \tag{99}$$

which constitute the correlation energy:

$$E_{\text{corr}} = \sum_{i<j} e_{ij}. \tag{100}$$

Equations (98-99) are solved iteratively until the values t_{ij}^{ab} and e_{ij} no longer change. We call this approach TCEPA (truncated coupled electron pair approximation) because its formulas naturally arise from the truncation of a summation in the well-known CEPA equations [286, 287]:

$$\langle \Psi_{ij}^{ab}|H|\Psi_0\rangle + \sum_{\substack{k<l \\ c<d}} \langle \Psi_{ij}^{ab}|H - E_0|\Psi_{kl}^{cd}\rangle t_{kl}^{cd} = e_{ij} c_{ij}^{ab}, \tag{101}$$

and e_{ij} is

$$e_{ij} = \sum_{c<d} \langle \Psi_{ij}^{cd}|H|\Psi_0\rangle t_{ij}^{cd}. \tag{102}$$

Observe that the neglect of e_{ij} in the denominator of (98) brings us to the second order EN perturbation theory (which is equivalent to EN pair-correlation theory), and further approximation of $\langle \Psi_{ij}^{ab}|H - E_0|\Psi_{ij}^{ab}\rangle$ through $\varepsilon_i + \varepsilon_j - \varepsilon_a - \varepsilon_b$ yields the MP2 theory. Some denominators in the EN perturbation theory approach zero as the bond is being broken. This may be explained by the fact that certain orbitals i and a (as well as j and b) necessarily become degenerate along the dissociation coordinate and the expression $\langle \Psi_{ij}^{ab}|H|\Psi_{ij}^{ab}\rangle$ approaches E_0. A few computations convinced us that the EN perturbation theory diverges even faster than MP2. Murray and Davidson [288], who compared the MP theory with one of the flavors of the EN theory for equilibrium geometries and up to the fifth order in the perturbation, also arrived at the conclusion that MP gives more predictable energies. TCEPA, however, promises a better dissociation behavior than the regular EN perturbation theory. If e_{ij} remains in the denominator (as in TCEPA) then the denominator is not likely

to turn into zero since e_{ij} is the part of the correlation energy which actually becomes constant at the end of the dissociation. We also constructed the hybrid TCEPA-CCSD(I) and TCEPA-CCSD(II) models built exactly after the MP2-CCSD(I) and MP2-CCSD(II) models, respectively (the types of the amplitudes updated are the same). In TCEPA-CCSD(I) and TCEPA-CCSD(II) the t-amplitudes which are not updated in the course of solving the CCSD equations come from equations (98-99). Observe that by combining TCEPA with CCSD we do not attempt to correct or improve some particular feature of TCEPA (as we did it with MP2 by substituting its AAAA amplitudes with the CCSD amplitudes). We merely wish to describe as many amplitudes as possible by a higher-quality method (CCSD) without disturbing the computational scaling of the lower-quality method (TCEPA).

One more $\mathcal{O}(N^5)$ candidate for a possible hybridization with coupled cluster method is CC2. As demonstrated below, the divergence of CC2 at large interatomic separations is even worse than that of MP2, and therefore we ruled out the idea of constructing a hybrid method built upon CC2.

6.3 Results and Discussion

Our first hybrid method based on MP2 amplitudes, MP2-CCSD(I), produces NPE's which are typically several times lower than those of MP2, but still somewhat larger than those of CCSD. MP2-CCSD(II) systematically improves the NPE's even further – it almost always works better than MP2-CCSD(I) and in four cases out of six (BH, HF, H_2O,and CH_4) rivals CCSD. Except for the CH^+ molecule, they are lower than those of MP2, but this improvement is not predictable: sometimes TCEPA improves on MP2 by a factor of two or so (BeH^+, BH, HF, H_2O), and sometimes it even outperforms MP2-CCSD(II) and CCSD. The TCEPA-CCSD(I) and TCEPA-CCSD(II) methods are more systematic in this regard: the NPE's of TCEPA-CCSD(II) are always lower than those of TCEPA-CCSD(I) but they are still typically higher than those of MP2-CCSD(II). Figure 33 displays the NPE's averaged over the test cases considered here. Among the $\mathcal{O}(N^5)$ methods considered here, MP2-CCSD(II) performs best. It is remarkable that the average NPE of MP2-CCSD(II) is just as low as that of CCSD. The second best method is TCEPA-CCSD(II), which confirms

our assumption that the inclusion of some additional amplitudes at the CCSD level should result in higher accuracy.

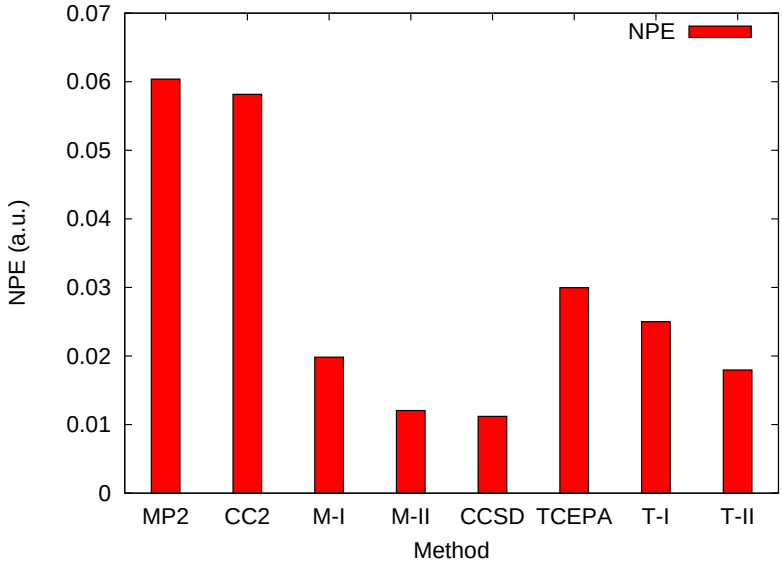

Figure 33: The average non-parallelity errors (NPE) in 6-31G* basis set relative to FCI.

Although MP2 fails at large interatomic distances, it works well near the bottom of the potential energy well. Therefore it is interesting to explore whether the new MP2-CCSD(II) method improves not only the behavior at large internuclear separations, but also the quality of results near equilibrium. If so, MP2-CCSD(II) might be preferable to MP2 not only for bond-breaking applications or cases where electronic near-degeneracies can become important, but also for routine computations of equilibrium molecular properties. Tables 29 and 30 present results for a number of spectroscopic properties, computed by fitting nine energy points evenly spaced by 0.005 Å about the equilibrium bond distance, r_e, to an eighth-order polynomial, $U(r)$. Each energy calculation was converged to at least 10^{-12} Hartrees and fitting errors are monitored to avoid numerical instabilities.

The familiar spectroscopic constants are computed by evaluating the zeroth to fourth-order derivatives of $U(r)$ at r_e and utilizing the following relations [33, 48]:

$$B_e \equiv \frac{h}{8\pi^2 \mu r_e^2}, \quad \omega_e \equiv \frac{1}{2\pi}\left(\frac{U''|_{r_e}}{\mu}\right)^{1/2}, \tag{103}$$

$$\omega_e x_e \equiv \frac{B_e^2\, r_e^4}{4h\omega_e^2}\left(\frac{10B_e\, r_e^2\, \left(U'''|_{r_e}\right)^2}{3h\omega_e^2} - U^{\mathrm{iv}}|_{r_e}\right), \tag{104}$$

$$\alpha_e \equiv -\frac{2B_e^2}{\omega_e}\left(\frac{2B_e\, r_e^3\, U'''|_{r_e}}{h\omega_e^2} + 3\right), \overline{D}_e \equiv \frac{4B_e^3}{\omega_e^2}. \tag{105}$$

Here, μ is the reduced mass, B_e is the rotational constant, ω_e is the harmonic vibrational frequency, $\omega_e x_e$ is the anharmonicity constant, α_e is the vibration-rotation coupling constant, and $\overline{D}_e$ is the centrifugal distortion constant.

Table 29: Spectroscopic constants of H_2, BeH^+, and BH computed using different methods in the 6-31G* basis set

Molecule	Method[a]	E_{min}	r_e	ω_e	$\omega_e x_e$	B_e	α_e	$\overline{D}_e$ (x10^{-4})
	MP2	-1.144141	0.7375	4533.58	126.1	61.502	3.0529	452.75
	CC2	-1.144174	0.7377	4527.85	126.7	61.466	3.0647	453.08
	MP2-CCSD(I)	-1.146218	0.7448	4367.81	143.2	60.305	3.4182	459.83
	MP2-CCSD(II)	-1.149402	0.7499	4297.58	140.1	59.483	3.3815	455.82
H_2	CCSD	-1.151698	0.7462	4367.09	141.7	60.080	3.3615	445.49
	TCEPA	-1.151003	0.7442	4403.38	141.8	60.404	3.3403	454.66
	TCEPA-CCSD(I)	-1.151508	0.7455	4384.19	140.1	60.199	3.3257	454.00
	TCEPA-CCSD(II)	-1.152484	0.7473	4354.30	141.1	59.910	3.3506	453.66
	FCI	-1.151698	0.7462	4367.09	141.7	60.080	3.3615	454.85
	MP2	-14.87313	1.3208	2280.90	34.3	10.660	0.2631	9.315
	CC2	-14.87338	1.3215	2275.49	34.5	10.649	0.2651	9.330
	MP2-CCSD(I)	-14.87368	1.3240	2251.12	37.8	10.609	0.2799	9.426
	MP2-CCSD(II)	-14.87656	1.3338	2176.70	42.6	10.454	0.3086	9.644
BeH^+	CCSD	-14.88154	1.3311	2193.06	40.4	10.496	0.2985	9.618
	TCEPA	-14.87941	1.3264	2269.61	39.1	10.571	0.2322	9.172
	TCEPA-CCSD(I)	-14.87980	1.3283	2252.92	43.2	10.541	0.2437	9.230
	TCEPA-CCSD(II)	-14.88146	1.3339	2214.01	44.3	10.451	0.2492	9.316
	FCI	-14.88159	1.3312	2192.20	40.4	10.495	0.2988	9.621
	MP2	-25.17587	1.2331	2451.40	47.6	12.007	0.3946	11.522
	CC2	-25.17634	1.2339	2443.36	48.3	11.993	0.3986	11.556
	MP2-CCSD(I)	-25.17660	1.2373	2399.63	55.1	11.926	0.4306	11.783
	MP2-CCSD(II)	-25.17780	1.2436	2336.48	57.7	11.805	0.4556	12.054
BH	CCSD	-25.20077	1.2443	2355.06	53.1	11.793	0.4281	11.183
	TCEPA	-25.20511	1.2371	2441.54	48.7	11.930	0.3828	11.393
	TCEPA-CCSD(I)	-25.20505	1.2370	2449.62	45.7	11.933	0.3723	11.327
	TCEPA-CCSD(II)	-25.20541	1.2393	2427.72	47.0	11.887	0.3797	11.400
	FCI	-25.20265	1.2448	2347.73	54.1	11.784	0.4333	11.874

Regarding the total energies at equilibrium, E_{min}, note that those of the TCEPA-based methods are often significantly lower than those of FCI (as mentioned above). The MP2-based hybrid methods as well as CC2 tend to act like MP2 itself in their prediction of E_{min}. Considering the equlilibrium bond length r_e, MP2 systematically underestimates this parameter (except for Li_2), while TCEPA behaves irregularly. Figure 34 shows the root mean square (RMS) errors for the spectroscopic constants. After CCSD, the lowest

Table 30: Spectroscopic constants of CH^+, Li_2 and HF computed using different methods in the 6-31G* basis set

Molecule	Method[a]	E_{min}	r_e	ω_e	$\omega_e x_e$	B_e	α_e	$\overline{D_e}$ (x10^{-4})
	MP2	-37.96526	1.1195	3039.74	62.3	14.468	0.4876	13.111
	CC2	-37.96565	1.1199	3033.28	63.0	14.457	0.4911	13.136
	MP2-CCSD(I)	-37.97142	1.1143	3054.53	74.1	14.601	0.5326	13.346
	MP2-CCSD(II)	-37.97990	1.1160	3024.52	72.3	14.558	0.5385	13.492
CH^+	CCSD	-37.99427	1.1284	2930.87	68.5	14.240	0.5245	13.446
	TCEPA	-37.99884	1.1236	2955.43	43.5	14.362	0.5709	13.566
	TCEPA-CCSD(I)	-37.99592	1.1267	2915.13	37.2	14.282	0.5701	13.713
	TCEPA-CCSD(II)	-37.99712	1.1297	2882.33	21.0	14.208	0.5186	13.809
	FCI	-37.99628	1.1293	2919.43	69.5	14.218	0.5297	13.489
	MP2	-14.88685	2.7731	339.34	2.2	0.625	0.0050	0.085
	CC2	-14.88694	2.7753	337.67	2.2	0.624	0.0051	0.085
	MP2-CCSD(I)	-14.89129	2.7701	330.79	2.4	0.626	0.0055	0.090
	MP2-CCSD(II)	-14.89719	2.7387	334.71	2.8	0.641	0.0058	0.094
Li_2	CCSD	-14.89790	2.7254	340.09	2.8	0.647	0.0054	0.094
	TCEPA	-14.89943	2.7566	329.53	2.4	0.632	0.0054	0.094
	TCEPA-CCSD(I)	-14.89793	2.7381	339.06	2.3	0.641	0.0050	0.092
	TCEPA-CCSD(II)	-14.89932	2.7259	340.08	2.6	0.647	0.0054	0.094
	FCI	-14.89799	2.7249	339.96	2.7	0.647	0.0057	0.094
	MP2	-100.1842	0.9339	4040.83	83.5	20.196	0.7379	20.180
	CC2	-100.1851	0.9349	4019.61	84.8	20.153	0.7458	20.265
	MP2-CCSD(I)	-100.1845	0.9355	3989.97	91.4	20.125	0.7780	20.480
	MP2-CCSD(II)	-100.1856	0.9391	3922.40	90.0	19.974	0.7874	20.719
HF	CCSD	-100.1884	0.9342	4024.03	86.9	20.183	0.7543	20.309
	TCEPA	-100.2339	0.9446	3857.97	97.7	19.742	0.8143	20.678
	TCEPA-CCSD(I)	-100.2337	0.9433	3901.95	87.2	19.793	0.7672	20.373
	TCEPA-CCSD(II)	-100.2328	0.9420	3914.49	90.2	19.849	0.7798	20.413
	FCI	-100.1906	0.9355	3997.62	88.4	20.125	0.7634	20.401

[a] Core 1s electrons in carbon frozen

RMS values of r_e belong to TCEPA-CCSD(II), TCEPA-CCSD(I) and MP2-CCSD(II). The individual equilibrium distances produced by the MP2-CCSD methods are typically smaller than those produced by the TCEPA-CCSD methods. The constants α_e and $\omega_e x_e$ depend on the third and fourth derivatives, respectively, of the potential and so are sensitive to the shape of the potential. MP2-CCSD(II) is the best performer out of hybrid methods for these constants, while the TCEPA-based hybrid methods are inferior to the MP2-based hybrids for these characteristics.

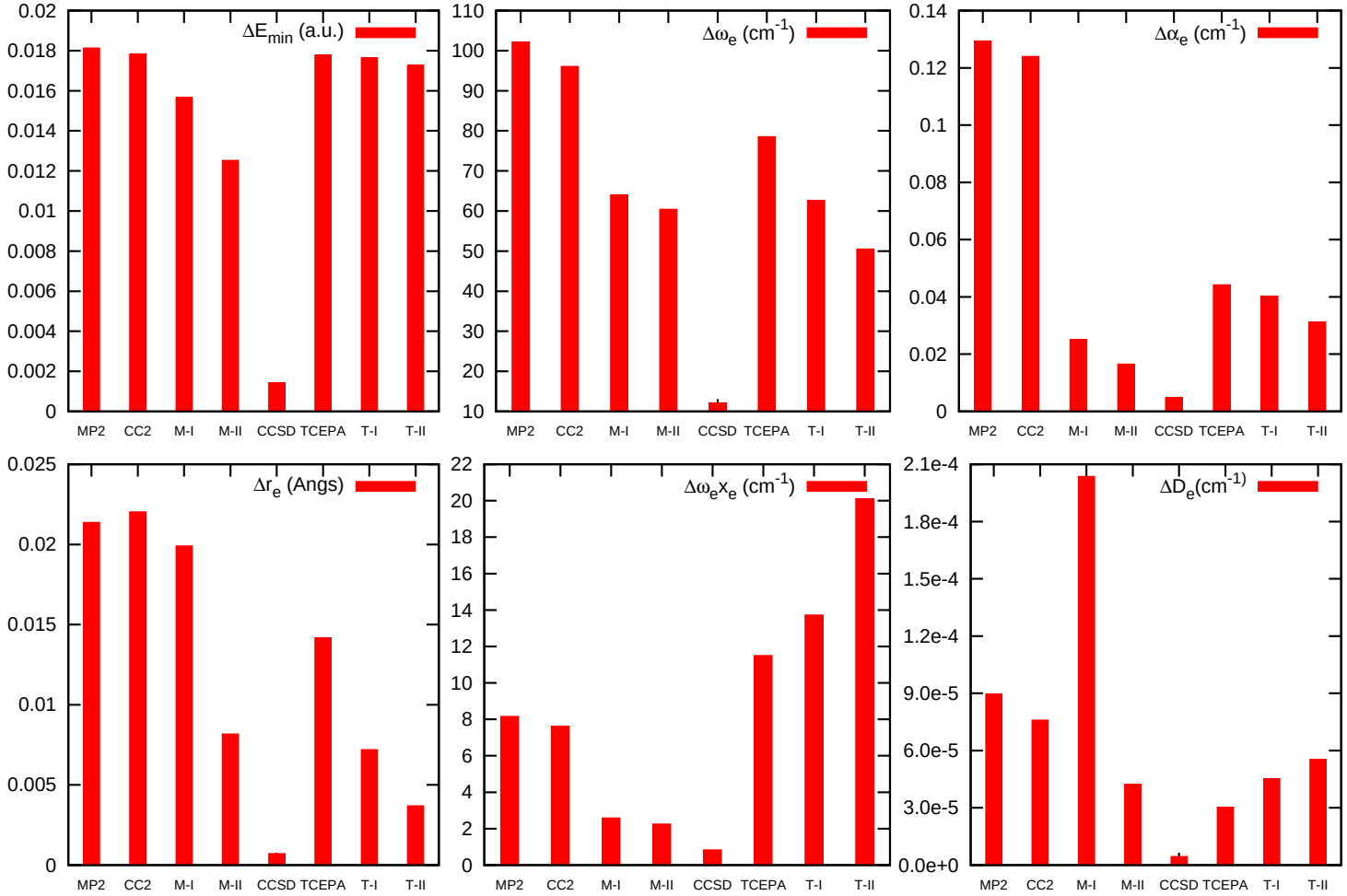

Figure 34: The root mean square (RMS) errors of various spectroscopic constants in 6-31G* basis set relative to FCI. M-I, M-II, T-I, and T-II denote MP2-CCSD(I), MP2-CCSD(II), TCEPA-CCSD(I), and TCEPA-CCSD(II), respectively.

Somewhat unexpectedly, the errors of MP2-CCSD(II) for the α_e, ω_e, and $\overline{D}_e$ constants frequently have the sign different from those of all other methods. The centrifugal distortion constant $\overline{D}_e$ is estimated with similar quality by MP2-CCSD(II) and the TCEPA-based methods, all of which perform better than MP2 or CC2. The larger RMS error observed for MP2-CCSD(I) is due almost entirely to a single poor result for the H_2 molecule. RMS errors for B_e are omitted from Figure 34 because this characteristic is proportional to r_e^{-2} and its errors are tied to r_e errors. Judging from the magnitude of the RMS errors of the spectroscopic constants, we conclude that MP2-CCSD(II) is the most consistent among the $\mathcal{O}(N^5)$ methods near equilibrium. The CC2 method shows only a slight improvement over MP2, while the TCEPA-based methods are apparently the worst performers.

4.5. Conclusions

In this work we have employed hybrid methodology to construct several new methods referred to as MP2-CCSD(II), TCEPA-CCSD(I), and TCEPA-CCSD(II) anticipating to find an $\mathcal{O}(N^5)$ scheme that improves upon the performance of the previous, MP2-CCSD(I), method. The computation of the NPE's and several spectroscopic constants for a number of simple molecules has shown that MP2-CCSD(II) works noticeably better than MP2 and sometimes rivals even CCSD, which scales as $\mathcal{O}(N^6)$. The average NPE error of MP2-CCSD(II) is not worse than that of CCSD. The simplicity of formulation, the inexpensiveness and the accuracy of the MP2-CCSD(II) method express the hope that it might be used instead of MP2 in many situations where the latter is currently applied.

A few limitations of MP2-CCSD(II) (equally applicable to our other hybrid methods) must be mentioned, however. First, we do not expect it to exhibit an impressive performance in cases where CCSD itself should fail. Such cases may include breaking multiple bonds or other cases of strong electronic near-degeneracies. A more sophisticated hybrid scheme may be desirable to deal with these issues. For example, the inclusion of higher than double excitations or accounting for the multireference character of the ground state may be needed. Indeed, work is in progress on such schemes as MP2-CCSDTQ and MP2-MCSCF which will be more suitable to conform to these requirements. Second, as all the methods based on the

active space partitionings, MP2-CCSD(II) obliges the researcher to select a proper active space. We believe than in many cases the minimal dimension of the active space (i.e., only σ and σ^* for single bonds) should be satisfactory, but sometimes slightly larger active spaces may be required. Such complications arise when there are orbitals whose energies are very close to those of σ and σ^*, or when σ and σ^* are of different character at different interatomic separations.

An attractive application for the new MP2-CCSD(II) method would be to systems for which CCSD performs well but MP2 misbehaves. In a separate study[289], where we investigate radical hydrogen abstraction reactions, the enthalpies produced by CCSD with non-iterative triples, CCSD(T), are relatively insensitive to the choice of the reference function, whether UHF or ROHF. However, the enthalpies computed with MP2 depend crucially on the choice of the reference. Additionally, the ROHF-based MP2 method produces some unacceptable artifacts whereas the UHF-based MP2 method suffers from serious spin contamination. We believe that the MP2-CCSD(II) method would alleviate such problems of MP2 if applied to these systems and plan to explore this in future work.

Part of the material of this chapter was published as a paper in the *Journal of Chemical Physics* [290].

CHAPTER VII

CONCLUSION

The limit of *ab initio* electronic structure methods in predicting molecular properties has been explored in a variety of contexts. First, we demonstrated that spectroscopic accuracy for the spectroscopic constants of three first row hydrides, BH, CH^+, and NH can be achieved by including small effects that are assumed to be negligible in conventional quantum chemical calculations. By accounting for the completeness of one- and n-particle basis sets, as well as relativistic, adiabatic and nonadiabatic corrections, our predicted ω_e and r_e for the three diatomic hydrides matched experiment within 0.5 cm^{-1} and 0.0007 Å, respectively. We also compared the magnitude of these corrections and discovered that both the adiabatic and nonadiabatic corrections to the bond lengths are abnormally large for BH an CH^+. In the following work, we studied the structure and properties of lithium hexamers using studied using CCSD(T) with large basis sets. For the neutral Li_6 cluster, the D_{4h} isomer was shown to be the most stable structure by virtue of its high total atomization/binding energy and the close agreement between its electron affinity, ionization potential and vertical excitation spectrum with experimental analogs. At the ZPVE-corrected CCSD(T)/cc-vCVQZ level, the C_{5v} and D_{3h} isomers lies 5.14 and 7.09 kcal mol^{-1} higher, respectively. The D_{4h} global minimum contrasts with many other metal hexamers such as Na_6 and Au_6 which are thought to have a D_{3h} global minimum. Some features from an experimental optical absorption spectrum of Li_6 compare well with those from our EOM-CCSD vertical excitation spectrum for the D_{4h} isomer, but not so much for the D_{3h} and C_{5v} isomers. The existence of other relevant isomers on higher spin manifolds was investigated and a $^3B_1$ minimum of C_{2v} spatial symmetry was found to lie 0.7 kcal mol^{-1} below the singlet D_{3h} isomer. For Li_6^+, the global minimum corresponded to a structure of C_{2v} symmetry, resulting from a stabilizing Jahn-Teller distortion and the anion, Li_6^-, had a D_{4h} structure. Theoretical predictions for these clusters were found to be sensitive both to the basis set used and to

electron correlation. The present, high-accuracy coupled-cluster results should help guide the interpretation of experiments on these clusters, which are at the size where 2D and 3D structures are energetically competitive.

In Chapter IV, the abstraction of hydrogens from prototypical hydrocarbon molecules was studied studied using high level *ab initio* techniques. The calculated activation barriers and enthalpies of reaction were found to be in good agreement with experiment. In general, MP2 overestimated barriers and was particularly sensitive to spin contamination of the reference wavefunction. Density functionals, namely B3LYP and BHLYP, significantly underestimated barriers due to self-interaction errors. The more reliable CCSD(T) method predicted barrier heights and enthalpies of reaction which were generally in excellent agreement with experiment. The hydrogen abstraction activation energy from sp^2 and sp^3 carbons by ethynyl radical was less than 3 kcal mol^{-1}. For the reaction of ethynyl radical with isobutane, the abstraction reaction was barrierless. The use of ethynyl-type radicals as possible tooltips for use in the mechanosynthesis of diamond, particularly at low temperatures is advocated on the basis of their high degree of positional selectivity and control. As a compliment to the hydrogen abstraction work, hydrogen donation reactions from Si, Ge, Sn and Pb bridgehead substituted methane and isobutane to methyl and t-butyl radical sites was investigated theoretically using high-level electronic structure theory methods. The importance of using a small-core pseudopotentials in getting accurate barriers and reaction energies was demonstrated. The use of a tooltip hydrogen attached to a bridgehead Group IVA element as a possible hydrogen donation tool in the mechanosynthesis of diamondoids appeared feasible, with reaction energy barriers decreasing and reaction exoergicities increasing for the Si $\rightarrow$ Ge $\rightarrow$ Sn $\rightarrow$ Pb methane and isobutane bridgehead substituent series.

Finally, the inexpensive MP2 method and favorable features of the more costly CCSD are combined in a hybrid MP2-CCSD approach and the new method is benchmarked both in the equilibrium as well as dissociation regime. The hybrid methods MP2-CCSD(II) is the best $\mathcal{O}(N^5)$ scaling method for both regimes.

APPENDIX A

DIAGONAL BORN-OPPENHEIMER CORRECTION TO ACTIVATION BARRIERS OF HYDROGEN TRANSFER REACTIONS

For a series of simple hydrogen exchange and abstraction reactions, the effect of the diagonal Born-Oppenheimer correction (DBOC) is evaluated for self-consistent field (SCF) and configuration interaction (CI) wavefunctions. While DBOC is normally considered to be a small correction for systems at equilibrium[34, 291], it has been shown to be indispensable in achieving spectroscopic accuracy ($\nu \leq 1$ cm^{-1}) particularly for systems containing light atoms[5, 48]. There have been many unusual findings with respect to DBOC - a contribution of 0.2 kcal mol^{-1} to the singlet-triplet gap of methylene[292]; a change in the equilibrium bond distance (r_e) of BH (0.00066 Å) and CH^+(0.00063 Å) that is three times larger than for H_2(0.0002 Å)[48]. In the reactive regime of a potential energy surface, the DBOC could conceivably be larger considering the Born-Oppenheimer potential energy surface would be less accurate in those regimes. Especially for hydrogen transfer reactions, the contribution of the DBOC to reaction barriers is an interesting subject that has not been studied very systematically.

There are a few studies which explore the impact of the DBOC on reactive systems. the DBOC changes the barriers to linearity of H_2O, and H_2S, and the reaction $H_2 + F \rightarrow H + HF$, by -17[293], +27[294] and +17 cm^{-1}[295], respectively. The simplest hydrogen exchange reaction, $H_2 + H \rightarrow H + H_2$, has been studied extensively since DBOC correction is most significant for light systems. Garrett and Truhlar[296] estimated the DBOC to the barrier height of this reaction to be +0.21 kcal mol^{-1} (+73 cm^{-1}) using the diatomics-in-molecules (DIMs) approximation and a London potential. Garashchuk *et al.*[297] studied the hydrogen exchange reaction and concluded that inclusion of the DBOC raises the reaction barrier by approximately 72 cm^{-1} at the UMP2 level[297]. Mielke *et al.*[298] calculated the

DBOC at the FCI level using a truncated 32-orbital CISD/aug-cc-pVQZ natural orbital basis and found a value of +0.154 kcal mol^{-1}. The most complete characterization of the effect of DBOC on the reaction H_2 + H and its isotopomers (D + H_2 and H + D_2) yielded corrections of 0.1532 (53.57), 0.1395 (48.80) and 0.0903 (31.57) kcal mol^{-1} (cm^{-1}) at the MRCI(11)/aug-cc-pV5Z//MRCI(3)/aug-cc-pVTZ level[299]. Other notable conclusions from the same work include the narrowing of the barrier width by 2.2% as a result of DBOC and the importance of correlation effects, as indicated by CASSCF and UHF DBOC predictions that were 55% and 22% higher than MRCI. The last work has further been used to resolve discrepancies between experimental and theoretical thermal reaction rates[300]. Despite the significant amount of work done on the smallest hydrogen exchange reaction, H +H_2 $\rightarrow$ H_2 + H, the effect of DBOC on other hydrogen transfer reactions remains largely unexplored and systematic studies are noticably absent. We attempt to study the dependence of DBOC correction on hydrogen transfer barriers for a series of reactions with varying barrier heights. Any correlation between the size of DBOC, the barrier heights and transition state geometries is noted. The basis set and correlation dependence of DBOC corrections to barriers are also studied carefully. The hydrogen transfer reactions studied have the form X + HY $\rightarrow$ XH + Y, where X,Y = H, C, F, O, CH_3, and C_2H.

A.1 Methodology

All DBOC computations were carried out using the PSI 3.2[29] package. For open-shell systems, the DBOC at SCF level was calculated using both UHF and ROHF references. while at the CI level we were limited to using ROHF reference. Configuration interaction with single and double excitations (CISD) and full CI (FCI) computations were performed using the DETCI module[28] in PSI 3.2 and employ ROHF references for open-shell systems. FCI is insensitive to the choice of zeroth order reference while CISD has small dependence.

DBOC corrections were computed using finite differences with two steps of 0.0005 Bohrs which ensure an accuracy in the DBOC correction of $0.0005^2 a.u. \sim 0.05$ cm^{-1}[29]. All SCF and CI energies were converged to $\sim 10^{-12}$ a.u.. As suggested by Handy and Lee[34], we have computed the DBOC using atomic masses instead of nuclear masses despite a small difference that has been observed between the two schemes. Geometries for reactants and transition states were optimized at the partially spin restricted [RHF-RCCSD(T)] open-shell coupled cluster singles, doubles and perturbative triples level, as implemented in MOLPRO[243] with Dunning's[13, 16] quadruple-ζ basis (cc-pVQZ).

A.2 Preliminary Results

A.2.1 DBOC Across A Potential Energy Surface

The diagonal correction to the Born-Oppenheimer energy is largest around the transition state regime and its effect on hydrogen transfer barriers is not negligible. For example, Figures 35 shows the DBOC correction for the linear H_3 having a large value around its transition state ($R[H\text{-}H]_1 = R[H\text{-}H]_2 \sim 0.94$ Å).

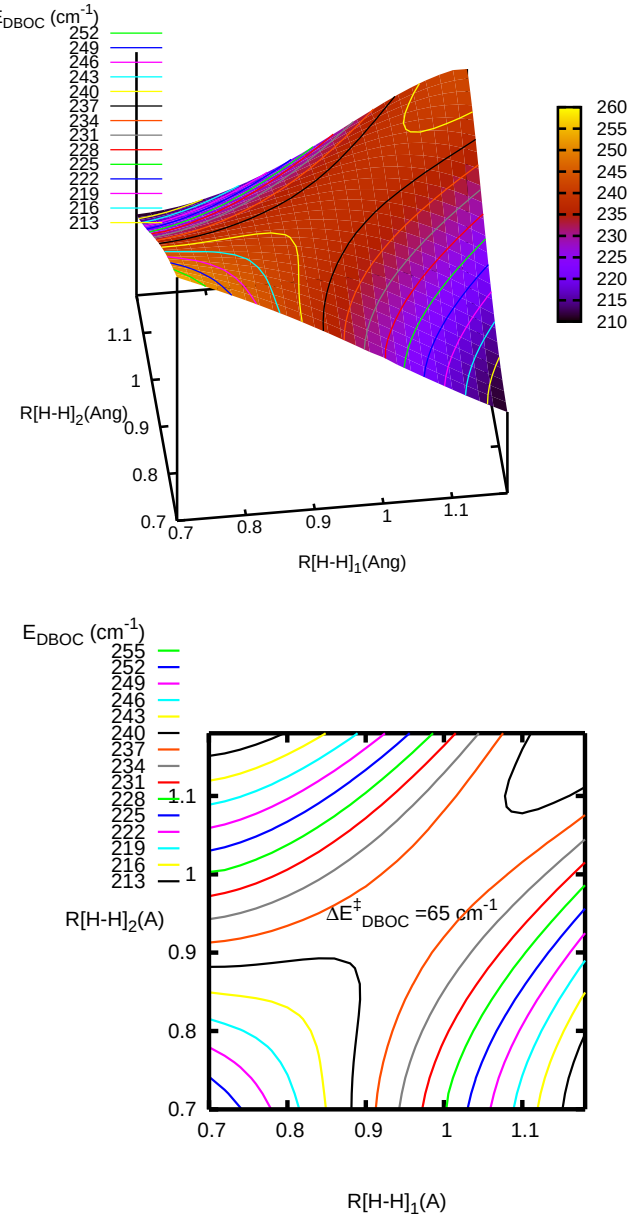

Figure 35: FCI/TZ DBOC across the linear H_3 potential energy surface (top) and contour (bottom). The DBOC to the classical barrier is 65 cm^{-1}

A.2.2 Basis Set and Correlation Dependence of DBOC

Basis set effects are somewhat minimal but correlation effects are very significant. Even for a system like H_3, correlation effects change DBOC by as much as 30 cm^{-1}. The ROHF DBOC for the transition state is much larger ($\sim$ 450 cm^{-1}) than that predicted by other methods ($\sim$ 240 cm^{-1}). The reason for this is not immediately obvious, and we did not have an opportunity to investigate it. It is possible that it could be a numerical artifact.

Table 31: One- and n-particle dependence of DBOC[a]

	ROHF			R/UHF			RO-CISD			FCI		
	DZ	TZ	QZ	DZ	TZ	QZ	DZ	TZ	QZ	DZ	TZ	QZ
H	59.7	59.7	59.8	59.7	59.7	59.8	59.7	59.7	59.8	59.7	59.7	59.8
H_2	99.4	101.0	101.2	99.4	101.0	101.2	111.9	114.6	114.6	111.9	114.6	114.6
H-H-H	440.6	448.2	448.7	251.2	253.7	254.1	240.0	242.5	241.0	237.3	239.0	237.2
$\Delta E^{\ddagger}_{DBOC}$	281.5	287.4	287.7	92.1	93.0	93.1	68.4	68.2	66.6	65.7	64.7	62.9

[a]-All DBOC calculations performed at the RCCSD(T)/cc-pVQZ optimized geometries

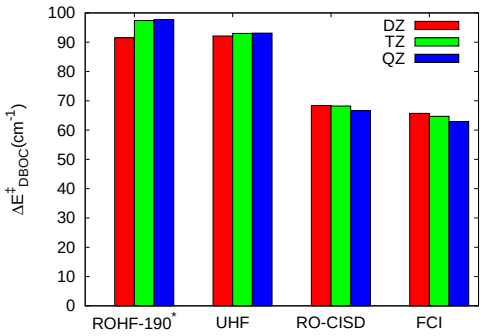

Figure 36: Basis set and correlation dependence of DBOC for H_3. * "ROHF-190" indicates that 190 cm^{-1} has been subtracted from ROHF DBOC values.

A.2.3 Magnitude of DBOC to Hydrogen Transfer Barriers

DBOC to hydrogen transfer barriers could be as large as 3% for some reactions, as listed in the table below.

Table 32: RO-CISD/DZ DBOC correction to barriers of reactions of type X + HY $\rightarrow$ XH + Y. [a]

X	HY	$\delta E^{\ddagger}_{DBOC}$ (cm^{-1})	$\delta E^{\ddagger}_{DBOC}/E^{\ddagger}$(%)
H	H_2	68.41	2.0
F	H_2	17.77	2.9
H	HF	28.33	0.2
H	HO	83.35	2.3
O	H_2	107.83	2.4
OH	H_2	31.25	1.6
H	H_2O	54.14	0.7
CCH	HCCH	19.61	0.6
H	HCH_3	18.31	0.3
CH_3	H_2	10.71	0.3

[a] All barrier and DBOC calculations performed at the RCCSD(T)/cc-pVQZ optimized geometries

APPENDIX B

UNUSUAL ARTIFACTS INTRODUCED BY OPEN-SHELL PERTURBATION THEORIES FOR SYMMETRIC HYDROGEN TRANSFER REACTIONS

During our study of hydrogen abstraction reactions[225], we were plagued by the spin contamination problem when we used unrestricted orbitals for open-shell systems. Unrestricted orbitals are frequently easier to converge, and the extra flexibility they provide often improves results for bond-breaking and bond-making reactions when electronic near degeneracy effects are strong. On the other hand, unrestricted orbitals can lead to poorer results in less severe cases of electronic near-degeneracies (e.g., in the spin-recoupling region of unimolecular dissociation reactions)[154, 155, 156, 157]. Additionally, the use of unrestricted orbitals means that the wave function is no longer an eigenfunction of the $\hat{S}^2$ operator and is contaminated by states with higher spin multiplicities. Using restricted orbitals remedies the spin contamination problem but it has been known to artificial symmetry breaking and other artifacts. One such problem we encountered is that second-order restricted open-shell Møller-Plesset perturbation theory (RMP2)[301] predicts an asymmetric transition state for symmetric reactions. At the symmetric location where a transition state is expected resides a shallow minimum, with two asymmetric transition states lying on opposite sides of the shallow minimum. Our objective is to investigate the presence of this artifact in other versions of open-shell perturbation theory and uncover the cause of this erroneous prediction using the reaction $H_2 + H \rightarrow H + H_2$ as our primary test case.

B.1 Methodology

The flexibility in the definition of ROHF Fock matrices in restricted open-shell perturbation theory (ROSPT) has led to the formulation of many flavors. The two main classes are those using the configuration state-function (CSF) basis and spin-orbital determinant basis.

Among the CSF-based methods areOPT1[302] and OPT2[302] while RMP(equivalent to ROHF-MBPT)[301, 303], ROMP[304], and z-averaged perturbation theory (ZAPT2)[305] comprise of the second kind. Our study mainly focuses on the failures of RMP2 since energy points and geometry optimizations with numerical gradients can be readily performed using MOLPRO[243] and many other packages. Single point energies for the less prevalent OPT1, OPT2, and ZAPT2 were calculated using the MPQC package[306] with the minima and transition states being located using Mathematica[307].

B.2 Preliminary Results

B.2.1 The Case of RMP2

Our finding is unique in that ROHF and RCCSD(T) predict the proper symmetric transition state while in other literature, when artificial symmetry breaking appears due to restricted orbitals, it is seen both at the reference ROHF level as well as RMP2. Figure 37 shows ROHF and RCCSD(T) show a symmetric transition state for symmetric reactions, in contrast to RMP2 (Figure 38) which predicts an asymmetric transition state.

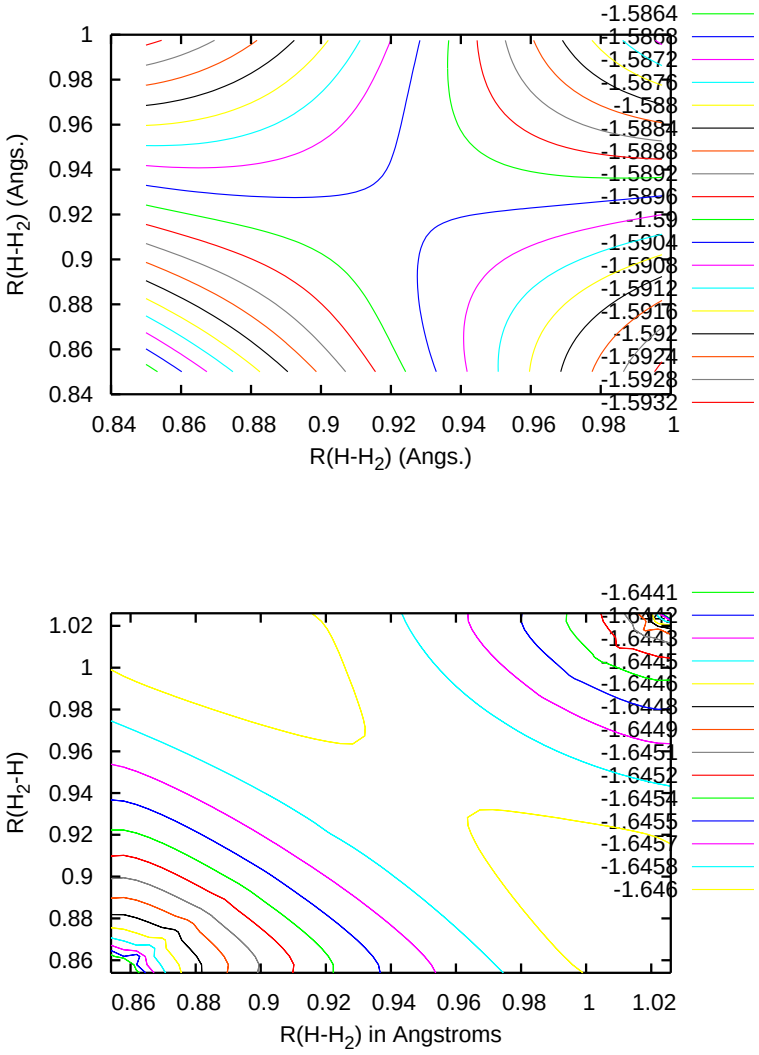

Figure 37: ROHF/DZ (top) and RCCSD(T) (bottom) potential energy contours for H_3

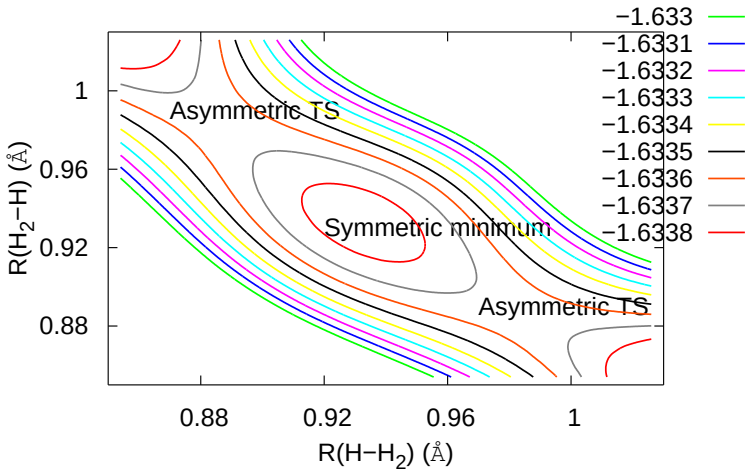

Figure 38: RMP2/DZ potential energy contours for H_3

Table 33: Normal mode analysis of RMP2 stationary points

Mode	Asymmetric	Symmetric
1	2153.2i	0.0i
2	0.0i	0.0i
3	0.0i	0.0
4	0.0i	0.0
5	0.0	0.0
6	0.0	959.9
7	927.2	959.9
8	927.2	2162.4
9	2258.8	2164.0

The shallow minimum does not disappear with increasing basis set size; it actually gets deeper, as shown in Table 34.

Table 34: Geometries and energies of the RMP2 transition state and minimum for H· + $H_2 \rightarrow H_2$ + ·H.

	Minimum		TS		
	R1	R2	R1	R2	E_{ts}-E_{min}(kcal mol^{-1})
DZ	0.9328	0.9328	0.8858	0.9845	0.1282
TZ	0.9195	0.9195	0.8689	0.9757	0.1481
QZ	0.9192	0.9192	0.8672	0.9771	0.1612

B.2.2 Decomposing the RMP2 Correlation Energy

What part of the correlation energy accounts for the asymmetry of the RMP2 transition state? Plotting the components of the RMP2 correlation energy along the reaction coordinate of H_3 shows that both the singles and pairs correlation energy have a minimum at the symmetric location (R=0) and thus they both contribute to the artifact.

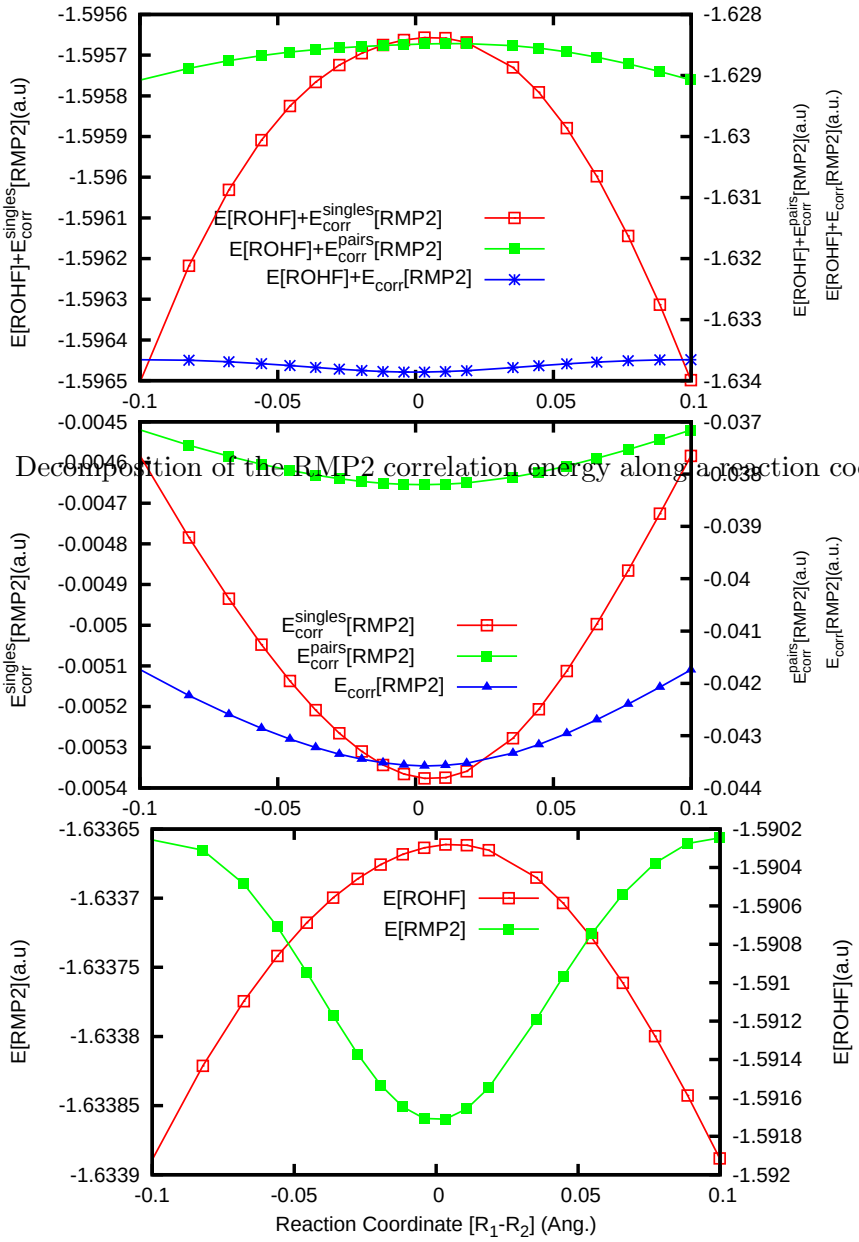

Figure 39: Decomposition of the RMP2 correlation energy along a reaction coordinate for linear H_3

B.2.3 Other Flavors of ROSPT

This curious artifact is not only seen on the RMP2 potential energy surfaces, but also for other flavors of open-shell perturbation theories like ZAPT2, OPT1 and OPT2. Table 35 shows the location of the shallow minimum and Figures 40 and 41 show potential energy contours in the region of the symmetric minimium for the ZAPT2, OPT1, and OPT2 methods.

Table 35: Location of shallow minimum for the reaction H· + H_2 → H_2 + ·H

	E_{min}	R1	R2
RMP2/DZ	-1.63387	0.932890	0.932843
ZAPT2/DZ	-1.63346	0.930637	0.934203
OPT1/DZ	-1.63741	0.935932	0.936406
OPT2/DZ	-1.63627	0.936331	0.936405

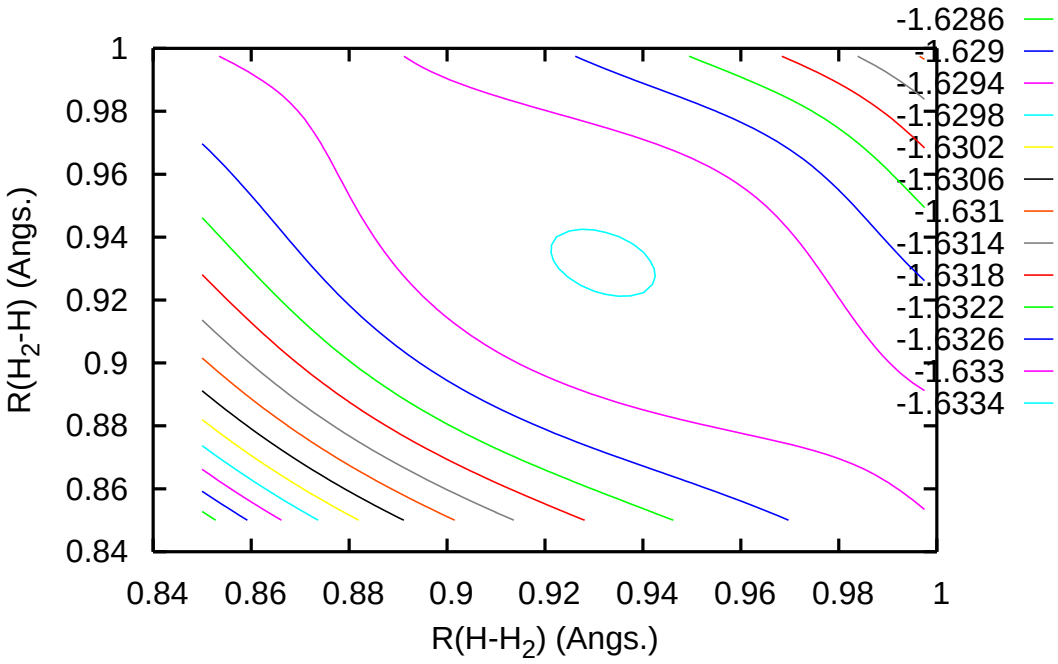

Figure 40: ZAPT2/DZ potential energy contours for H_3

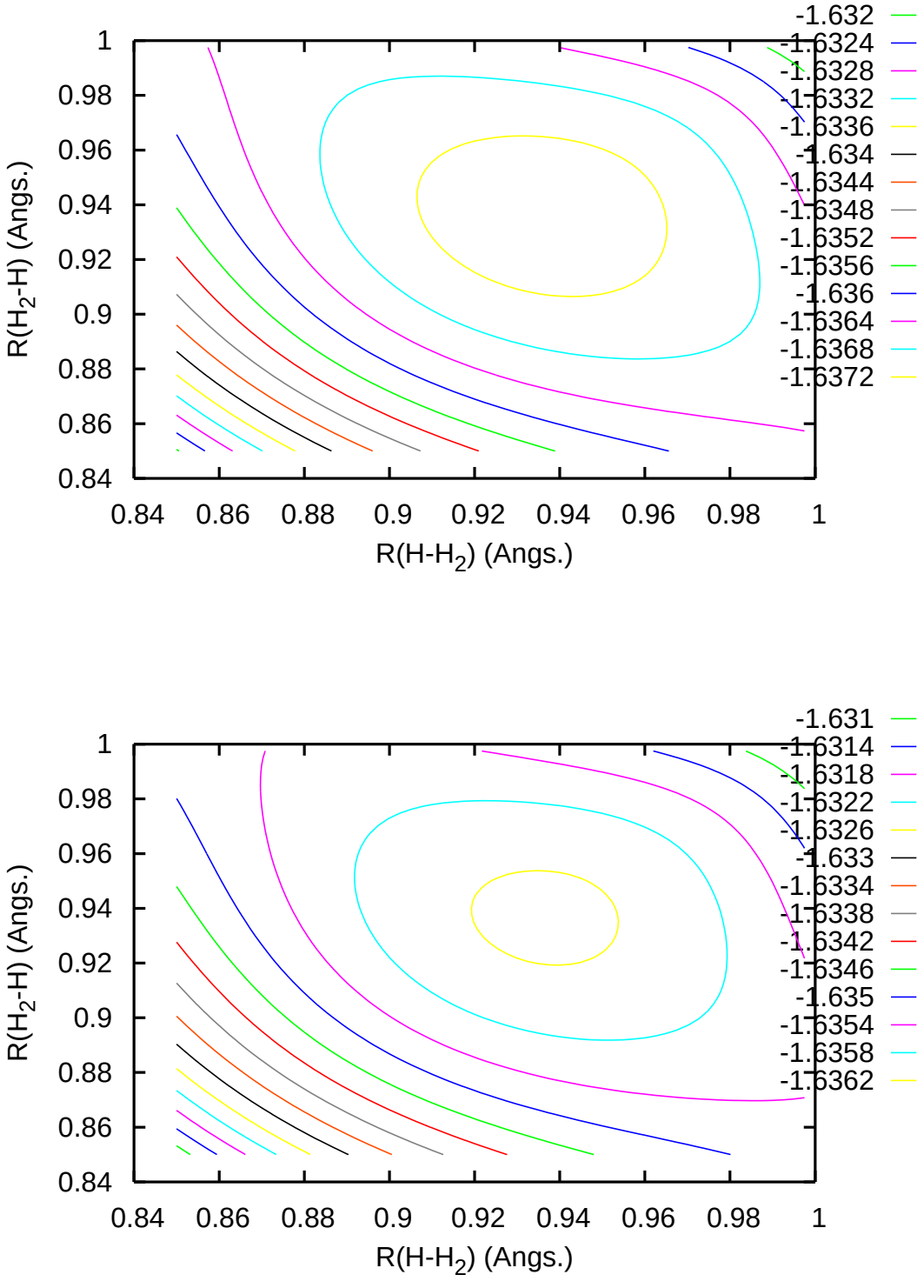

Figure 41: OPT1/DZ (top) and OPT2/DZ (bottom) potential energy contours for H_3

REFERENCES

[1] M. Born and J. Oppenheimer, Ann. Phys. Lpz. **84**, 457 (1927).

[2] J. C. Tully, Theor. Chem. Acc. **103**, 173 (2000).

[3] A. Szabo and N. S. Ostlund, *Modern Quantum Chemistry: Introduction to Advanced Electronic Structure Theory*, McGraw-Hill, New York, 1989.

[4] F. Jensen.

[5] O. L. Polyansky et al., Science **277**, 346 (1997).

[6] O. L. Polyansky, A. G. Császár, S. V. Shirin, N. F. Zobov, and Barletta, Science **299**, 539 (2003).

[7] J. M. L. Martin, Chem. Phys. Lett. **283**, 283 (1998).

[8] J. M. L. Martin, Chem. Phys. Lett. **292**, 411 (1998).

[9] J. M. L. Martin, Spectrochimica Acta A **57**, 875 (2001).

[10] D. Feller and J. A. Sordo, J. Chem. Phys. **112**, 5604 (2000).

[11] F. Pawlowski et al., J. Chem. Phys. **113**, 2539 (2003).

[12] M. O. Sinnokrot and C. D. Sherrill, J. Chem. Phys. **115**, 2439 (2001).

[13] T. H. Dunning Jr., J. Chem. Phys. **90**, 1007 (1989).

[14] D. E. Woon and T. H. Dunning Jr., J. Chem. Phys. **103**, 4572 (1995).

[15] A. K. Wilson, T. V. Mourik, and T. H. Dunning Jr., J. Mol. Struct (THEOCHEM) **388**, 339 (1996).

[16] R. A. Kendall, T. H. Dunning Jr., and R. J. Harrison, J. Chem. Phys. **96**, 6796 (1992).

[17] 2002 basis sets were obtained from the Extensible Computational Chemistry Environment Basis Set Database, Version 7/29/02, as developed and distributed by the Molecular Sciences Computing Facility, Environmental and Molecular Sciences Laboratory (EMSL), which is a part of Pacific Northwest National Laboratories, P.O.Box 999, Richland, Washington 99352 and funded by effects", the US Department of Energy. The Pacific Northwest Laboratory is a multiprogram laboratory operated by Battelle Memorial Institute for the US Department of Energy under Contract DE-AC06-76RLO 1830. Contact David Feller or Karen Schuchardt for more information.

[18] D. Feller, J. Chem. Phys. **96**, 7059 (1992).

[19] T. Helgaker, W. Klopper, H. Koch, and J. Noga, J. Chem. Phys. **106**, 9639 (1997).

[20] A. G. Császár, J. S. Kain, O. L. Polyansky, N. F. Zobov, and J. Tennyson, Chem. Phys. Lett **293**, 317 (1998).

[21] J. M. L. Martin and G. D. Oliviera, J. Chem. Phys. **111**, 1843 (1999).

[22] C. W. Bauschlicher Jr. and A. Ricca, J. Phys. Chem. A **102**, 8014 (1998).

[23] N. C. Handy, Y. Yamaguchi, and H. F. Schaefer, J. Chem. Phys. **84**, 4481 (1986).

[24] W. Kutzelnigg, Mol. Phys. **90**, 909 (1997).

[25] E. F. Valeev and C. D. Sherrill, J. Chem. Phys. **118**, 3921 (2003).

[26] P. Bunker and R. Moss, Mol. Phys. **33**, 417 (1977).

[27] D. Schwenke, J. Phys. Chem. A **105**, 2352 (2001).

[28] C. D. Sherrill and H. F. Schaefer, The configuration interaction method: Advances in highly correlated approaches, in *Advances in Quantum Chemistry*, edited by P.-O. Löwdin, volume 34, pages 143–269, Academic Press, New York, 1999.

[29] T. D. Crawford et al., 2003, PSI3.2: An Open-Source, *Ab Initio* Electronic Structure Package.

[30] J. F. Stanton, J. Gauss, W. J. Lauderdale, J. D. Watts, and R. J. Bartlett, The package also contains modified versions of the MOLECULE Gaussian integral program of J. Almlöf and P. R. Taylor, the ABACUS integral derivative program written by T. U. Helgaker, H. J. Aa. Jensen, P. Jørgensen and P. R. Taylor, and the PROPS property evaluation integral code of P. R. Taylor.

[31] R. D. Cowan and M. Griffith, J. Opt. Soc. Am. **66**, 1010 (1976).

[32] J. L. Dunham, Phys. Rev. **41**, 721 (1932).

[33] I. N. Levine, *Molecular Spectroscopy*, Wiley & Sons, New York, 1975.

[34] N. C. Handy and A. M. Lee, Chem. Phys. Lett. **252**, 425 (1996).

[35] W. T. M. L. Fernando and P. F. Bernath, J. Mol. Spec. **145**, 392 (1991).

[36] A. Carrington and D. A. Ramsey, Phys. Scripta **25**, 272 (1982).

[37] C. R. Brazier, R. S. Ram, and P. F. Bernath, J. Mol. Spec. **120**, 381 (1986).

[38] R. S. Ram and P. F. Bernath, J. Mol. Spec. **176**, 329 (1996).

[39] E. Tiemann and J. F. Ogilvie, J. Mol. Spec. **165**, 377 (1994).

[40] J. K. G. Watson, J. Mol. Spec. **45**, 99 (1973).

[41] J. A. Coxon and R. Colin, J. Mol.Spec. **181**, 215 (1997).

[42] A. Halkie, T. Helgaker, W. Klopper, P. Jørgensen, and A. Császár, Chem. Phys. Lett. **310**, 385 (1999).

[43] S. Hirata, T. Yanai, W. A. de Jong, T. Nakajima, and K. Hirao, J. Chem. Phys. **121**, 3297 (2004).

[44] G. Tarczay, A. Császár, W. Klopper, and H. Quiney, Mol. Phys. **99**, 1769 (2001).

[45] C. W. Bauschlicher Jr., J. Phys. Chem. A **104**, 2281 (2000).

[46] M. Douglas and N. M. Kroll, Ann. Phys. **82**, 89 (1974).

[47] H. M. Quiney et al., Chem. Phys. Lett. **344**, 413 (2001).

[48] B. Temelso, E. F. Valeev, and C. D. Sherrill, J. Phys. Chem. A **108**, 3068 (2004).

[49] P. Ballone and W. Andreoni, *Metal Clusters*, Wiley, New York, 1999.

[50] M. Brack, Rev. Mod. Phys. **65**, 677 (1993).

[51] W. A. de Heer, Rev. Mod. Phys. **65**, 611 (1993).

[52] J. Blanc et al., J. Chem. Phys. **96**, 1793 (1992).

[53] V. Bonačić-Koutecký, J. Pittner, C. Scheuch, M. F. Guest, and J. Koutecký, J. Chem. Phys. **96**, 7938 (1992).

[54] P. Dugourd et al., Phys. Rev. Lett. **67**, 2638 (1991).

[55] V. Bonačić-Koutecký, P. Fantucci, and J. Koutecký, Phys. Rev. B **37**, 4369 (1988).

[56] V. Bonačić-Koutecký, P. Fantucci, and J. Koutecký, Chem. Rev. **91**, 1035 (1991).

[57] J. Koutecký, I. Boustani, and V. Bonačić-Koutecký, Int. J. Quan. Chem. **38**, 149 (1990).

[58] R. Rousseau and D. Marx, Chem. Eur. J. **6**, 2982 (2000).

[59] R. Rousseau and D. Marx, Phys. Rev. A **56**, 617 (1997).

[60] S. E. Wheeler, K. W. Sattelmeyer, P. v. R. Schleyer, and H. F. Schaefer, III, J. Chem. Phys. **120**, 4683 (2004).

[61] W. D. Knight et al., Phys. Rev. Lett. **52**, 2141 (1984).

[62] J. L. Martins, R. Car, and J. Buttet, Surf. Sci. **106**, 265 (1981).

[63] Z. Penzar and W. Ekardt, Z. Phys. D **19**, 109 (1991).

[64] G. Gardet, F. Rogemond, and H. Chermette, J. Chem. Phys. **105**, 9933 (1996).

[65] C. Bréchignac, H. Busch, P. Cahuzac, and J. Leygnier, J. Chem. Phys. **101**, 6992 (1994).

[66] C. Yannouleas and U. Landman, Phys. Rev. Lett. **78**, 1424 (1997).

[67] C. Yannouleas and U. Landman, J. Chem. Phys. **107**, 1032 (1997).

[68] Y. Sakurai et al., Phys. Rev. Lett. **74**, 2252 (1995).

[69] W. Schulke, G. Stutz, F. Wohlert, and A. Kaprolat, Phys. Rev. B **54**, 14381 (1997).

[70] M. W. Sung, R. Kawai, and K. H. Weare, Phys. Rev. Lett. **73**, 3552 (1994).

[71] R. O. Jones, A. I. Lichtenstein, and J. Hutter, J. Chem. Phys **106**, 4566 (1997).

[72] I. Boustani, W. Pewestorf, P. Fantucci, V. Bonačić-Koutecký, and J. Koutecký, Phys. Rev. B **35**, 9437 (1987).

[73] A. Grassi, G. M. Lombardo, G. G. N. Angilella, N. H. March, and R. Pucci, J. Chem. Phys **120**, 11615 (2004).

[74] M. J. McAdon and I. W. A. Goddard, Phys. Rev. Lett. **25**, 2563 (1985).

[75] M. J. McAdon and I. W. A. Goddard, J. Non-Cryst. Solids **75**, 149 (1985).

[76] M. J. McAdon and I. W. A. Goddard, J. Phys. Chem **91**, 2607 (1987).

[77] P. Fantucci et al., Chem. Phys. Lett. **250**, 47 (1996).

[78] R. Rousseau and D. Marx, Phys. Rev. Lett. **80**, 2574 (1998).

[79] R. Rousseau and D. Marx, J. Chem. Phys. **111**, 5091 (1999).

[80] Y. Ishikawa, Y. Sugita, T. Nishikawa, and Y. Okamoto, Chem. Phys. Lett. **333**, 199 (2001).

[81] A. Ishii, K. Ohno, Y. Kawazoe, and S. G. Louie, Phys. Rev. B. **65**, 245109 (2002).

[82] S. K. Lai, P. J. Hsu, K. L. Wu, W. K. Liu, and M. Iwamatsu, J. Chem. Phys. **117**, 10715 (2002).

[83] K. J. Taylor et al., J. Chem. Phys. **93**, 7515 (1990).

[84] K. Balasubramanian and D. Liao, J. Chem. Phys. **94**, 5233 (1991).

[85] D. Liao and K. Balasubramanian, J. Chem. Phys. **97**, 2548 (1992).

[86] H. Hakkinen and U. Landman, Phys. Rev. B. **62**, 2287 (2000).

[87] G. Mills, M. S. Gordon, and H. Metiu, J. Chem. Phys. **118**, 4198 (2003).

[88] C. Massobrio, A. Pasquarello, and A. D. Corso, J. Chem. Phys. **109**, 6626 (1998).

[89] C. Massobrio, A. Pasquarello, and A. D. Corso, Chem. Phys. Lett. **238**, 215 (1995).

[90] I. A. Solov'yov, A. V. Solov'yov, and W. Greiner, Phys. Rev. A. **65**, 053203 (2002).

[91] K. Raghavachari, J. A. P. G. W. Trucks, and M. Head-Gordon, Chem. Phys. Lett. **157**, 479 (1989).

[92] MOLPRO 2002.6 is a package of ab initio programs designed by Werner, H.-J. and Knowles, P. J., with contributions from Amos, R. D., Bernhardosson, A., Berning, A., Celani, P., Cooper, D. L., Deegan, M. J. O., Dobbyn, A. J., Eckert, F., Hampel, C., Hetzer, G., Knowles, P. J., Korona, T., Lindh, R., Lloyd, A. W., McNicholas, S. J., Manby, F. R., Meyer, W., Mura, M. E., Nicklass, A., Palmieri, P., Pitzer, R., Rauhut, G., Schutz, M., Schumann, U., Stoll, H., Stone, A. J., Tarroni, R., Thorsteinsson, T., and Werner, H.-J.

[93] G. Schaftenaar and J.H. Noordik, "Molden: a pre- and post-processing program for molecular and electronic structures", J. Comput.-Aided Mol. Design, 14 (2000) 123-134.

[94] J. F. Stanton and R. J. Bartlett, J. Chem. Phys. **98**, 7029 (1993).

[95] T. J. Lee, J. E. Rice, G. E. Scuseria, and H. F. Schaefer, Theor. Chim. Acta. **75**, 81 (1989).

[96] T. J. Lee and P. R. Taylor, Int. J. Quantum Chem. Symp. **23**, 199 (1989).

[97] M. A. Iron, M. Oren, and J. M. L. Martin, Mol. Phys. **101**, 1345 (2003).

[98] K. A. Peterson and T. H. Dunning, Jr, J. Chem. Phys. **117**, 10548 (2002).

[99] R. Krishnan, R. S. J.S. Binkley, and J. Pople, J. Chem. Phys. **72**, 650 (1980).

[100] H. B. C. Bréchignac, P. Cahuzac, and J. Leygnier, J. Phys. Chem. **101**, 6992 (1994).

[101] B. Temelso, E. F. Valeev, and C. D. Sherrill, J. Phys. Chem. A **108**, 3068 (2004).

[102] J. L. Martins, J. Buttet, and R. Car, Phys. Rev. B. **31**, 1804 (1985).

[103] P. Dugourd et al., Chem. Phys. Lett. **197**, 433 (1992).

[104] B. Vezin et al., Chem. Phys. Lett. **206**, 521 (1993).

[105] B. Temelso and C. D. Sherrill, J. Chem. Phys. **122**, 064315 (2005).

[106] M. J. Knapp and J. Klinman, Eur. J. Biochem. **269**, 3113 (2002).

[107] B. Balasubramanian, W. K. Pogozelskidagger, and T. D. Tullius, Proc. Natl. Acad. Sci. **95**, 9738 (1998).

[108] M. D. Le Page and B. R. James, Chem. Comm. , 1647 (2000).

[109] P. W. May, Endeavour **19**, 101 (1995).

[110] H. T. Hall, J. Chem. Ed. **38**, 484 (1961).

[111] K. E. Drexler, J. Vac. Sci. Technol. B **9**, 1394 (1991).

[112] H. H. Farrell and M. Levinson, Phys. Rev. B **31**, 3593 (1985).

[113] K. E. Drexler, *Nanosystems: Molecular Machinery, Manufacturing, and Computation*, John Wiley & Sons, New York, 1992.

[114] R. C. Merkle, Chem. Design Automation News **9**, 1 (1993).

[115] R. C. Merkle, Nanotechnology **8**, 149 (1997).

[116] R. C. Merkle and R. A. Freitas Jr., J. Nanosci. Nanotech. **3**, 319 (2003).

[117] J. Peng, R. A. Freitas Jr., and R. C. Merkle, J. Comput. Theor. Nanosci. **1**, 62 (2004).

[118] J. Peng, R. A. Freitas Jr., R. C. Merkle, J. R. Von Ehr, and G. D. Skidmore, J. Comput. Theor. Nanosci. **3**, 28 (2006).

[119] D. J. Mann, J. Peng, R. A. Freitas Jr., and R. C. Merkle, J. Comput. Theor. Nanosci. **1**, 71 (2004).

[120] X. Y. Chang, M. Perry, J. Peploski, D. L. Thompson and L. M. Raff, J. Chem. Phys. **99**, 4748 (1993); J. W. Lyding, K. Hess, G. C. Abeln, D. S. Thompson, J. S. Moore, M. C. Hersam, E. T. Foley, J. Lee, Z. Chen, S. T. Hwang, H. Choi, P. H. Avouris and I. C. Kizilyalli, Appl. Surf. Sci. **130**, 221 (1998); W. Ho and H. Lee, Science. **286**, 1719(1999); L. J. Lauhon and W. Ho, J. Phys. Chem. **105**, 3987 (2000); S. Hla and K. Rieder, Ann. Rev. Phys. Chem. **54**, 307 (2003).

[121] E. T. Foley, A. F. Kam, J. W. Lyding and P.H. Avouris, Phys. Rev. Lett. **80**, 1336 (1998); M. C. Hersam, G. C. Abeln and J. W. Lyding, Microelectronic Engineering. **47**, 235 (1999); N. Oyabu, O. Custance, I. Yi, Y. Sugawaran and S. Morita. Phys. Rev. Lett. **90**, 176102 (2003).

[122] C. B. Musgrave, J. K. Perry, R. C. Merkle, and W. A. Goddard III, Nanotechnology **2**, 187 (1991).

[123] S. B. Sinnott, R. J. Colton, C. T. White, and D. W. Brenner, Surf. Sci. **316**, L1055 (1994).

[124] D. W. Brenner, S. B. Sinnott, J. A. Harrison, and O. A. Shenderova, Nanotechnology **7**, 161 (1996).

[125] J. A. Pople, M. Head-Gordon, D. J. Fox, K. Raghavachari, and L. A. Curtiss, J. Chem. Phys. **90**, 5622 (1989).

[126] L. A. Curtiss, K. Raghavachari, G. W. Trucks, and J. A. Pople, J. Chem. Phys. **94**, 7221 (1991).

[127] L. A. Curtiss, K. Raghavachari, and J. A. Pople, J. Chem. Phys. **98**, 1293 (1993).

[128] L. A. Curtiss, K. Raghavachari, P. C. Redfern, V. Rassolov, and J. A. Pople, J. Chem. Phys. **109**, 7764 (1998).

[129] L. A. Curtiss, P. C. Redfern, K. Raghavachari, V. Rassolov, and J. A. Pople, J. Chem. Phys. **110**, 4703 (1999).

[130] A. G. Baboul, L. A. Curtiss, P. C. Redfern, and K. Raghavachari, J. Chem. Phys. **110**, 7650 (1999).

[131] J. M. L. Martin and G. de Oliveira, J. Chem. Phys. **111**, 1843 (1999).

[132] A. D. Boese, M. Oren, O. Atasoylu, J. M. L. M. J. Gauss, and M. Kállay, J. Chem. Phys. **111**, 1843 (1999).

[133] A. Tajti et al., J. Chem. Phys. **121**, 11599 (2004).

[134] A. Dybala-Defratyka, P. Paneth, J. Pu, and D. G. Truhlar, J. Phys. Chem. A **108**, 2475 (2004).

[135] Y. Chuang, E. L. Coitiño, and D. G. Truhlar, J. Phys. Chem. A **104**, 446 (2000).

[136] J. A. Litwinowicz, D. W. Ewing, S. Jurisevic, and M. J. Manka, J. Phys. Chem **99**, 9709 (1995).

[137] S. Skokov and R. A. Wheeler, Chem. Phys. Lett. **271**, 251 (1997).

[138] J. Peeters, H. Van Look, and B. Ceursters, J. Phys. Chem. **100**, 15124 (1996).

[139] H. Van Look and J. Peeters, J. Phys. Chem. **99**, 16284 (1995).

[140] H. M. T. Nguyen, A. K. Chandra, S. A. Carl, and M. T. Nguyen, J. Mol. Struct (THEOCHEM) **732**, 219 (2005).

[141] J. Peeters, B. Ceursters, H. M. T. Nguyen, and M. T. Nguyen, J. Chem. Phys. **116**, 3700 (2002).

[142] J. Peeters, B. Ceursters, H. M. T. Nguyen, and M. T. Nguyen, Chem. Phys. **262**, 243 (2000).

[143] M. Page and D. W. Brenner, J. Amer. Chem. Soc. **113**, 3270 (1991).

[144] S. P. Walch and R. C. Merkle, Nanotechnology **9**, 285 (1998).

[145] F. N. Dzegilenko, D. Srivastava, and S. Saini, Nanotechnology **9**, 325 (1998).

[146] K. Raghavachari, G. W. Trucks, J. A. Pople, and M. Head-Gordon, Chem. Phys. Lett. **157**, 479 (1989).

[147] P. J. Stephens, F. J. Devlin, C. F. Chabalowski, and M. J. Frisch, J. Phys. Chem. **98**, 11623 (1994).

[148] A. D. Becke, J. Chem. Phys. **98**, 1372 (1993).

[149] R. J. Sreeruttun et al., Intl. J. of. Mass. Spec. **241**, 295 (2005).

[150] J. Xiao, Z. Li, J. Liu, L. Sheng, and C. Sun, J. of. Comp. Chem. **23**, 1456 (2002).

[151] A. D. Becke, Phys. Rev. A **38**, 3098 (1988).

[152] C. Lee, W. Yang, and R. G. Parr, Phys. Rev. B **37**, 785 (1988).

[153] B. J. Lynch, P. Fast, M. Harris, and D. J. Truhlar, J. Phys. Chem. A **104**, 4811 (2000).

[154] M. L. Abrams and C. D. Sherrill, Chem. Phys. Lett. **404**, 284 (2005).

[155] A. Dutta and C. D. Sherrill, J. Chem. Phys. **118**, 1610 (2003).

[156] H. K. A. B. J. Olsen, P. Jørgensen, J. Chem. Phys. **104**, 8007 (1996).

[157] R. J. Bartlett and J. F. Stanton, Applications of post-hartree-fock methods: A tutorial, in *Reviews in Computational Chemistry*, edited by K. B. Lipkowitz and D. B. Boyd, volume 5, pages 65–169, VCH Publishers, New York, 1994.

[158] R. D. Amos, J. S. Andrews, N. C. Handy, and P. J. Knowles, Chem. Phys. Lett. **185**, 256 (1991).

[159] P. J. Knowles, C. Hampel, and H.-J. Werner, J. Chem. Phys. **99**, 5219 (1993).

[160] J. D. Watts, J. Gauss, and R. J. Bartlett, J. Chem. Phys. **98**, 8718 (1993).

[161] C. D. Sherrill, Annu. Rep. Comp. Chem. **1**, 45 (2004).

[162] M. R. Hoffmann and K. G. Dyall, editors, *Low-Lying Potential Energy Surfaces*, volume 828 of *ACS Symposium Series*, American Chemical Society, Washington, D.C., 2002.

[163] K. Hirao, editor, *Recent Advances in Multireference Methods*, volume 4 of *Recent Advances in Computational Chemistry*, World Scientific, Singapore, 1999.

[164] J. F. Stanton and R. J. Bartlett, J. Chem. Phys. **98**, 7029 (1993).

[165] D. R. Lide, ed., *Handbook of Chemistry and Physics*, CRC Press, Boca Raton, FL, 1996.

[166] A. H. Laufer and A. Fahr, Chem. Rev. **104**, 2814 (2004).

[167] W. R. Shulz and D. J. Leroy, J. Chem. Phys. **42**, 3869 (1965).

[168] J. M. Tedder, Agnew. Chem. Int. Ed. Engl. **21**, 401 (1982).

[169] B. J. Opansky and S. R. Leone, J. Phys. Chem. **100**, 19904 (1996).

[170] B. J. Opansky and S. R. Leone, J. Phys. Chem. A. **100**, 4888 (1996).

[171] R. J. Hobbler, B. J. Opansky, and S. R. Leone, J. Phys. Chem. **101**, 1338 (1997).

[172] J. I. Steinfeld, J. S. Francisco, and W. L. Hase, Prentice Hall, New Jersey, USA, 1989.

[173] E. Wigner, Z. Phys. Chem. B **19**, 203 (1932).

[174] R. P. Bell, *The Tunnel Effect in Chemistry*, Chapman and Hall, London, 1980.

[175] G. S. Hammond, J. Am. Chem. Soc. **77**, 334 (1955).

[176] W. T. Borden, E. R. Davidson, and D. Feller, Tetrahedron **38**, 737 (1982).

[177] E. R. Davidson and W. T. Bowden, J. Phys. Chem. **87**, 4783 (1983).

[178] B. Johnson, C. Gonzalez, P. Gill, and J. Pople, Chem. Phys. Lett. **221**, 100 (1994).

[179] S. Patchkovskii and T. Ziegler, J. Chem. Phys. **116**, 7806 (2002).

[180] Y. Zhang and W. Yang, J. Chem. Phys. **109**, 2604 (1999).

[181] B. J. Lynch, P. L. Fast, M. Harris, and D. G. Truhlar, J. Phys. Chem. A **104**, 4811 (2000).

[182] B. J. Lynch and D. G. Truhlar, J. Phys. Chem. A **105**, 2936 (2001).

[183] M. L. Coote, J. Phys. Chem. A **108**, 3865 (2004).

[184] H. Basch and S. Hoz, J. Phys. Chem. A **101**, 4416 (1997).

[185] F. Goulay and S. R. Leone, J. Phys. Chem. A. **110**, 1875 (2006).

[186] K. D. Tucker, M. L. Kutner, and P. Thaddeus, Astrophys. J. **193**, L115 (1974).

[187] C. Henkel, J. B. Whiteoak, L. A. Nyman, and J. Hajru, Astron. Astrophys. **230**, L5 (1990).

[188] K. C. Smyth, P. J. H. Tjossem, A. Hamines, and J. H. Miller, Combust. Flame **79**, 366 (1990).

[189] Y.-C. Hsu, J. J.-M. Lin, D. Papoušek, and J.-J. Tsai, J. Chem. Phys. **98**, 6690 (1993).

[190] S. Shih, S. D. Peyerimhoff, and R. J. Buekner, J. Mol. Spect. **64**, 167 (1977).

[191] Q. Cui and M. Morokuma, J. Chem. Phys. **108**, 8 (1998).

[192] M. Perić, S. D. Peyerimhoff, and R. J. Buekner, Z. Phys. D. **24**, 177 (1992).

[193] P. G. Carrick, A. J. Merer, and R. F. Curl, J. Chem. Phys. **78**, 3652 (1983).

[194] Y. C. Hsu, Y. J. Shui, and C. M. Lin, J. Chem. Phys. **103**, 5919 (1995).

[195] H. Thümmel, M. Perić, S. D. Peyerimhoff, and R. J. Buekner, Z. Phys. D. **13**, 307 (1989).

[196] D. Duflot, J. Robbe, and J. P. Flament, J. Chem. Phys. **100**, 1236 (1994).

[197] M. Boggio-Pasqua, P. Halvick, M. T. Rayez, J. C. Rayez, and J. M. Robbe, J. Phys. Chem. A **102**, 2009 (1998).

[198] A. Mebel, M. Baer, and S. Lin, J. Chem. Phys. **112**, 10703 (200).

[199] L. A. Eriksson and A. Laaksonen, J. Chem. Phys. **105**, 8195 (1996).

[200] P. A. Szalay, L. S. Thøgersen, M. Kállay, and J. Gauss, J. Phys. Chem. A. **108**, 3030 (2004).

[201] A. D. Isaacson and D. G. Truhlar, J. Chem. Phys. **76**, 1380 (1982).

[202] I. Sims et al., Chem. Phys. Lett. **211**, 461 (1993).

[203] X. Zhang, Y. Ding, Z. Li, X. Huang, and C. Sun, J. Phys. Chem. A **104**, 8375 (2000).

[204] Y. Kurosaki and T. Takayanagi, J. Chem. Phys. **113**, 4060 (2000).

[205] B. Ceursters, H. M. T. Nguyen, J. Peeters, and M. T. Nguyen, Chem. Phys. Lett. **329**, 412 (2000).

[206] K. A. Jackson, *Proceedings of the Second International Conference*, Materials Research Society, Pittsburgh,PA, 1991.

[207] A. Ricca, C. Bauschlicher Jr., J. Kang, and C. Musgrave, Surf. Sci. **429**, 199 (1999).

[208] P. G. Szalay, J. Vázquez, C. Simmons, and J. F. Stanton, J. Chem. Phys. **121**, 1 (2004).

[209] A. I. Krylov, J. Chem. Phys. **113**, 6052 (2000).

[210] H. B. Schlegel, J. Phys. Chem. **92**, 3075 (1987).

[211] W. Chen and W. B. Schlegel, J. Chem. Phys. **101**, 5957 (1994).

[212] M. W. Wong and L. Radom, J. Phys. Chem. **99**, 8582 (1995).

[213] D. J. Henry, C. J. Parkinson, and L. Radom, J. Phys. Chem. A **106**, 7927 (2002).

[214] J. Baker, A. Scheiner, and J. Andzelm, Chem. Phys. Lett. **216**, 380 (1993).

[215] T. J. Lee, J. E. Rice, G. E. Scuseria, and H. F. Schaefer, Theor. Chim. Acta **75**, 81 (1989).

[216] T. J. Lee and P. R. Taylor, Int. J. Quantum Chem. Symp. **23**, 199 (1989).

[217] K. Kawaguchi, T. Amano, and E. Hirato, J. Mol. Spec.. **131**, 58 (1988).

[218] E. F. C. Byrd, C. D. Sherrill, and M. Head-Gordon, J. Phys. Chem. A **105**, 9736 (2001).

[219] P. G. Carrick, J. Pfeiffer, E. Koester, F. K. Tittel, and J. Kasper, J. Chem. Phys. **76**, 3336 (1982).

[220] F. Shokoohi, T. A. Watson, R. F. Kong, and A. R. andC. Wittig, J. Phys. Chem. **80**, 5695 (1986).

[221] P. Rosmus and H.-J. Werner, J. Chem. Phys. **80**, 5085 (1984).

[222] H. Pedersen et al., J. Chem. Phys. **109**, 5849 (1998).

[223] A. Einstein, Verh. d. Deutsch. Phys. Ges. **18**, 318 (1916).

[224] A. Einstein, Z. Phys. **18**, 121 (1917).

[225] B. Temelso, C. D. Sherrill, R. C. Merkle, and R. A. Freitas, J. Phys. Chem. A **110**, 11160 (2006).

[226] H.-F. Lu and Y.-C. Sun, Surf. Sci. **494**, L787 (2001).

[227] D. Huang and Y. Yamamoto, Appl. Phys. A **64**, 419 (1997).

[228] C. Thirstrup, M. Sakurai, and T. Nakayama, Surf. Sci. **411**, 203 (1998).

[229] B. J. McIntyre, M. Salmeron, and G. A. Somorjai, Science **265**, 1415 (1994).

[230] W. T. Müller, D. L. Klein, T. Lee, J. Clarke, and P. G. S. P. L. McEuen, Science **268**, 272 (1995).

[231] L. Song, W. Wu, K. Dong, P. C. Hiberty, and S. Shaik, J. Phys. Chem. A **106**, 11361 (2002).

[232] (a) Hiberty, P.C; Flament, J. P.; Noizet, E. Chem. Phys. Lett. 1992, 189, 259. (b) Hiberty, P. C.; Humbel, S.; Byrman, C. P.; Van Lenthe, J. H. J. Chem. Phys. 1994, 101, 5969. (c) Hiberty, P. C.; Humbel, S.; Archirel, P. J. Phys. Chem. 1994, 98, 11697. (d) Hiberty, P. C. In Modern Electronic Structure Theory and Applications in Organic Chemistry; Davidson, E. R., Ed.; Word Scientific: River Edge, NY, 1997; pp 289-367. (e) Hiberty, P. C.; Shaik, S. In Valence Bond Theory, Cooper, D. L., Ed.; Elsevier: Amsterdam, 2002; pp 187-225.

[233] T. I. Drozdova and E. T. Denisov, Kinet. and Catal. **43**, 10 (2002).

[234] C. Chatgilialoglu, M. Ballestri, J. Escudié, and I. Pailhous, Organometallics **18**, 2395 (1999).

[235] N. L. Arthur and L. A. Miles, J. Chem. Soc., Faraday Trans. **94**, 2741 (1998).

[236] A. A. Zavitsas and C. ChatgiliaIoglu, J. Am. Chem. Soc. **117**, 10645 (1995).

[237] S. Shimokawa, A. Namiki, M. N.-Gamo, and T. Ando, J. Chem. Phys. **113**, 6916 (2000).

[238] S. Sugahara, K. Hosaka, and M. Matsumura, App. Surf. Sci. **130**, 327 (1998).

[239] J. Olander and K. Larsson, Thin Solid Films **458**, 191 (2004).

[240] E. Srinivasan, H. Yang, and G. N. Parsons, J. Chem. Phys. **105**, 5467 (1996).

[241] K. A. Peterson, J. Chem. Phys. **119**, 11099 (2003).

[242] K. A. Peterson, D. Figgen, E. Goll, H. Stoll, and M. Dolg, J. Chem. Phys. **119**, 11113 (2003).

[243] H.-J. Werner et al., 2006, see http://www.molpro.net.

[244] J. M. L. Martin and A. Sundermann, J. Chem. Phys. **114**, 3408 (2001).

[245] N. Arthur and L. Miles, J. Chem. Soc. Faraday Trans. **93**, 4259 (1997).

[246] Y. Matsui, A. Yuuki, N. Morita, and K. Tachibana, Jpn. J. Appl. Phys. Part 1 **26**, 1575 (1987).

[247] A. Goumri, W. Yuan, L. Ding, Y. Shi, and P. Marshall, Chem. Phys. **177**, 233 (1993).

[248] N. Arthur and T. Bell, Rev. Chem. Intermed. **2**, 37 (1978).

[249] R. Berkley, I. Safarik, O. Strausz, and H. Gunning, J. Phys. Chem. **77**, 1741 (1973).

[250] H. O'Neal, S. Pavlou, T. Lubin, M. Ring, and L. Batt, J. Phys. Chem. **75**, 3945 (1971).

[251] O. Strausz, E. Jakubowski, H. Sandhu, and H. Gunning, J.Chem. Phys. **51**, 552 (1969).

[252] E. Morris and J. Thynne, J. Phys. Chem. **73**, 3294 (1969).

[253] R. Berkley, I. Safarik, H. Gunning, and O. Strausz, J. Phys. Chem. **77**, 1734 (1973).

[254] J. Kerr, D. Slater, and J. Young, J. Chem. Soc. A. **1**, 134 (1967).

[255] N. Arthur, I. Cooper, and L. Miles, Int. J. Chem. Kinet. **29**, 237 (1997).

[256] N. Arthur and I. Cooper, J. Chem. Soc. Faraday Trans. **91**, 3367 (1995).

[257] D. Nava, W. Payne, G. Marston, and L. Stief, J. Geophys. Res. **98**, 5531 (1993).

[258] C. Janssen and I. Nielsen, Chem. Phys. Lett. **290**, 423 (1998).

[259] T. J. Lee, Chem. Phys. Lett. **290**, 423 (1998).

[260] T. Schaich, J. Braun, J. Toennies, M. Buck, and C. Woll, Surf. Sci. **385**, L958 (1997).

[261] C. Su et al., J. Chem. Phys. **107**, 7543 (1997).

[262] K. Bobrov, B. Fisgeer, H. Shechter, M. Folman, and A. Hoffman, Diam. Rel. Mater **6**, 736 (1997).

[263] A. D. Bochevarov and C. D. Sherrill, J. Chem. Phys. **122**, 234110 (2005).

[264] F. Moscardó, A. J. Pérez-Jiménez, Sancho-García, and E. San Fabián, Chem. Phys. Lett. **288**, 418 (1998).

[265] T. V. Voorhis and M. Head-Gordon, Chem. Phys. Lett. **317**, 575 (2000).

[266] T. V. Voorhis and M. Head-Gordon, J. Chem. Phys. **112**, 5633 (2000).

[267] G. J. O. Beran, M. Head-Gordon, and S. R. Gwaltney, J. Chem. Phys. **124**, 114107 (2006).

[268] A. I. Krylov, Chem. Phys. Lett. **338**, 375 (2001).

[269] A. I. Krylov, Chem. Phys. Lett. **350**, 522 (2001).

[270] A. I. Krylov and C. D. Sherrill, J. Chem. Phys. **116**, 3194 (2002).

[271] J. S. Sears, C. D. Sherrill, and A. I. Krylov, J. Chem. Phys. **118**, 9084 (2003).

[272] Y. H. Shao, M. Head-Gordon, and A. I. Krylov, J. Chem. Phys. **118**, 4807 (2003).

[273] P. Piecuch, K. Kowalski, I. S. O. Pimienta, and S. A. Kucharski, Method of moments coupled-cluster equations: A new theoretical framework for designing "black box" approaches for molecular potential energy surfaces, in *Low-Lying Potential Energy Surfaces,* ACS Symposium Series, volume 828, page 31, Washington, D.C., 2002, American Chemical Society.

[274] P. Piecuch, K. Kowalski, I. S. O. Pimienta, and M. J. McGuire, Int. Rev. Phys. Chem. **21**, 527 (2002).

[275] K. Kowalski and P. Piecuch, J. Chem. Phys. **116**, 7411 (2002).

[276] M. Włoch, J. R. Gour, K. Kowalski, and P. Piecuch, J. Chem. Phys. **122**, 214107 (2005).

[277] G. D. Purvis and R. J. Bartlett, Chem. Phys. Lett. **76**, 1910 (1982).

[278] J. F. Stanton, J. Gauss, J. D. Watts, and R. J. Bartlett, Mol. Phys. **98**, 1185 (2000).

[279] M. Musial and R. J. Bartlett, J. Chem. Phys. **122**, 224102 (2005).

[280] O. Christiansen, H. Koch, and P. Jørgensen, Chem. Phys. Lett. **243**, 409 (1995).

[281] H. Larsen, J. Olsen, P. Jørgensen, and J. Gauss, Chem. Phys. Lett. **342**, 200 (2001).

[282] C. Hättig, J. Chem. Phys. **118**, 7751 (2003).

[283] A. I. Krylov, J. Chem. Phys. **113**, 6052 (2000).

[284] A. D. Bochevarov and C. D. Sherrill, J. Chem. Phys. **122**, 234110 (2005).

[285] M. Nooijen, J. Chem. Phys. **111**, 10815 (1999).

[286] W. Meyer, J. Chem. Phys. **58**, 1017 (1973).

[287] W. Kutzelnigg, Pair correlation theories, in *Methods of Electronic Structure Theory*, volume 828, page 129, New York, 1977, Plenum Press.

[288] C. Murray and E. R. Davidson, Int. J. Quant. Chem. **43**, 755 (1992).

[289] B. Temelso, C. D. Sherrill, R. C. Merkle, and J. R. A. Freitas, J. Phys. Chem. A , submitted.

[290] A. D. Bochevarov, B. Temelso, and C. D. Sherrill, J. Chem. Phys. **125**, 054109 (2006).

[291] D. Feller, K. A. Peterson, and T. D. Crawford, J. Chem. Phys. **124**, 054107 (2006).

[292] N. C. Handy, Y. Yamaguchi, and H. F. Schaefer, J. Chem. Phys. **84**, 4481 (1986).

[293] G. Tarczay, A. Császár, W. Klopper, W. Allen, and H. Schaefer, J. Chem. Phys. **110**, 11971 (1999).

[294] G. Tarczay, A. Császár, M. L. Leininger, and W. Klopper, Chem. Phys. Lett. **322**, 119 (2000).

[295] N. H. A.G. Ioannou, R.D. Amos, Chem. Phys. Lett. **251**, 52 (1996).

[296] B. C. Garrett and D. G. Truhlar, J. Chem. Phys. **82**, 4543 (1985).

[297] S. Garashchuk, J. C. Light, and V. A. Rassolov, Chem. Phys. Lett. **333**, 459 (2001).

[298] S. L. Mielke, B. C. Garrett, and K. A. Peterson, J. Chem. Phys. **116**, 4142 (2002).

[299] S. L. Mielke, D. W. Schwenke, and K. A. Peterson, J. Chem. Phys. **122**, 224313 (2005).

[300] S. L. Mielke et al., Phys. Rev. Lett. **91**, 063201 (2003).

[301] P. J. Knowles, J. S. Andrews, R. D. Amos, N. C. Handy, and J. A. Pople, Chem. Phys. Lett. **186**, 130 (1991).

[302] C. Murray and E. R. Davidson, Chem. Phys. Lett. **187**, 451 (1991).

[303] W. L. Lauderdale, J. F. Stanton, J. Gauss, J. D. Watts, and R. J. Bartlett, Chem. Phys. Lett. **187**, 21 (1991).

[304] R. D. Amos, J. S. Andrews, N. C. Handy, and P. J. Knowles, Chem. Phys. Lett. **185**, 256 (1991).

[305] T. Lee and D. Jayatilaka, Chem. Phys. Lett. **201**, 1 (1993).

[306] C. L. Janssen, I. B. Nielsen, M. L. Leininger, E. F. Valeev, and E. T. Seidl, 2004, The Massively Parallel Quantum Chemistry Program (MPQC), Version 2.3.1, Sandia National Laboratories, Livermore, CA, USA.

[307] Wolfram Research, Inc., Mathematica, Version 5.2, Champaign, IL (2005).

VITA

Berhane Temelso was born in 1979 in Addis Ababa, Ethiopia to Eritrean parents, Temelso Gayim and Ametsion Hadgu. He attended the Atse Tewodros School before getting a four year scholarship to attend the International Community School (ICS) of Addis Ababa in 1993. In August 1998, he moved to Berea, KY to do his undergraduate work in physics and continued onto Georgia Institute of Technology in 2002 to study computational chemistry under the direction of Dr. C. David Sherrill. He is currently seeking an industrial computational chemist and/or Unix/Linux administrator position.